Tools and Methods for the Analysis and Simulation of Large Transmission Systems Using 100% Power Electronics

Quentin Cossart

HESAM UNIVERSITÉ

Arts et Métiers Sciences et Technologies

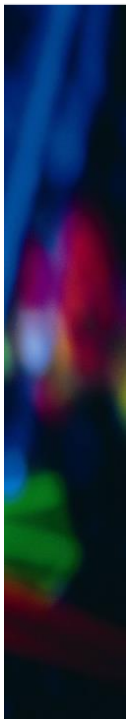

2019-ENAM-0031

École doctorale n°432 : Sciences des Métiers de l'ingénieur

Doctorat

T H È S E

pour obtenir le grade de docteur délivré par

l'École Nationale Supérieure d'Arts et Métiers

Spécialité " Génie Électrique "

présentée et soutenue publiquement par

Quentin COSSART

le 24 Septembre 2019

Outils et Méthodes pour l'Analyse et la Simulation de Réseaux de Transport 100% Électronique de Puissance

Directeur de thèse : **Xavier KESTELYN**
Co-encadrement de la thèse : **Frédéric COLAS**

Jury

M. Stéphane CLENET, Professeur, L2EP, Arts et Métiers ParisTech	Président
M. Bogdan MARINESCU, Professeur, LS2N, École Centrale de Nantes	Rapporteur
M. Seddik BACHA, Professeur, G2ELAB, Université Grenoble Alpes	Rapporteur
Mme Héloïse BARAFFE, Docteure, EDF	Examinateur
M. Xavier KESTELYN, Professeur, L2EP, Arts et Métiers ParisTech	Examinateur
M. Frédéric COLAS, Docteur, L2EP, Arts et Métiers ParisTech	Examinateur
M. Guillaume DENIS, Docteur, RTE	Invité

T H È S E

Arts et Métiers - Campus de Lille
Laboratoire d'Électrotechnique et d'Électronique de Puissance de Lille

This project has received funding from the European Union's Horizon 2020 research and innovation programme under grant agreement No 691800. This report reflects only the author's views and the European Commission is not responsible for any use that may be made of the information it contains.

Acknowledgement

Plusieurs personnes ont contribué à la réussite de ce projet de thèse.

J'adresse tout d'abord mes remerciements aux membres de mon jury pour leur relecture attentive de mon rapport et leurs conseils. Je remercie donc le président de mon jury le professeur Stéphane Clénet, les rapporteurs de mon mémoire les professeurs Bogdan Marinescu et Seddik Bacha et l'examinatrice de ma thèse la docteure Héloïse Baraffe.

Je remercie bien évidemment mes encadrants de thèse qui m'ont accompagné pendant ces trois ans, à savoir mon directeur de thèse le professeur Xavier Kestelyn et mon co-encadrant le docteur Frédéric Colas. Je les remercie pour l'expertise scientifique qu'ils m'ont apportée, leur investissement durant ces trois années de thèse et la confiance qu'ils m'ont accordée en me laissant travailler avec beaucoup d'autonomie.

Je remercie les membres du laboratoire L2EP avec qui j'ai eu la chance de travailler, en particulier le professeur Xavier Guillaud pour son accompagnement, lorsque j'étais étudiant en école d'ingénieur, qui m'a permis de m'orienter dans la voie de la recherche dans les réseaux électriques.

Je remercie les stagiaires, doctorants et post-doctorants des laboratoires L2EP, LISPEN et LMFL du campus de l'ENSAM de Lille que j'ai côtoyés pendant cette thèse et avec qui j'ai passé de très bons moments. Je remercie en particulier mes collègues de bureau Martin Legry, Pierre Vermeersch, Jérôme Buire, Nnaemeka Ugwuanyi, Artur Avazov et Taoufik Qoria.

Je remercie les membres du projet MIGRATE avec qui j'ai travaillé durant mon doctorat, en particulier les ingénieurs de RTE Thibault Prevost, Marie-Sophie Debry et le docteur Guillaume Denis.

Je remercie ma famille, en particulier mes parents, grâce à qui j'ai pu réussir mes études et aboutir à ce doctorat.

Enfin, je remercie ma compagne Émilie, pour son soutien, sa compréhension et sa patience pendant ces trois années.

List of Figures

List of Tables

List of abbreviations

DAE	Differential Algebraic Equations
DQ0	Direct-Quadrature-Zero
EMT	Electromagnetic Transient
EVD	Eigenvalue Decomposition
HSV	Hankel Singular Values
HVAC	High Voltage Alternating Current
HVDC	High Voltage Direct Current
IGBT	Insulated Gate Bipolar Transistor
LTI	Linear Time Invariant
MIMO	Multiple Inputs Multiple Output
MMC	Modular Multilevel Converter
MOR	Model Order Reduction
ODE	Ordinary Differential Equations
PCC	Point of Common Coupling
PE	Power Electronics
PGD	Proper Generalised Decomposition
PI	Proportional Integral controller
PLL	Phase-Locked Loop
POD	Proper Orthogonal Decomposition
pu	per unit
SISO	Single Input Single Output
SVD	Singular Value Decomposition
TSO	Transmission System Operator
TSP	Transient Stability Program
VSC	Voltage Source Converter
VSM	Virtual Synchronous Machine

Contents

Introduction

Contents

General context

Since the beginning of electricity generation in the 19^{th} century, fossil energies like coal or gas have been the most used resources. It is a cheap energy but it resulted in huge greenhouse gases emissions, responsible for global warming and climate change.

To fight climate change and reduce greenhouse gases emissions, governments of most countries have decided to massively invest in renewable energies such as wind power or photovoltaic power. These renewable energy generators are connected to the power system through Power Electronics (PE) converters, which is not the case for the coal, gas or nuclear power plants that use Synchronous Machines (SM).

In parallel, several High Voltage Direct Current (HVDC) links are built to interconnect asynchronous power systems (between France and England for example) or synchronous power systems on long distances (between France and Spain for example) between each other, and they too use PE converters. Figure 1 shows the existing HVDC links (in red) and some planed projects (in blue) in Europe. The green line represents the France-Spain link that was built recently.

Finally, most of the new generation loads use PE converters as well (like computers or household appliances). And the fast development of the electric vehicles induces an increase in the PE penetration too.

For all these reasons, the PE penetration in the power systems hugely increases. It can be high very soon in some places like Ireland, which is an island with a lot of wind generation.

But this trend is not without any consequence. The dynamic behaviour of SM and PE converters are indeed very different. For example, while SM have an inertia because of their rotating mass, PE devices haven't got any. Another example is the over current capability that is way higher for SM than for PE converters. Moreover, PE converters are currently controlled as simple current sources (they are called grid feeding or grid following converters). They do not create the voltage like SM. Soon this will be mandatory for them to create this voltage and replace the SM. This is what is called a grid forming capability and this necessitates a change in the way the converters are controlled. But when controlled as voltage sources (grid forming converters), the converters are even more subject to over current which is a great issue that should be taken into account in the analysis and simulations.

As a result, if the PE penetration keeps on increasing, which is highly probable, there is a non negligible possibility that the power system security and stability are not ensured any more if nothing changes in the way it is controlled. Moreover, protection issues will arise, as well as power quality challenges.

To anticipate and prepare for this challenge, several European Transmission System Operators (TSO) and universities have gathered to form a European project to work on these issues. This is the MIGRATE project, which is presented in the next section.

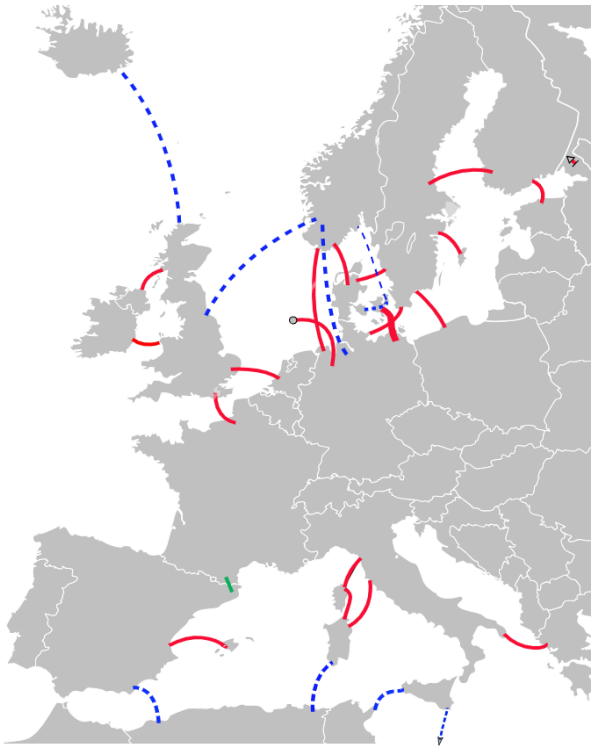

Figure 1: Example of HVDC links in Europe

Presentation of the MIGRATE project

MIGRATE stands for Massive InteGRATion of power Electronic devices [1]. It is an EU-funded project under the framework of European Union's Horizon 2020.

It gathers several partners, that are presented in Figure 2 [1]. There are 11 TSO, 12 universities and one manufacturer from 13 countries working together in this project. Their main objective is to propose innovative solutions to progressively adjust the HVAC system operations.

The different objectives of the project are addressed in 8 work packages that are presented in Figure 3 [1].

This PhD is part of the work package 3 that aims at developing controls and operations of a grid with 100% converter based devices.

The goals of this PhD are to simulate and analyse transmission systems with 100% PE. The increase in the PE penetration is indeed a challenge and it changes the way we need to simulate transmission systems as their dynamic behaviour greatly changes. To do so, it aims at developing new tools and methods to analyse and simulate such systems. Then it can give some insights on how a power system with 100% PE behave and how it should be modelled to guarantee that the simulations and analyses fit what is observed in reality. The final aim is to ensure the security and stability of a power system with 100% PE in the future.

Figure 2: Members of the MIGRATE project

Figure 3: Work packages of the MIGRATE project

Contributions

This work has brought several contributions that are listed here.

First, a review of the existing tools and methods to simulate and analyse power systems has been done. It has been assessed for each one of these tools, whether they can be used with a large PE penetration and in which cases.

Then three Model Order Reduction (MOR) methods have been developed to reduce the simulation time and to simplify the analysis by reducing the number of state variables. Unlike most of the existing methods, these developed methods keep the physical structure and the variables of the system, making the analysis easier. These methods are described in details in this report.

The developed methods have been validated and compared using realistic test cases. Thanks to these applications, the advantages and drawbacks of each method have been presented. Moreover, the results of these test cases give recommendations on how to model, simulate and analyse a transmission system with a high PE penetration. Among these test cases, a real transmission system (the Irish transmission system) has been modelled using 100% PE generation and it proves to be stable with the converter control developed in the MIGRATE project.

Outline of the thesis

This report is organized in four chapters.

The first chapter reviews the existing tools and methods that are used to simulate and analyse transmission systems and the most common MOR methods. The presented simulation tools are the EMT simulations that use detailed models, the phasor simulations that use a phasor approximation to simplify the models and thus reduce the simulation time and the dynamics phasor simulations that are a compromise between the two. The presented analysis tools are the small-signal stability analysis, the sensitivity analysis and the participation factors. The presented MOR methods are the modal truncation that is based on a modal analysis, the balanced truncation that is based on a study of the Hankel singular values of the system, the proper orthogonal decomposition that uses a snapshot of the system taken from a previous simulation or an experiment and the Krylov methods that use moment matching techniques.

The second chapter presents the models that are used for the rest of the report. Each element of a transmission system is modelled: converters (grid forming, grid feeding and modular multilevel converter), lines, transformers, synchronous machines, loads, etc. In each case, the equations of the model are given in the DQ0 representation and block diagrams illustrate the different controls.

The third chapter presents the three developed MOR methods. The process is detailed for each one of them. These methods use the presented analysis tools but they are also inspired by the existing MOR methods to take the best of them. One method consists in discarding the fastest poles of the system, the second one discards the poles

of the system that are linked to the less energetic states in the balanced realization (link with the balanced truncation) and the third one uses an optimisation to minimize an error criterion. All the methods preserve the variables, parameters and physical structure of the system which are important features for a MOR method applied to power systems.

The fourth and last chapter applies the developed methods to realistic test cases using the models presented in the second chapter. The conclusions for each test case are recommendation on how to model, simulate and analyse a transmission system with a high PE penetration. One conclusion is that depending on the studied converter in the system and the simulated event, the most adapted reduced model is not the same. And this is taken into account by the developed MOR methods.

Publications

The work done in this PhD resulted in several publications that are listed below:

- Q. Cossart, F. Colas, X. Kestelyn, "Model reduction of converters for the analysis of 100% power electronics transmission systems," in *2018 IEEE International Conference on Industrial Technology (ICIT)*, Lyon, 2018.

  In this paper, the first developed method is presented and applied to a simple test case consisting in one grid forming converter connected to an infinite grid.

- Q. Cossart, F. Colas, X. Kestelyn, "Modèles réduits de convertisseurs pour l'étude de réseaux 100% électronique de puissance," in *Symposium de Génie Électrique*, Nancy, 2018.

  This paper presents the results of the previous paper in french and in a national conference.

- Q. Cossart, F. Colas, X. Kestelyn, "Simplified converters models for the analysis and simulation of large transmission systems using 100% power electronics," in *2018 20th European Conference on Power Electronics and Applications (EPE'18 ECCE Europe)*, Riga, 2018.

  In this paper, the first developed method is applied to a test case consisting in a two-converter system.

- Q. Cossart, F. Colas, X. Kestelyn, "A priori error estimation of the structure-preserving modal model reduction by state residualization of a grid forming converter for use in 100% power electronics transmission systems," in *15th IET International Conference on AC and DC Power Transmission (ACDC 2019)*, Coventry, 2019.

  In this paper, the third developed method (in its first version, with a brute-force optimization) is applied to a two-converter system. The idea is to find the most

adequate model for each element of the system (converter and line) depending on the simulated event and the observed variable.

Two journal papers have been submitted and are under review:

- Q. Cossart, F. Colas, X. Kestelyn, "A novel strategy of modal model order reduction by state residualization for 100% power electronic-based grids," *EPE Journal*.

  In this paper, the second developed method is applied to the Irish transmission system in phasor mode. The idea is to find the most adequate model for each converter in the system depending on the observed variable.

- Q. Cossart, F. Colas, X. Kestelyn, "A novel method for choosing the most suitable model order reduction of a 100% renewable power grid subject to various events," *IEEE Transactions on Power Systems*.

  In this paper, the third strategy (in its final version, with a genetic algorithm optimization) is applied to the Irish transmission system in EMT mode. The idea is to find the most adequate model for each element in the system (converter, line, transformer, load) depending on the observed variable and the simulated event.

CHAPTER 1

Scientific context

Contents

As presented in the introduction, the aim of this thesis is to study transmission systems with a large PE penetration in order to assess their stability, security and expected performances. Given the size and the complexity of the transmission systems, experimentations are limited and at-scale prototypes are nearly impossible to build. To cope with that, a solution is the use of numerical simulations and analysis tools. They make it possible to test different test cases and validate the developed controls at limited cost compared to experimentations.

In this chapter, a bibliographic work has been carried out to set the scientific context of this work. The first section presents the existing tools to simulate and analyse transmission systems. It is shown that some tools, especially some approximations, might not be relevant any more with a large PE penetration. This is why a need for Model Order Reduction (MOR) is identified, in order to accelerate the simulation and simplify the analysis of large systems. A focus is made here on the case of a power system with a high PE penetration.

As a result, the second section presents the existing MOR methods, their characteristics, advantages and drawbacks. It is explained why they are not always suitable for the study of power systems with a large PE penetration.

1.1 Tools and methods for the simulation and analysis of transmission systems

This section presents the existing tools to simulate and analyse transmission systems. The first subsection deals with the simulation tools while the second one is about the analysis tools. The idea is to assess whether these tools are still relevant when the PE penetration is very high, and if not, what are the alternatives.

1.1.1 Simulation tools

Electromagnetic transient programs

The Electromagnetic Transient (EMT) programs are software used to simulate power systems that have been introduced in [2].

As their name says it, they consider the fast electromagnetic transients in addition to the slow electromechanical transients (see Figure 1.1 [3]). The computation time of such a simulation is high due to the level of details of the models and the fact that the time-step needs to be small (tens of μs) to capture the fast transients and simulate the fast electromagnetic dynamics [4]. Moreover, because of the high number of variables and parameters of EMT simulations, the analysis is complex. As a consequence, only local parts of the system are simulated with EMT programs and during a short time-span.

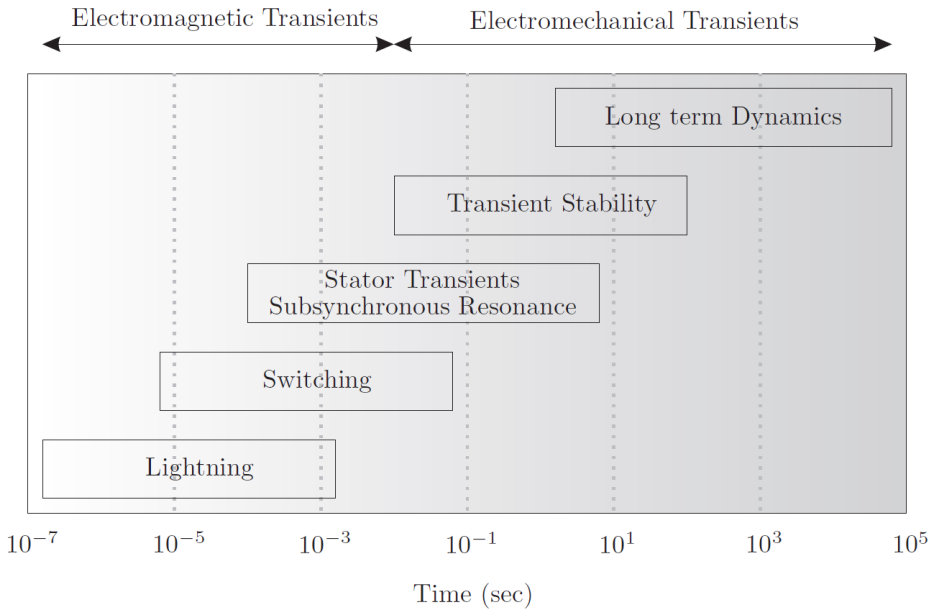

Figure 1.1: Time frame of power system transients

Unbalances can be taken into account with EMT programs, and the models are most of the time in the ABC representation, that uses the natural/physical variables (unlike the DQ0 representation that uses a basis change. See appendix for more information).

For all these reasons, they are particularly adapted to the simulation of PE devices, where the switching of the IGBT can be simulated with high-fidelity. Today, EMT programs are for instance used for the simulation of Modular Multilevel Converter (MMC) [5], wind turbines converters [6] or switching in transmission lines [7].

An overview of the existing EMT programs have been made in [8]. The most famous ones are EMTP-RV [9] and PSCAD/EMTDC [10], which are commercial software.

In this work, large systems (transmission systems) are simulated and analysed. It means that using EMT programs could lead to high computation times and complex analyses.

Phasor approximation and transient stability programs

The phasor approximation is an approximation that has been used in the power system community for a long time [11]. It is applied to balanced systems and consists in neglecting the electromagnetic dynamics of the lines as they are faster (and therefore less relevant for stability analyses) than the slow electromechanical dynamics of the SM. As a result, the only dynamics of the model are the dynamics of the SM and their controls. Moreover, the models for all the elements of the system only take into account the slow dynamics and not the fastest one. For example, simplified models are used for the SM.

For example, consider a model of a line as illustrated in 1.2. This is a simple R,L model. The system is considered to be balanced. As a result, the DQ0 representation is used and only the d-axis and q-axis components are considered. The equations modelling this line are shown in (1.1).

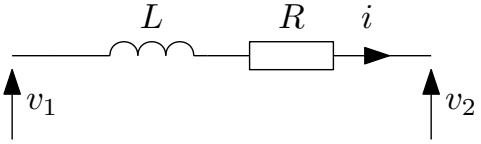

Figure 1.2: Example of a model of a line

$$\begin{cases} \dfrac{L}{\omega_b}\dfrac{di_d}{dt} = v_{1_d} - v_{2_d} - Ri_d + \omega L i_q \\ \dfrac{L}{\omega_b}\dfrac{di_q}{dt} = v_{1_q} - v_{2_q} - Ri_q - \omega L i_d \end{cases} \tag{1.1}$$

With the phasor approximation, the derivative parts of the variables i_d and i_q are neglected. It leads to (1.2).

$$\begin{cases} 0 = v_{1_d} - v_{2_d} - Ri_d + \omega L i_q \\ 0 = v_{1_q} - v_{2_q} - Ri_q - \omega L i_d \end{cases} \tag{1.2}$$

It can be seen in these equations that the line behaviour is now quasi-static, which simplifies the model and accelerate the simulation. It is indeed now possible to use larger time steps for the simulation and analysing the system becomes faster as there are less state variables. Of course, this approximation leads to errors when considering the transient behaviour [12]. The question is to decide whether these transients are important or not for the study. Over-current transients are for instance less important with SM (which can handle high over-currents) than with converters (which have a low over-current capability [13] and therefore need an accurate simulation to ensure that the device can handle the transient).

Programs that use the phasor approximation are called Transient Stability Programs (TSP). Examples of TSP are the commercial software EUROSTAG [14], PSS/E (for Power System Simulator for Engineering) and RAMSES (for RApid Multiprocessor Simulation of Electric power Systems) [15, 16].

This phasor approximation is still widely used today when there are PE devices in the power system [17, 18]. But the hypothesis on which it is based (which is that the fast electromagnetic transients can be neglected as they are faster than the electromechanical transients of the SM) might not be verified any more if the SM penetration decreases and the PE penetration increases.

Dynamic phasor

The dynamic phasors were developed in [19]. Their advantages are the possibility to consider the unbalances [20], a better accuracy than the classical phasor approximation (although the model is more complex), and a lower computation time than with EMT models (although they are less precise).

This tool is based on a Fourier series decomposition. Consider a nearly-periodical variable x of a period T and a pulsation ω (which is the case for the currents and voltages in a power system for example). This variable can be approximated by a Fourier decomposition in (1.3).

$$\forall \tau,\ \forall t \in [\tau - T; \tau],\ x(t) \approx \sum_{k=-\infty}^{+\infty} X_k(\tau) e^{jk\omega t} \tag{1.3}$$

The coefficient X_k, called dynamic phasor k is calculated in (1.4).

$$X_k(\tau) = \frac{1}{T} \int_{\tau - T}^{\tau} x(t) e^{-jk\omega t} dt = < x >_k (\tau) \tag{1.4}$$

To go further, the variable x can be approximated with its first K dynamic phasors in (1.5). The bigger K is, the more accurate the model is but the higher the computation time is. The choice of K determines the number of equations suitable to model the system.

$$x(t) \approx \sum_{k=-K}^{K} X_k(\tau) e^{jk\omega t} \tag{1.5}$$

The following property in (1.6) helps writing the differential equations in the dynamic phasor domain and thus writing an entire model in the dynamic phasor domain.

$$< \frac{dx}{d\tau} >_k (\tau) = \frac{d < x >_k}{d\tau}(\tau) + jk\omega < x >_k (\tau) = \frac{dX_k}{d\tau}(\tau) + jk\omega X_k(\tau) \tag{1.6}$$

One advantage of the dynamic phasors is that it is more accurate than the phasor approximation and it has a lower computation time than EMT simulations. It is used today to simulate 2-level VSC [21], MMC [22] or electrical machines [23].

One drawback of the dynamic phasors is that it increases the number of variables and equations (two for each k), which makes the analysis complicated. Moreover, it is not easily applicable on the classical simulation software.

Comparison of the three simulation methods on a simple example

To illustrate the three simulation methods (EMT, phasors and dynamic phasors), consider the simple test case in Figure 1.3.

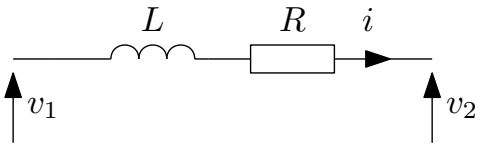

Figure 1.3: Test case under consideration

The two voltages v_1 and v_2 are fixed. A short-circuit at v_2 is simulated at $t = 1s$ ($v_2 = 0$ at $t = 1s$) and cleared after $150ms$. The current in the RL line is shown on Figure 1.4 for each of the three simulation methods. For the dynamic phasors, $K = 1$.

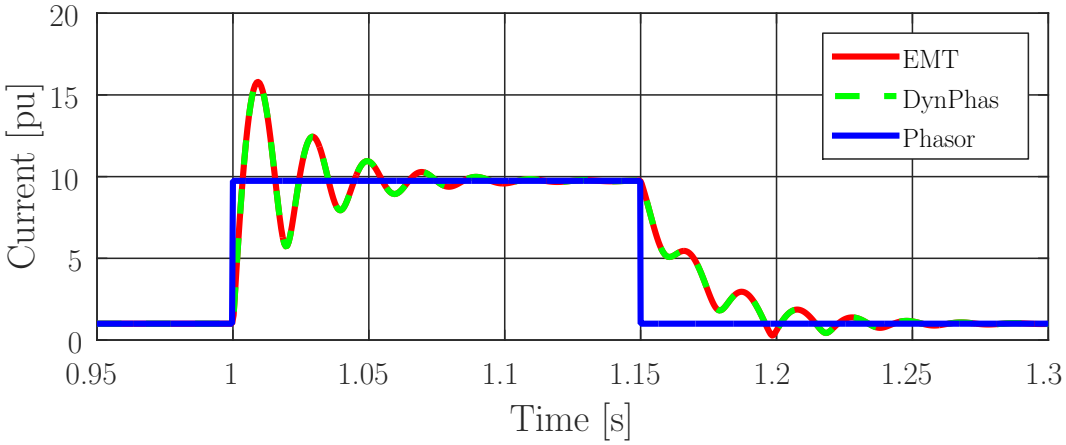

Figure 1.4: Comparison of EMT, dynamic phasors and phasors simulations

One can see that the phasor approximation misses the transient during the short-circuit and the clearing of the fault. On the other hand, the EMT and dynamic phasors simulations give the same result on this particular test case.

Conclusion

In this subsection, different tools to simulate power systems have been presented:

- The phasor approximation simplifies the equations in the DQ0 representation by neglecting the fast electromagnetic transients. This approximation is based on the fact that SM have slow electromechanical dynamics, which are more important for the stability than the fast electromagnetic transients. As a result, a larger time step can be used which makes the simulation faster. Moreover, as the number of state variables has decreased, the analysis gets easier. With a 100% PE transmission system however, this approximation might not be relevant any more. Moreover, it is important with PE devices (more than with SM) to capture fast transients, which can damage the converter (over-current for example).

- The EMT programs allow to simulate accurately PE converters. However, the simulation time with these programs is high because of the level of details and the number of variables and parameters makes the analysis complicated. Moreover, a small time step needs to be used. As a result, EMT programs cannot easily be used for simulating large power systems.

- The dynamic phasors are an interesting tool between the phasor simulation and the EMT simulation. They are based on a Fourier series decomposition of all the variables in the system. The needed time step is larger than with an EMT simulation, which decreases the simulation time. However, they induce an increase in the number of variables and equations that can complicate the analysis, which is not what is looked for in this report, although they reduce the computation time compared to EMT simulations [3].

1.1.2 Analysis tools

This subsection presents three analysis tools that are used today to study transmission systems. The aim here is to check whether they are still relevant when studying transmission systems with a high PE penetration.

One can remark that these tools are applicable on linear systems only. Several tools exist for nonlinear systems like the Lyapunov stability [24] or the nonlinear participation factors [25] but using them is not straightforward and it can complicate the analysis which is not what is wanted here. As a consequence, it has been chosen here to focus only on tools for linear systems. To proceed, the studied systems are linearised around their operating point in steady state.

Small-signal stability analysis

The first analysis tool to be presented here is called small-signal stability analysis. It is a widely used tool in the power system analysis [26].

First, a nonlinear Differential Algebraic Equations (DAE) system, modelling the studied transmission system, is considered in (1.7).

$$\begin{cases} \dfrac{dx_{diff}}{dt} = f(x_{diff}, x_{alg}, u) \\ \quad 0 = g(x_{diff}, x_{alg}, u) \\ \quad y = h(x_{diff}, x_{alg}, u) \\ x_{diff} \in \mathbb{R}^{N_{diff}}, x_{alg} \in \mathbb{R}^{N_{alg}}, u \in \mathbb{R}^{p}, y \in \mathbb{R}^{q} \end{cases} \tag{1.7}$$

This system is linearised around its operating point $x_0 = (x_{diff_0}, x_{alg_0}, u_0)$ at steady state. It is important that the system is time-invariant at steady state. This is why the DQ0 representation is used (see Appendix for more explanation). To simplify the writing, all the derivatives $\frac{\partial f}{\partial x}(x_0)$ are written $\frac{\partial f}{\partial x}$. It gives (1.8).

$$\begin{cases} \dfrac{d\Delta x_{diff}}{dt} = \dfrac{\partial f}{\partial x_{diff}}\Delta x_{diff} + \dfrac{\partial f}{\partial x_{alg}}\Delta x_{alg} + \dfrac{\partial f}{\partial u}\Delta u \\ 0 = \dfrac{\partial g}{\partial x_{diff}}\Delta x_{diff} + \dfrac{\partial g}{\partial x_{alg}}\Delta x_{alg} + \dfrac{\partial g}{\partial u}\Delta u \\ \Delta y = \dfrac{\partial h}{\partial x_{diff}}\Delta x_{diff} + \dfrac{\partial h}{\partial x_{alg}}\Delta x_{alg} + \dfrac{\partial h}{\partial u}\Delta u \\ \Delta x_{diff} \in \mathbb{R}^{N_{diff}}, \Delta x_{alg} \in \mathbb{R}^{N_{alg}}, \Delta u \in \mathbb{R}^{p}, \Delta y \in \mathbb{R}^{q} \end{cases} \tag{1.8}$$

If $\frac{\partial g}{\partial x_{alg}}$ is not singular, the following matrices are defined in (1.9).

$$\begin{cases} A = \dfrac{\partial f}{\partial x_{diff}} - \dfrac{\partial f}{\partial x_{alg}} \times \dfrac{\partial g}{\partial x_{alg}}^{-1} \times \dfrac{\partial g}{\partial x_{diff}} \in \mathbb{R}^{N_{diff} \times N_{diff}} \\ B = \dfrac{\partial f}{\partial u} - \dfrac{\partial f}{\partial x_{alg}} \times \dfrac{\partial g}{\partial x_{alg}}^{-1} \times \dfrac{\partial g}{\partial u} \in \mathbb{R}^{N_{diff} \times p} \\ C = \dfrac{\partial h}{\partial x_{diff}} - \dfrac{\partial h}{\partial x_{alg}} \times \dfrac{\partial g}{\partial x_{alg}}^{-1} \times \dfrac{\partial g}{\partial x_{diff}} \in \mathbb{R}^{q \times N_{diff}} \\ D = \dfrac{\partial h}{\partial u} - \dfrac{\partial h}{\partial x_{alg}} \times \dfrac{\partial g}{\partial x_{alg}}^{-1} \times \dfrac{\partial g}{\partial u} \in \mathbb{R}^{q \times p} \end{cases} \tag{1.9}$$

With these matrices, it is possible to write the system in state-space representation in (1.10) by injecting the algebraic equations in the differentials equations and in the output equations.

$$\begin{cases} \dfrac{d\Delta x_{diff}}{dt} = A\Delta x_{diff} + B\Delta u \\ \Delta y = C\Delta x_{diff} + D\Delta u \\ \Delta x_{diff} \in \mathbb{R}^{N_{diff}}, \Delta u \in \mathbb{R}^{p}, \Delta y \in \mathbb{R}^{q} \end{cases} \tag{1.10}$$

To simplify, this system is written as in (1.11). The system is now a simple Linear Time Invariant (LTI) system represented in state-space.

$$\begin{cases} \dfrac{dx}{dt} = Ax + Bu \\ y = Cx + Du \\ x \in \mathbb{R}^{N_{diff}}, u \in \mathbb{R}^{p}, y \in \mathbb{R}^{q} \end{cases} \tag{1.11}$$

The poles of this LTI system are defined as the eigenvalues of the state matrix A. The set of the eigenvalues of A is noted σ_A and is called its spectrum. The eigenvalues of A are the roots of the characteristic polynomial of A, as presented in (1.12).

$$\lambda_i \in \sigma_A \Leftrightarrow det(A - \lambda_i I_{n_{diff}}) = 0 \tag{1.12}$$

A LTI system is exponentially stable if the real part of all its poles are strictly negative. This is explained in (1.13).

$$\text{The system is exponentially stable} \Leftrightarrow \forall \lambda_i \in \sigma_A, Re(\lambda_i) < 0 \tag{1.13}$$

An operating point of a non-linear system is stable if the corresponding linearised system at this operating point is stable.

To illustrate it, ten poles are considered in Figure 1.5. The poles that are on the left side of the imaginary axis of the complex plane are stable. The one that are on the right side are unstable.

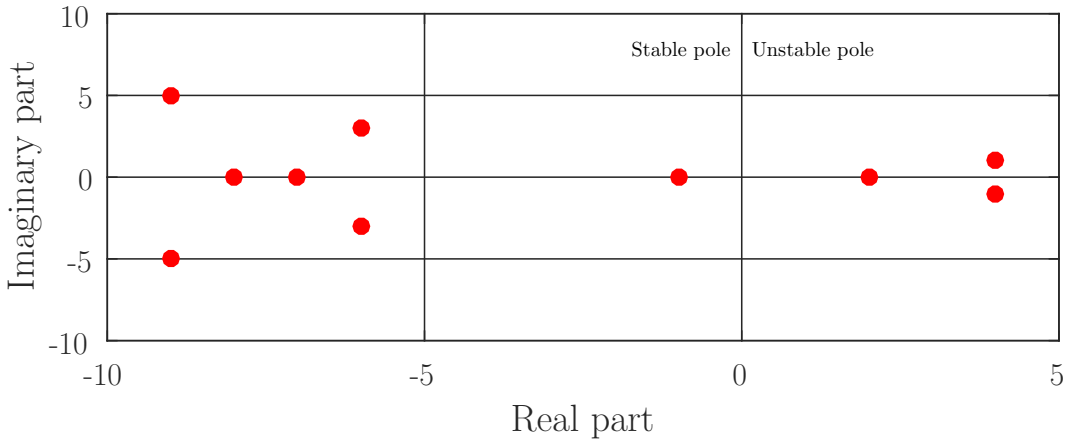

Figure 1.5: Example of stable and unstable poles

The analysis of the stability of the poles of the linearised system is what is called the small-signal stability analysis. This analysis is still relevant with a high PE penetration and is applied on several test cases in chapter 4.

One can note that a limit to the small-signal stability analysis is that it is only valid when the system is close to its operating point (small-signal). Moreover, it doesn't take into account the non-linearities of the system that can have an impact on the stability. To cope with that, nonlinear stability analyses using Lyapunov functions can be used. But there is no systematic method to find the Lyapunov function which makes it difficult to apply in such complex systems like power systems. This is why the focus of the report is on small-signal stability analysis.

Sensitivity analysis

The second presented tool is called sensitivity analysis. It is based on the small-signal stability analysis presented previously.

A pole λ_i of the A matrix is considered. If this pole is unstable or at risk of becoming unstable (close to the imaginary axis), it is interesting to know which parameters of the model influence the most this pole. Knowing this, it might be possible to change a parameter (the tuning of some PI controllers for instance) in order to stabilize this pole or improve the performance of the system [27].

The sensitivity $s_{r_{i,j}}$ of the real part of the eigenvalue λ_i with respect to the parameter p_j is defined in (1.14).

$$s_{r_{i,j}} = \frac{\partial Re(\lambda_i)}{\partial p_j} \tag{1.14}$$

The sensitivity gives the evolution of the considered eigenvalue when the considered parameter changes. If it is positive, the real part of the eigenvalue increase when the parameter increase. If it is negative, the real part of the eigenvalue decrease when the parameter increase.

As a consequence, if $s_{r_{i,j}}$ is positive, it means that p_j must decrease to stabilize the pole. If it is negative, it means that it must increase to stabilize the pole.

One can remark that the sensitivity depends on the unit and the value of each parameter. It is thus arduous to compare the sensitivities of an eigenvalues with respect to different parameters of different values and unit.

This tool is very important for the tuning of the controllers of the converters in a transmission system with a large PE penetration. It helps tuning the controllers to obtain a stable power system.

Participation factors

The last presented tool are the participation factors.

The eigenvalues of A, that are defined in (1.12) can also be defined as in (1.15).

$$\lambda_i \in \sigma_A \Leftrightarrow \exists y_i \in \mathbb{R}^{N_{diff}} / Ay_i = \lambda_i y_i \tag{1.15}$$

In (1.15), y_i is called a right eigenvector of A associated to the eigenvalue λ_i. In the same way, the definition in (1.15) can be rewritten with a left eigenvector as in (1.16).

$$\lambda_i \in \sigma_A \Leftrightarrow \exists u_i \in \mathbb{R}^{N_{diff}} / u_i^T A = \lambda_i u_i^T \tag{1.16}$$

For each eigenvalue, the left and right eigenvectors are not unique. They can be chosen to be normalized, which means that they respect (1.17).

$$\begin{cases} i = j \Rightarrow u_i^T y_j = 1 \\ i \neq j \Rightarrow u_i^T y_j = 0 \end{cases} \tag{1.17}$$

The participation factors are a linear algebra tool introduced in [28]. They have been constantly used since in the power system community [29–31] and for MOR [32]. More generally, their meaning and how they can be used for the analysis of dynamical systems is also still discussed today [33–35].

They give the links between the eigenvalues of a linear system and its state variables. More precisely, the participation factor $p_{k,i}$ is a complex number whose modulus gives the participation of the state x_k in the eigenvalue λ_i (and vice-versa). It tells how much this state variables influences the considered pole. It is calculated as in (1.18).

$$p_{k,i} = u_i(k)y_i(k) \tag{1.18}$$

In this equation, $u_i(k)$ is the k^{th} entry of the left eigenvector of A associated to λ_i and $y_i(k)$ is the k^{th} entry of the right eigenvector of A associated to λ_i.

If the left and right eigenvectors of A are normalized, the sum of the participation factors of a state in all the eigenvalues is equal to 1 and the sum of all the participation factors of all the states in one eigenvalue is equal to 1 (note that this is not true when the modulus are summed). This allows comparing the degree of participation of each state in an eigenvalue (and vice-versa).

The participation factors helps identifying which state variables are critical for the stability. They are the states that participate the most in the unstable poles or the poles at risk of becoming unstable.

To better understand the physical meaning of the participation factors, consider the simple LTI system in (1.19).

$$\begin{cases} \dfrac{dx}{dt} = Ax \\ A \in \mathbb{R}^{n \times n} \end{cases} \tag{1.19}$$

The solution of this system is given in (1.20).

$$x(t) = \sum_{i=1}^{n} (u_i^T x(0)) e^{\lambda_i t} y_i \tag{1.20}$$

Consider now the initial conditions $x_k(0) = 1$ and $x_i(0) = 0, \forall i \neq k$. In these conditions, the solution of the system can be rewritten in (1.21).

$$x_k(t) = \sum_{i=1}^{n} p_{k,i} e^{\lambda_i t} \tag{1.21}$$

This equation clearly shows the role played by the participation factors. They link the state variables to the the poles of the system.

In this thesis, the participation factors are used for the development of MOR methods in chapter 3.

1.1.3 Conclusion

In this section, several simulation and linear analysis tools, that can be used to study transmission systems with a high PE penetration, have been presented: the phasor approximation and the Transient Stability Programs, the Electromagnetic Transients Programs, the dynamic phasors, the small-signal stability analysis, the sensitivity analysis and the participation factors.

As seen in this section, the EMT programs can lead to a too high computation time and a too complex analysis when applied to large transmission systems, and the phasor approximation might not be applicable when there are a lot of PE devices. However, to

study and simulate large systems, like it is the case in this report, simplifications and approximations, just like the phasor approximation, are needed. These simplifications are called Model Order Reduction (MOR) in the literature. This is why the focus of the next section is on MOR. The aim is to list the existing methods and assess if they are adapted to the study of power systems with a large PE penetration and thus to simplify an EMT model. And if not, what are the alternatives.

1.2 Model order reduction

A MOR is a process that finds a model with an output that is close to the output of the initial model (in other words, the error has to be bounded) but of reduced order. For example, consider a nonlinear DAE system in (1.22).

$$\begin{cases} \dfrac{dx_{diff}}{dt} = f(x_{diff}, x_{alg}, u) \\ \quad 0 = g(x_{diff}, x_{alg}, u) \\ \quad y = h(x_{diff}, x_{alg}, u) \\ x_{diff} \in \mathbb{R}^{N_{diff}}, x_{alg} \in \mathbb{R}^{N_{alg}}, u \in \mathbb{R}^p, y \in \mathbb{R}^q \end{cases} \tag{1.22}$$

A second nonlinear DAE system is considered in (1.23).

$$\begin{cases} \dfrac{dx_{diff_r}}{dt} = f_r(x_{diff_r}, x_{alg_r}, u) \\ \quad 0 = g_r(x_{diff_r}, x_{alg_r}, u) \\ \quad y_r = h_r(x_{diff_r}, x_{alg_r}, u) \\ x_{diff_r} \in \mathbb{R}^{N_{diff_r}}, x_{alg_r} \in \mathbb{R}^{N_{alg_r}}, u \in \mathbb{R}^p, y_r \in \mathbb{R}^q \end{cases} \tag{1.23}$$

The system in (1.23) is a reduction of the system in (1.22) if the equation (1.24) is respected, for a given accepted error ϵ.

$$\begin{cases} ||y - y_r|| < \epsilon \\ \quad N_{diff_r} << N_{diff} \end{cases} \tag{1.24}$$

The principle of MOR is to find the smallest reduced model like (1.23) for a given reference model like (1.22) and for a given accepted error. It results in a system that gives approximately the same results but that is faster to simulate and easier to analyse as it has a reduced number of state variables.

This section presents the most used MOR methods: the modal truncation, the balanced truncation, the Proper Orthogonal Decomposition (POD) and the Krylov methods. The first three methods are called Singular Value Decomposition (SVD) methods as they are based on the SVD of matrices. They are illustrated in this chapter with a small order 4 example. For each method, the idea is to assess whether it is relevant for the MOR of transmission systems with a high PE penetration.

1.2.1 Modal truncation

The first method to be presented is called modal truncation [36]. Although not new [37], it is today a widely used method in the power system community [38,39] as it is quite easy to apply it and it preserves some physical dynamics of the system, which is what is looked for in this work. It is indeed based on the preservation of some poles of the system and the suppression of others. Because it preserves the poles of the system, it ensures that the operating point remains stable: no pole is moved during the MOR.

As illustration, the method is applied on the LTI system in (1.25).

$$\begin{cases} \dfrac{dx}{dt} = Ax + Bu \\ y = Cx + Du \\ x \in \mathbb{R}^{N_{diff}}, u \in \mathbb{R}^p, y \in \mathbb{R}^q \end{cases} \tag{1.25}$$

One can remark that this method can be used only with linear systems.

Eigenvalue decomposition and basis change

First, the Eigenvalue Decomposition (EVD) of A [40] is done using a matrix P that can easily be found using the eigenvectors of A (see Appendix for more explanation). This decomposition is presented in (1.26).

$$A = P^{-1}\Lambda P = P^{-1} diag(\lambda_i) P \tag{1.26}$$

By writing $x_m = Px$, $B_m = PB$, $C_m = CP^{-1}$, the system can be rewritten in (1.27). For now, no approximation has been made. The system is just written in a different basis.

$$\begin{cases} \dfrac{dx_m}{dt} = \Lambda x_m + B_m u \\ y = C_m x_m + Du \\ x_m \in \mathbb{R}^{N_{diff}}, u \in \mathbb{R}^p, y \in \mathbb{R}^q \end{cases} \tag{1.27}$$

Fast poles/Slow poles

The system is organized as follows in (1.28). In this equations, Λ_1 contains the poles to keep and Λ_2 the poles to discard. In general, the slowest poles are kept and the fastest are discarded. In other word, the poles that are the closest to the imaginary axis (with a real part close to 0) are kept, and the one that are far from it (large negative real part) are discarded.

$$\begin{cases} \dfrac{d}{dt}\begin{pmatrix} x_{m_1} \\ x_{m_2} \end{pmatrix} = \begin{pmatrix} \Lambda_1 & 0 \\ 0 & \Lambda_2 \end{pmatrix}\begin{pmatrix} x_{m_1} \\ x_{m_2} \end{pmatrix} + \begin{pmatrix} B_{m_1} \\ B_{m_2} \end{pmatrix} u \\ y = \begin{pmatrix} C_{m_1} & C_{m_2} \end{pmatrix}\begin{pmatrix} x_{m_1} \\ x_{m_2} \end{pmatrix} + Du \\ x_{m_1} \in \mathbb{R}^{N_{diff_1}}, x_{m_2} \in \mathbb{R}^{N_{diff_2}}, u \in \mathbb{R}^p, y \in \mathbb{R}^q \end{cases} \tag{1.28}$$

The choice of N_{diff_1} determines the size of the reduced model.

In the next two parts, the modal truncation is explained in two different representations: in the state-space representation first and then in the Laplace representation. One can notice that this is the same approximation in both cases.

Modal truncation in state-space representation

The modal truncation consists in truncating the model in (1.28) and keeping only x_{m_1}. It gives the following reduced model in (1.29)

$$\begin{cases} \dfrac{dx_{m_{1_r}}}{dt} = \Lambda_1 x_{m_{1_r}} + B_{m_1} u \\ y_r = C_{m_1} x_{m_{1_r}} + Du \\ x_{m_{1_r}} \in \mathbb{R}^{N_{diff_1}}, u \in \mathbb{R}^p, y_r \in \mathbb{R}^q \end{cases} \tag{1.29}$$

The aim is to have the smallest N_{diff_1} while still having a good accuracy (error lower than the chosen maximum accepted error ϵ).

The poles of the obtained reduced models are Λ_1 which are also poles of the initial full model. The poles in Λ_2 are deleted with this reduction.

However, the state variables are not the same any more between the full and the reduced model because of the basis change and the truncation. As a result, this might complicate the analysis. It is indeed for example more complicated to identify the critical variables in the reduced model using the participation factors as these variables have changed during the process. As a consequence, the structure of the model is not preserved.

Modal truncation in Laplace representation

Consider the system in (1.27) and apply the Laplace transform to it. The transfer function of the system can be written as in (1.30).

$$Y(s) = (C_m(I_{N_{diff}} s - \Lambda)^{-1} B_m + D)U(s) = F(s)U(s) \tag{1.30}$$

The transfer function F can be decomposed in (1.31) using partial fraction decomposition [40]. In this equation R_i is called residue and can be calculated using the eigenvectors of A. One can remark that the eigenvalues here are all taken separately, even the complex ones, that all have their conjugate among the other eigenvalues.

$$F(s) = \sum_{i=1}^{N_{diff}} \frac{R_i}{s - \lambda_i} + D \tag{1.31}$$

The reduced model obtained by modal truncation is written in (1.32). It is the same model as in (1.29) but represented in the Laplace domain.

$$F_r(s) = \sum_{i=1}^{N_{diff_1}} \frac{R_i}{s - \lambda_i} + D \tag{1.32}$$

Error

By subtracting (1.32) to (1.31), an error is obtained in (1.33).

$$F(s) - F_r(s) = \sum_{i=N_{diff_1}+1}^{N_{diff}} \frac{R_i}{s - \lambda_i} \tag{1.33}$$

One advantage of this method is that the error is bounded, as shown in (1.34). This guarantees the accuracy of the reduced model.

$$||F - F_r|| \leq \sum_{i=N_{diff_1}+1}^{N_{diff}} \frac{||R_i||}{|Re\lambda_i|} \tag{1.34}$$

Illustration with an order 4 model

To illustrate the method, the order 4 LTI model in 1.35 is considered.

$$\begin{cases} \dfrac{dx}{dt} = Ax + Bu = \begin{pmatrix} -50 & -25 & 5 & 1 \\ -10 & -20 & 1 & 1 \\ 5 & 1 & -10 & -10 \\ 10 & 1 & 10 & -10 \end{pmatrix} x + \begin{pmatrix} 1 \\ 1 \\ 1 \\ 1 \end{pmatrix} u \\ y = \begin{pmatrix} 0 & 0 & 0 & 0 \\ 0 & 1 & 0 & 0 \\ 0 & 0 & 0 & 0 \\ 0 & 0 & 0 & 0 \end{pmatrix} x \end{cases} \tag{1.35}$$

The EVD of A is done and the system is expressed in the modal basis in 1.36.

$$\begin{cases} \dfrac{dx_m}{dt} = \begin{pmatrix} -9.4 + 10.5i & 0 & 0 & 0 \\ 0 & -9.4 - 10.5i & 0 & 0 \\ 0 & 0 & -13.4 & 0 \\ 0 & 0 & & -57.8 \end{pmatrix} x_m + \begin{pmatrix} 0.9 - 0.6i \\ 0.9 + 0.6i \\ 0.9 \\ -1.3 \end{pmatrix} u \\ y = \begin{pmatrix} 0 & 0 & 0 & 0 \\ 0.006 - 0.028i & 0.006 + 0.028i & 0.779 & -0.257 \\ 0 & 0 & 0 & 0 \\ 0 & 0 & 0 & 0 \end{pmatrix} x_m \end{cases} \tag{1.36}$$

The reduced system is then obtained by truncating this system. An example is given for an order 2 reduced model in 1.37

$$\begin{cases} \dfrac{dx_{m_r}}{dt} = \begin{pmatrix} -9.4 + 10.5i & 0 \\ 0 & -9.4 - 10.5i \end{pmatrix} x_{m_r} + \begin{pmatrix} 0.9 - 0.6i \\ 0.9 + 0.6i \end{pmatrix} u \\ y_r = \begin{pmatrix} 0 & 0 \\ 0.006 - 0.028i & 0.006 + 0.028i \\ 0 & 0 \\ 0 & 0 \end{pmatrix} x_{m_r} \end{cases} \tag{1.37}$$

One can remark that the system is completely different from the initial one. The matrices describing it are now complex and not real any more.

1.2.2 Balanced truncation and singular perturbation approximation

The method presented here is called balanced truncation. It was introduced in 1981 in [41]. It has been widely used since, in different fields, including power systems [42]. Various versions of this method exist [43] but they are all based on the same principles, which are presented here.

A similar method, the singular perturbation approximation, was introduced in [44]. It is also presented here.

The system to reduce is an LTI system in (1.38). Like the modal truncation, the balanced truncation can only be applied on linear systems.

$$\begin{cases} \dfrac{dx}{dt} = Ax + Bu \\ \quad y = Cx + Du \\ \quad x \in \mathbb{R}^{N_{diff}}, u \in \mathbb{R}^p, y \in \mathbb{R}^q \end{cases} \tag{1.38}$$

The reachability and observability Gramians

The first step of the method is to define the reachability Gramian P and the observability Gramian Q in (1.39).

$$\begin{cases} P = \displaystyle\int_0^{+\infty} e^{At} B B^T e^{A^T t} dt \\ Q = \displaystyle\int_0^{+\infty} e^{A^T t} C^T C e^{At} dt \end{cases} \tag{1.39}$$

They can be calculated by solving the following Lyapunov equations in (1.40), of which they are solutions.

$$\begin{cases} AP + PA^T + BB^T = 0 \\ A^T Q + QA + C^T C = 0 \end{cases} \tag{1.40}$$

Consider the system expressed in another basis b in (1.41).

$$\begin{cases} \dfrac{dx_b}{dt} = A_b x_b + B_b u \\ \quad y = C_b x_b + Du \end{cases} \tag{1.41}$$

The variables and matrices in this new basis are calculated using the T_b matrix as in (1.42).

$$\begin{cases} x_b = T_b x \\ A_b = T_b A T_b^{-1} \\ B_b = T_b B \\ C_b = C T_b^{-1} \end{cases} \tag{1.42}$$

The Gramian in the new basis are then expressed as follows in (1.43). They change when the basis changes.

$$\begin{cases} P_b = T_b P T_b^T \\ Q_b = T_b^{-T} Q T_b^{-1} \end{cases} \tag{1.43}$$

Hankel Singular Values

The Hankel Singular Values (HSV) are defined as the square root of the eigenvalues of the product PQ and written σ_i like in (1.44).

$$\sigma_i = \sqrt{\lambda_i(PQ)} \tag{1.44}$$

One can remark that in the basis b, the HSV do not change, as explained in (1.45).

$$\begin{cases} \sigma_{i_b} = \sqrt{\lambda_i(P_b Q_b)} \\ \quad = \sqrt{\lambda_i(T_b P T_b^T T_b^{-T} Q T_b^{-1})} \\ \quad = \sqrt{\lambda_i(T_b P Q T_b^{-1})} \\ \quad = \sqrt{\lambda_i(PQ)} \\ \quad = \sigma_i \end{cases} \tag{1.45}$$

The fact that the HSV don't change when the basis changes is very important. It means that they are an inherent characteristic of the system.

Balancing transformation

Consider an upper triangular matrix U and a lower triangular matrix L so that $P = UU^T$ and $Q = LL^T$.

An SVD decomposition of the product $U^T L$ is made in (1.46).

$$U^T L = Z \Sigma Y^T \tag{1.46}$$

The balancing transformation T_b is then defined in (1.47).

$$T_b = \Sigma^{\frac{1}{2}} Z^T U^{-1} \tag{1.47}$$

It has been proven that in the new basis b, the Gramians are equal and diagonal, as in (1.48). And the diagonal contains the HSV of the system.

$$P_b = Q_b = diag(\sigma_i) \tag{1.48}$$

The way the system is expressed in the new basis is called a balanced realization. The other way in (1.38) is called a physical realization in this report.

Most reachable and observable states

In these conditions, a HSV σ_i is associated to each state in the balanced realization x_{b_i}. It is a positive real which gives the degree of reachability and observability of this state. The bigger it is, the more reachable and observable the considered state is.

The system is rearranged so that x_{b_1} is the most observable and reachable state (biggest HSV) and $x_{b_{N_{diff}}}$ the less observable and reachable state (lowest HSV).

In these conditions, the model can be expressed as in (1.49). In this model x_{b_1} contains the most observable and reachable states.

$$\begin{cases} \dfrac{d}{dt}\begin{pmatrix} x_{b_1} \\ x_{b_2} \end{pmatrix} = \begin{pmatrix} A_{b_{11}} & A_{b_{12}} \\ A_{b_{21}} & A_{b_{22}} \end{pmatrix}\begin{pmatrix} x_{b_1} \\ x_{b_2} \end{pmatrix} + \begin{pmatrix} B_{b_1} \\ B_{b_2} \end{pmatrix} u \\ y = \begin{pmatrix} C_{b_1} & C_{b_2} \end{pmatrix}\begin{pmatrix} x_{b_1} \\ x_{b_2} \end{pmatrix} + Du \\ x_{b_1} \in \mathbb{R}^{N_{diff_1}}, x_{b_2} \in \mathbb{R}^{N_{diff_2}}, u \in \mathbb{R}^p, y \in \mathbb{R}^q \end{cases} \tag{1.49}$$

Balanced truncation

The balanced truncation consists in truncating the model in (1.49) and keeping only the most observable and reachable states x_{b_1}. This leads to the reduced model in (1.50).

$$\begin{cases} \dfrac{dx_r}{dt} = A_{b_{11}} x_r + B_{b_1} u \\ y_r = C_{b_1} x_r + Du \end{cases} \tag{1.50}$$

Singular perturbation approximation

The singular perturbation approximation consists in transforming the less observable and reachable states x_{b_2} into a singular perturbation by replacing their derivative part by 0. This gives the reduced model in (1.51).

$$\begin{cases} \begin{pmatrix} \frac{dx_r}{dt} \\ 0 \end{pmatrix} = \begin{pmatrix} A_{b_{11}} & A_{b_{12}} \\ A_{b_{21}} & A_{b_{22}} \end{pmatrix}\begin{pmatrix} x_r \\ x_{b_2} \end{pmatrix} + \begin{pmatrix} B_{b_1} \\ B_{b_2} \end{pmatrix} u \\ y_r = \begin{pmatrix} C_{b_1} & C_{b_2} \end{pmatrix}\begin{pmatrix} x_r \\ x_{b_2} \end{pmatrix} + Du \\ x_r \in \mathbb{R}^{N_{diff_1}}, x_{b_2} \in \mathbb{R}^{N_{diff_2}}, u \in \mathbb{R}^p, y \in \mathbb{R}^q \end{cases} \tag{1.51}$$

By injecting the algebraic equations of x_{b_2} into the differential equations of x_r, the model in (1.52) is obtained.

$$\begin{cases} \dfrac{dx_r}{dt} = (A_{b_{11}} - A_{b_{12}}A_{b_{22}}^{-1}A_{b_{21}})x_r + (B_{b_1} - A_{b_{12}}A_{b_{22}}^{-1}B_{b_2})u \\ y_r = (C_{b_1} - C_{b_2}A_{b_{22}}^{-1}A_{b_{21}})x_r + (D - C_{b_2}A_{b_{22}}^{-1}B_{b_2})u \end{cases} \tag{1.52}$$

While the balanced truncation provides a reduced-order system which approximates the original well at high frequencies, the singular perturbation approximation provides a good approximation at low frequencies [45].

Error

Both the balanced truncation and the singular perturbation approximation have a bounded error, which is explained in (1.53). In this equation, the reduced system is supposed to be of order k, that is with the k most observable and reachable states.

$$||Y(s) - Y_r(s)|| \leq 2(\sigma_{k+1} + \sigma_{k+2} + ... + \sigma_{N_{diff}-1} + \sigma_{N_{diff}}) \tag{1.53}$$

Moreover both methods guarantee a stability preservation [46]. It means that if the full model is stable then the reduced model is stable as well.

Illustration with an order 4 model

To illustrate the method, the order 4 LTI model in 1.54 is considered.

$$\begin{cases} \dfrac{dx}{dt} = Ax + Bu = \begin{pmatrix} -50 & -25 & 5 & 1 \\ -10 & -20 & 1 & 1 \\ 5 & 1 & -10 & -10 \\ 10 & 1 & 10 & -10 \end{pmatrix} x + \begin{pmatrix} 1 \\ 1 \\ 1 \\ 1 \end{pmatrix} u \\ y = \begin{pmatrix} 0 & 0 & 0 & 0 \\ 0 & 1 & 0 & 0 \\ 0 & 0 & 0 & 0 \\ 0 & 0 & 0 & 0 \end{pmatrix} x \end{cases} \tag{1.54}$$

The HSV of the systems are computed and the balanced truncation is done for a desired size of 2 (In chapter 3, when describing the second strategy, more details are given on how to compute the balanced realization). The obtained reduced model by balanced truncation is given in 1.55.

$$\begin{cases} \dfrac{dx_{m_r}}{dt} = \begin{pmatrix} -11.64 & 9.19 \\ -23.21 & -144.8 \end{pmatrix} x_{m_r} + \begin{pmatrix} 0.8215 \\ -0.9359 \end{pmatrix} u \\ y_r = \begin{pmatrix} 0 & 0 \\ 0.8701 & -0.5459 \\ 0 & 0 \\ 0 & 0 \end{pmatrix} x_{m_r} \end{cases} \tag{1.55}$$

Again, a projection and a basis change have been done and the reduced model is not physical any more, which complicates the analysis.

1.2.3 Proper orthogonal decomposition

The method presented in this subsection is called Proper Orthogonal Decomposition (POD) [47]. It has mainly been used for fluid mechanics [48]. Then the method gained some interest in electrical engineering, more precisely in magnetics [49] and to study semiconductors [50]. In the power system community, the method has been little used [51].

To start with, a nonlinear Ordinary Differential Equation (ODE) model is considered in (1.56).

$$\begin{cases} \dfrac{dx}{dt} = f(x,u) \\ \quad y = g(x,u) \\ \quad x \in \mathbb{R}^N, u \in \mathbb{R}^p, y \in \mathbb{R}^q \end{cases} \tag{1.56}$$

One can remark that unlike the two previous MOR methods, the POD can be applied to nonlinear models.

Snapshots matrix, eigenvalue decomposition and approximation

The first step of the method is to collect snapshots from a simulation of the full model or an experimentation. This gives the X matrix in (1.57).

$$X = \begin{pmatrix} x_1(t_1) & \dots & x_1(t_{N_{time}}) \\ \vdots & \ddots & \vdots \\ x_N(t_1) & \dots & x_N(t_{N_{time}}) \end{pmatrix} \tag{1.57}$$

In this matrix the number of time steps N_{time} should be way larger than the number of variables N.

An EVD of the matrix XX^T is performed in (1.58).

$$\begin{cases} XX^T = U\Sigma V \\ XX^T \in \mathbb{R}^{N\times N}, \Sigma \in \mathbb{R}^{N\times N}, U \in \mathbb{R}^{N\times N}, V \in \mathbb{R}^{N\times N} \end{cases} \tag{1.58}$$

In this equation, Σ is diagonal and contains the eigenvalues of XX^T. They correspond to the square of the singular values of X.

The equation (1.58) is reorganised in (1.59) so that σ_1 is the largest eigenvalue of XX^T and σ_N the smallest. In this equation, $\Sigma_k = diag(\sigma_1, ..., \sigma_k)$ contains the k largest eigenvalues of XX^T.

$$\begin{cases} XX^T = \begin{pmatrix} U_k & U_{rest} \end{pmatrix} \begin{pmatrix} \Sigma_k & 0 \\ 0 & \Sigma_{rest} \end{pmatrix} \begin{pmatrix} V_k \\ V_{rest} \end{pmatrix} \\ \qquad = U_k\Sigma_k V_k + U_{rest}\Sigma_{rest}V_{rest} \end{cases} \tag{1.59}$$

The matrix XX^T can be approximated in (1.60).

$$XX^T \approx U_k \Sigma_k V_k \tag{1.60}$$

Model order reduction

The MOR by POD consists in defining the reduced system in (1.61).

$$\begin{cases} \dfrac{dx_r}{dt} = V_k f(U_k x_r, u) \\ y_r = g(U_k x_r, u) \\ x_r \in \mathbb{R}^k, u \in \mathbb{R}^p, y_r \in \mathbb{R}^q \end{cases} \tag{1.61}$$

Functions f_r and g_r are defined in (1.62).

$$\begin{cases} f_r(x_r, u) = V_k f(U_k x_r, u) \\ g_r(x_r, u) = g(U_k x_r, u) \end{cases} \tag{1.62}$$

This allows writing the new reduced system in (1.63).

$$\begin{cases} \dfrac{dx_r}{dt} = f_r(x_r, u) \\ y_r = g_r(x_r, u) \\ x_r \in \mathbb{R}^k, u \in \mathbb{R}^p, y_r \in \mathbb{R}^q \end{cases} \tag{1.63}$$

The smaller k is, the more reduced the model is. To choose k, the decay of the eigenvalues of XX^T must be looked at. For instance, consider that the ten eigenvalues represented in Figure 1.6 are the eigenvalues of XX^T. This figure shows that a good choice for k could be 3 or 6 because of the way the eigenvalues decrease.

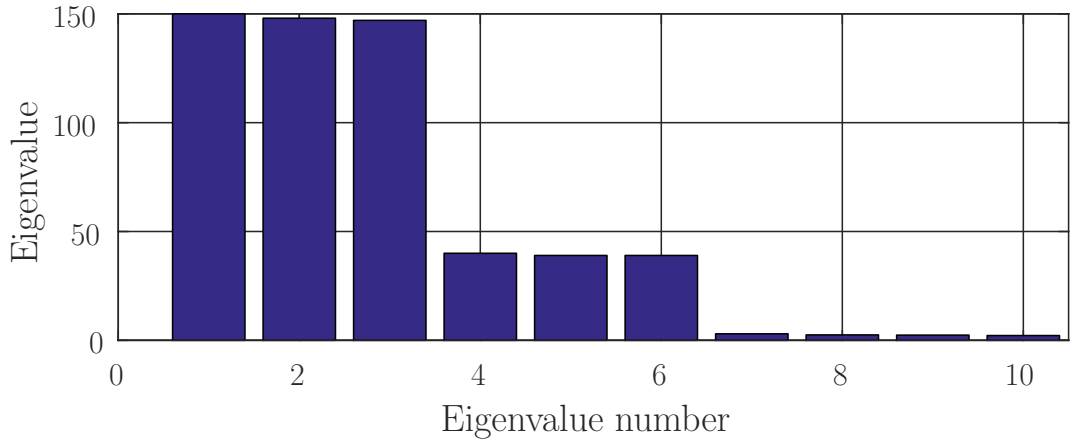

Figure 1.6: Examples of eigenvalues of XX^T

Remarks on the method

Unlike the modal truncation and the balanced truncation, the POD does not guarantee the stability preservation.

Moreover, as it is based on a snapshots matrix resulting from a specific simulation test case or experimentation, the reduced model obtained with a POD is only valid for this particular simulation. If the test case is not the same (a change in the simulated event for instance), the POD has to be done again. This makes this method not very flexible.

Finally, the induced error is not bounded a priori. There is not known maximum value for the error like it is the case for the modal truncation or the balanced truncation and the singular perturbation approximation.

Illustration with an order 4 model

To illustrate the method, the order 4 LTI model in 1.64 is considered.

$$\begin{cases} \dfrac{dx}{dt} = Ax + Bu = \begin{pmatrix} -50 & -25 & 5 & 1 \\ -10 & -20 & 1 & 1 \\ 5 & 1 & -10 & -10 \\ 10 & 1 & 10 & -10 \end{pmatrix} x + \begin{pmatrix} 1 \\ 1 \\ 1 \\ 1 \end{pmatrix} u \\ \quad y = \begin{pmatrix} 0 & 0 & 0 & 0 \\ 0 & 1 & 0 & 0 \\ 0 & 0 & 0 & 0 \\ 0 & 0 & 0 & 0 \end{pmatrix} x \end{cases} \tag{1.64}$$

The system is first simulated with a step in the input u. A snapshot matrix X is created and U_2 and V_2 are computed (an order 2 model is looked for). The reduced model is then given in 1.65.

$$\begin{cases} \dfrac{dx_{m_r}}{dt} = \begin{pmatrix} -20 & -10 \\ -25 & -50 \end{pmatrix} x_{m_r} + \begin{pmatrix} 1 \\ 1 \end{pmatrix} u \\ \quad y_r = \begin{pmatrix} 0 & 0 \\ 1 & 0 \\ 0 & 0 \\ 0 & 0 \end{pmatrix} x_{m_r} \end{cases} \tag{1.65}$$

1.2.4 Krylov methods

The last presented methods are the Krylov methods [52], which are also referred to as the moment matching methods. They were introduced by Freund [53] in several papers and are now widely used in many fields, including power systems [54, 55]. They are briefly described in this subsection.

To begin with, a LTI system is considered in (1.66). To simplify, the system is considered to be Single Input Single Output (SISO) instead of Multiple Inputs Multiple Outputs (MIMO). In other words, $p = 1$ and $q = 1$ here.

$$\begin{cases} \dfrac{dx}{dt} = Ax + Bu \\ \quad y = Cx + Du \\ \quad x \in \mathbb{R}^{N_{diff}}, u \in \mathbb{R}^p, y \in \mathbb{R}^q \end{cases} \tag{1.66}$$

This system is the system to reduce. The moment matching MOR methods are presented in the following.

The Laplace transformation is applied to this system, which gives the following transfer function $F(s)$ in (1.67).

$$Y(s) = (C(I_{N_{diff}}s - A)^{-1}B + D)U(s) = F(s)U(s) \tag{1.67}$$

As the system is SISO, this transfer function is a scalar.

Moment matching

The transfer function $F(s)$ is expanded in a Laurent series around $s_0 \in \mathbb{C}$. This gives (1.68).

$$F(s) = \sum_{n \geq 0} a_n (s - s_0)^n \tag{1.68}$$

In this equation, the a_n are called the moments of F at s_0.

The idea of MOR by moment matching is to find a transfer function F_r whose k first moments at s_0 match the k first moments at s_0 of F, with $k << N_{diff}$. This is summed up in (1.69) and (1.70).

$$F_r(s) = \sum_{n \geq 0} a_{r_n} (s - s_0)^n \tag{1.69}$$

$$\forall n \in \{1, ..., k\},\ a_{r_n} = a_n \tag{1.70}$$

If $s_0 = +\infty$, the moments are called Markov parameters and the process of moment matching is called partial realization.

If $s_0 = 0$ the process of moment matching is called Padé approximation.

If s_0 is an arbitrary complex the process of moment matching is called rational interpolation.

One should notice that the calculation of the moments can be problematic and time-consuming. However, methods exist to find F_r without calculating the moments. One can cite the Arnoldi or the Lanczos procedures that are presented in [45].

Remarks on the methods

Several remarks can be made on the Krylov methods:

- The computation time to obtain the reduced model is faster than for SVD methods like the balanced truncation.
- There is no error bound with these methods [56].
- The stability may not be preserved. The reduced model can be unstable while the full model is stable.

1.2.5 Methods comparison and applicability on transmission systems with a high PE penetration

This section has presented the most used MOR methods, their advantages and their drawbacks. Other methods like the Proper Generalised Decomposition (PGD) [57], the Hankel-norm approximation [58] or the SVD-Krylov methods [59] exist in the literature, but they are less used in power systems than the methods presented here.

Table 1.1 sums up the different characteristics of the presented methods, as well as the desired characteristics of a MOR methods for the case under consideration, i.e. the study of transmission systems with a large PE penetration.

The expected characteristics for a MOR are an applicability on nonlinear models (power systems are indeed nonlinear), a preservation of the physical variables to simplify the analysis and the tuning of new controllers directly on the reduced models, a poles preservation around the operating point to keep the main physical dynamics and guarantee that this operating point remains stable and a knowledge of the error.

It can be seen in this table that none of the classical methods meets these requirements.

	Applicability on nonlinear models	Variables preservation	Poles preservation	Stability preservation	Bounded error
Modal	No	No	Yes	Yes	Yes
Balanced	No	No	No	Yes	Yes
POD	Yes	No	No	No	No
Krylov	No	No	No	No	No
Expected	Yes	Yes	Yes	Yes	Yes

Table 1.1: Comparison of the characteristics of the classical MOR methods

To cope with that, research has been made to obtain adequate MOR methods but none of them is totally satisfying.

[60] generalizes the balanced truncation to nonlinear models but still changes the variables of the system with the change of basis and the truncation.

[61] neglects the second derivative of some state variables to reduce the order of the model. This results in a reduced model that preserves the variables of the system. Moreover, this method tries to keep the poles of the system as much as possible. However, it is only applicable on linear system and there is no guarantee that the given reduced model is the best one for the given size. Some dynamics are indeed neglected based on a time-scale separation, which might not be the best solution, especially with PE (see chapter 4 for some examples).

[62] neglects the first derivative of some variables, based on the same time-scale separation as the previous method. The same remarks apply on this method.

[63] proposes a mix between the modal and the balanced truncation. Yet it doesn't keep the variables of the system as it is still based on a truncation.

[64] mixes a MOR by moment matching with a poles preservation. But as for the other methods, it doesn't keep the variables of the system.

[65] preserves the poles but not the variables as it is based on a truncation.

[66] uses sparse representations, which preserves the variables of the system. However, the stability is not guaranteed.

To sum up, each of the solutions to cope with the drawbacks of the classical MOR methods has its own advantages and drawbacks. The aim of this thesis is to propose new MOR methods that combine as much as possible the advantages of all of them: a preservation of the physical variables and the poles, a guarantee that the operating point remains stable and an applicability on nonlinear models.

1.3 Chapter conclusion

In this chapter, a literature review on the existing tools and methods to simulate and analyse power systems has been made.

The analysis tools, which are the small-signal stability analysis, the sensitivity analysis and the participation factors are used in the rest of this report.

Concerning the simulation tools, the EMT programs are usually used to simulate PE on a local scale, the phasor approximation is usually used to simulate large systems with SM and the dynamic phasors are not suitable here as they induce a multiplication of the variables which makes the analysis more complicated than what is expected. The question is thus to find how to simulate a large system with a high PE penetration.

The idea is to start from the EMT models and make some adequate approximations (like the phasor approximation for SM) to have a simplified model of a transmission system with a high PE penetration. That is why a review of the classical MOR methods has been made in this chapter to find one that could be suitable for the case under consideration. The conclusion is that none of them is because they alter the structure and the variables of the system which is a problem for the analysis. Alternatives have been found in the literature but they are not completely satisfying.

As a consequence, the focus of this thesis is on the development of MOR methods that meet some requirements that are specific to the study of transmission systems with a large PE penetration. These developed methods need to preserve the parameters of the system as well as its variables to simplify the analysis and allow to tune controllers directly on the reduced models. It means that basis changes, truncations and projections are out of concern from now on. Moreover, they need to be applicable on nonlinear models and to preserve some poles of the system around the operating point to ensure that this operating point remains stable and keep some important physical dynamics. Finally they should easily be implemented in the classical DAE solvers (see chapter 4 for more explanations). These new methods are developed using the analysis tools presented in this chapter and they are inspired by the existing MOR methods to keep their advantages and try to get rid of their drawbacks for an application to power systems with a large PE penetration.

CHAPTER 2

Modelling of transmission systems with a high power electronics penetration

Contents

This chapter presents the different models that are used in this report. For each model, its differential and algebraic equations are given, as well as some block diagrams to illustrate them. In all cases, the equations are written in the DQ0 reference frame (the frequency/angle are specified in each case) and in pu (the basis is also specified in each case) to simplify the linear analysis and accelerate the simulation (see Appendix for more explanations). This is possible because all the models are considered as balanced. This hypothesis is made for the sake of simplicity but the developed MOR methods are easily applicable to unbalanced systems, provided that the model describing them is given.

The first section presents the basic elements in a power system: branches, transformers, loads, shunt capacitors and synchronous machines. The second section presents the different models used for PE converters: grid feeding two-level voltage source converter, grid forming converter and Modular Multilevel Converter (MMC). Finally, the third section presents how a complete model is deduced when all these elements are assembled in a transmission system.

2.1 Modelling of the basic elements of a transmission system

In this section, the models that are used for the branches, transformers, loads, shunt capacitors and synchronous machines are presented.

2.1.1 Branches

The modelling of the lines has been a particularly important topic in studying transmission systems [67] and it is still today [68]. Several models exist, from the most complex one to the simplest one. In this thesis, two models are used: a pi-line model and an RL-line model. They are presented in the following.

Pi-line model

The Pi-line model is presented in Figure 2.1. This model takes into account the capacitive effects of the line.

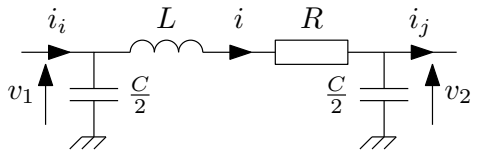

Figure 2.1: Pi-line model

The equations modelling this Pi-line are given in the following in pu and in the DQ0 reference frame of a frequency ω.

$$\frac{L}{\omega_b}\frac{di_d}{dt} = v_{1_d} - v_{2_d} - Ri_d + \omega L i_q \tag{2.1}$$

$$\frac{L}{\omega_b}\frac{di_q}{dt} = v_{1_q} - v_{2_q} - Ri_q - \omega L i_d \tag{2.2}$$

$$\frac{C}{2\omega_b}\frac{dv_{1_d}}{dt} = i_{i_d} - i_d + \omega\frac{C}{2}v_{1_q} \tag{2.3}$$

$$\frac{C}{2\omega_b}\frac{dv_{1_q}}{dt} = i_{i_q} - i_q - \omega\frac{C}{2}v_{1_d} \tag{2.4}$$

$$\frac{C}{2\omega_b}\frac{dv_{2_d}}{dt} = i_d - i_{j_d} + \omega\frac{C}{2}v_{2_q} \tag{2.5}$$

$$\frac{C}{2\omega_b}\frac{dv_{2_q}}{dt} = i_q - i_{j_q} - \omega\frac{C}{2}v_{2_d} \tag{2.6}$$

RL-line model

The RL-line model is presented in Figure 2.2. This model only takes into account the resistance and the inductive effect in the line.

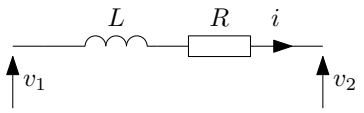

Figure 2.2: RL-line model

The equations modelling this RL-line are given in the following in pu and in the DQ0 reference frame of a frequency ω.

$$\frac{L}{\omega_b}\frac{di_d}{dt} = v_{1_d} - v_{2_d} - Ri_d + \omega L i_q \tag{2.7}$$

$$\frac{L}{\omega_b}\frac{di_q}{dt} = v_{1_q} - v_{2_q} - Ri_q - \omega L i_d \tag{2.8}$$

Summary

Two models of lines have been presented and are used in the following for the simulation. In each case, the dynamics of the line is taken into account (it is not a phasor model). The Pi-line model is more detailed than the RL-line model. In chapter 4, when doing a simulation, it is said which model is used for the lines.

2.1.2 Transformers

As for the lines, the choice of the model for transformers is a very important topic [69]. In this report, a generalized RL-model is used to model them in pu and in the DQ0 reference frame of a frequency ω. A phase shift δ can be taken into account with this model, as well as a change in the transformer ratio r. This model is represented in Figure 2.3.

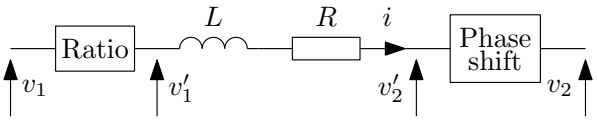

Figure 2.3: Transformer model

The equations corresponding to this model are presented in the following.

$$\frac{L}{\omega_b}\frac{di_d}{dt} = v'_{1_d} - v'_{2_d} - Ri_d + \omega L i_q \tag{2.9}$$

$$\frac{L}{\omega_b}\frac{di_q}{dt} = v'_{1_q} - v'_{2_q} - Ri_q - \omega L i_d \tag{2.10}$$

$$\begin{pmatrix} v'_{1_d} \\ v'_{1_q} \end{pmatrix} = \frac{1}{r}\begin{pmatrix} v_{1_d} \\ v_{1_q} \end{pmatrix} \tag{2.11}$$

$$\begin{pmatrix} v'_{2_d} \\ v'_{2_q} \end{pmatrix} = \begin{pmatrix} cos(\delta) & -sin(\delta) \\ sin(\delta) & cos(\delta) \end{pmatrix}\begin{pmatrix} v_{2_d} \\ v_{2_q} \end{pmatrix} = R(\delta)\begin{pmatrix} v_{2_d} \\ v_{2_q} \end{pmatrix} \tag{2.12}$$

One can note that in nominal conditions $r = 1$ in pu. And if the phase shift is equal to 0, the model of the transformer is a simple RL-line model.

2.1.3 Loads

In this report, the loads are modelled as RL-loads, as shown in Figure 2.4.

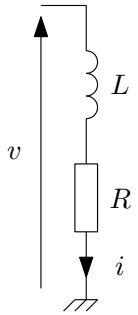

Figure 2.4: Load model

The dynamic equations modelling this load are given in the following in pu and in the DQ0 reference frame of a frequency ω.

$$\frac{L}{\omega_b}\frac{di_d}{dt} = v_d - Ri_d + \omega L i_q \tag{2.13}$$

$$\frac{L}{\omega_b}\frac{di_q}{dt} = v_q - Ri_q - \omega L i_d \tag{2.14}$$

If the active and reactive power consumed by a load in steady state are known, the resistance and inductance modelling it can be calculated so that the powers consumed by the equivalent RL model match the powers actually consumed by the load.

2.1.4 Shunt capacitors

In transmission systems there can be shunt capacitors that are put to help maintaining the voltage at a certain level. In this report, they are modelled as simple capacitors, as shown in Figure 2.5.

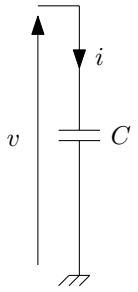

Figure 2.5: Shunt capacitor model

The equations modelling this shunt capacitor are given in the following in pu and in the DQ0 reference frame of a frequency ω.

$$\frac{C}{\omega_b}\frac{dv_d}{dt} = i_d + \omega C v_q \tag{2.15}$$

$$\frac{C}{\omega_b}\frac{dv_q}{dt} = i_q - \omega C v_d \tag{2.16}$$

2.1.5 Synchronous machines

In one test case in chapter 4, there is a PE converter but also one SM to study the interactions between the two. This is why a good synchronous machine model is needed. It is presented here and is taken from [11]. In this model, the equations are given in pu and in the reference frame of a frequency ω, the frequency of the SM rotor.

The general structure, detailed hereafter, is given in Figure 2.6. It is made of the machine itself, an RL line modelling a transformer and a control. Each part is detailed in the following.

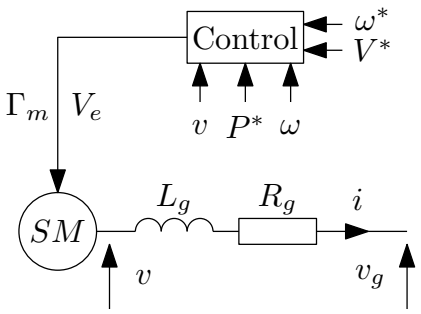

Figure 2.6: Structure of the synchronous machine and its control

Modelling of the machine

The equations modelling the physical part of the SM are given here. The first six equations model the dynamics of the fluxes in the SM.

$$\frac{1}{\omega_b}\frac{d\phi_d}{dt} = v_d + R_s i_d + \omega\phi_q \tag{2.17}$$

$$\frac{1}{\omega_b}\frac{d\phi_q}{dt} = v_q + R_s i_q - \omega\phi_d \tag{2.18}$$

$$\frac{1}{\omega_b}\frac{d\phi_{f_d}}{dt} = V_e - R_f i_{f_d} \tag{2.19}$$

$$\frac{1}{\omega_b}\frac{d\phi_{1_d}}{dt} = -R_{1_d} i_{1_d} \tag{2.20}$$

$$\frac{1}{\omega_b}\frac{d\phi_{1_q}}{dt} = -R_{1_q} i_{1_q} \tag{2.21}$$

$$\frac{1}{\omega_b}\frac{d\phi_{2_q}}{dt} = -R_{2_q} i_{2_q} \tag{2.22}$$

The following six equations model the calculation of the fluxes in the SM.

$$\phi_d = -L_d i_d + L_{a_d} i_{f_d} + L_{a_d} i_{1_d} \tag{2.23}$$

$$\phi_q = -L_q i_q + L_{a_q} i_{1_q} + L_{a_q} i_{2_q} \tag{2.24}$$

$$\phi_{f_d} = -L_{a_d} i_d + L_{f_d} i_{f_d} + L_{a_d} i_{1_d} \tag{2.25}$$

$$\phi_{1_d} = -L_{a_d} i_d + L_{a_d} i_{f_d} + L_{1_d} i_{1_d} \tag{2.26}$$

$$\phi_{1_q} = -L_{a_q} i_q + L_{1_q} i_{1_q} + L_{a_q} i_{2_q} \tag{2.27}$$

$$\phi_{2_q} = -L_{a_q} i_q + L_{a_q} i_{1_q} + L_{2_q} i_{2_q} \tag{2.28}$$

The following equation models the calculation of the electric torque.

$$\Gamma_e = \phi_d i_q - \phi_q i_d \tag{2.29}$$

The hereafter two equations model the RL line that connects the SM to the grid.

$$\frac{L_g}{\omega_b} \frac{di_d}{dt} = v_d - v_{g_d} - R_g i_d + \omega L_g i_q \tag{2.30}$$

$$\frac{L_g}{\omega_b} \frac{di_q}{dt} = v_q - v_{g_q} - R_g i_q - \omega L_g i_d \tag{2.31}$$

Finally, the last two equations model the mechanical dynamics of the SM.

$$2J \frac{d\omega}{dt} = \Gamma_m - \Gamma_e - k_d(\omega - \omega_g) \tag{2.32}$$

$$\frac{1}{\omega_b} \frac{d\delta}{dt} = \omega - \omega_g \tag{2.33}$$

Modelling of the control

The first six equations model the frequency control of the SM. It uses a droop control.

$$m_d \Delta P^* = \omega^* - \omega \tag{2.34}$$

$$T_d \frac{d\Delta P_d}{dt} = \Delta P^* - \Delta P_d \tag{2.35}$$

$$T_{se} \frac{d\Delta P_s}{dt} = P^* - \Delta P_s - \Delta P_d \tag{2.36}$$

$$T_{ac} \frac{d\Delta P_a}{dt} = \Delta P_s - \Delta P_a \tag{2.37}$$

$$T_1 \frac{d\Delta P_a}{dt} + \Delta P_a = T_2 \frac{d\Gamma_m}{dt} + \Gamma_m \tag{2.38}$$

These equations are summed up in the block diagram in Figure 2.7.

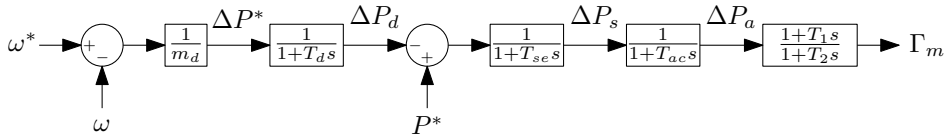

Figure 2.7: Structure of the frequency control of the synchronous machine

The following equations model the voltage control of the SM.

$$V = \sqrt{v_d^2 + v_q^2} \tag{2.39}$$

$$T_r \frac{dV_f}{dt} = V - V_f \tag{2.40}$$

$$u^* = V^* - V_f - V_{e_f} \tag{2.41}$$

$$T_a \frac{du_f^*}{dt} = K_a u^* - u_f^* \tag{2.42}$$

$$T_e \frac{dV_e}{dt} = K_e u_f^* - V_e \tag{2.43}$$

$$K_f \frac{dV_e}{dt} = V_{e_f} + T_f \frac{dV_{e_f}}{dt} \tag{2.44}$$

These equations are summed up in the block diagram in Figure 2.8.

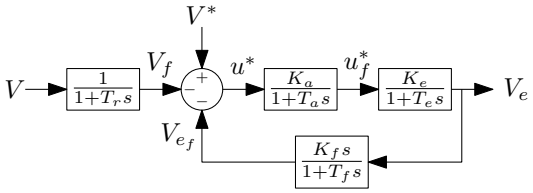

Figure 2.8: Structure of the voltage control of the synchronous machine

Parameters

The parameters of the model are given in Table 2.1.

L_d	1.22	L_q	1.16	L_{1_d}	1.74	L_{1_q}	1.52
L_{2_q}	1.48	R_{1_d}	0.067	R_{1_q}	0.0093	R_{2_q}	0.023
L_{a_d}	1.21	L_{a_q}	1.15	L_{f_d}	1.4	R_{f_d}	$5e^{-4}$
J	4.77	k_d	3	ω_b	314.159 rad/s	R_s	0.004
R_g	0.0055	L_g	0.17	ω_g	1	T_1	1.4
T_2	5	m_d	-0.04	T_d	0.083	T_{se}	0.2
T_{ac}	0.05	T_r	0.06	K_a	25	T_a	0.2
K_e	-0.06	T_e	0.68	K_f	0.11	T_f	0.35

Table 2.1: Parameters of the synchronous machine

Summary

The SM model studied in this report is an order 18 model. This model contains the modelling of the physical part of the machine as well of its control, made of a frequency regulation and a voltage regulation.

2.2 Converters models

As presented in the introduction, this section focuses on the models of PE converters. The first subsection presents the model of a grid feeding converter, the second one the model of a grid forming converter and the third one the model of an MMC.

2.2.1 Grid feeding converter

A grid feeding [70] or grid following converter is a PE converter that just injects power/current into the grid. Unlike the grid forming converter it is considered as a current source and not voltage source because it does not create the voltage. It is the most used type of converter today, mainly to connect renewable sources to the system [71].

General structure of the grid feeding converter

The structure of the grid feeding converter studied in this thesis and its control is presented in Figure 2.9.

This figure shows that the grid feeding converter is made of the DC/AC converter itself (here the DC part is modelled as a perfect voltage source), an RLC filter, an RL transformer and the control part is made of an external loop, a Phase-Locked Loop (PLL) to measure the angle and the frequency of the grid, and a current loop. All these parts are presented in the following.

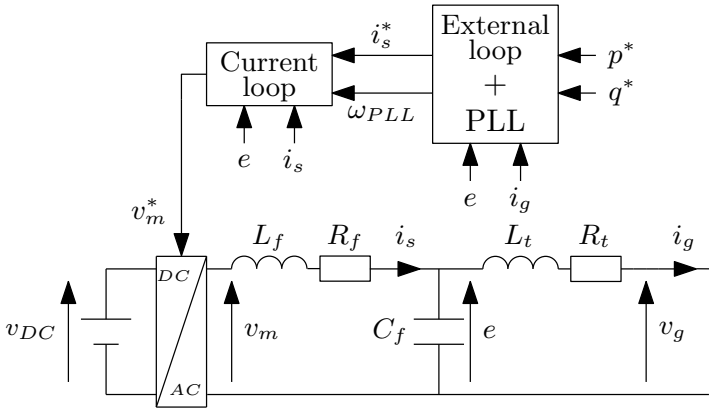

Figure 2.9: Structure of the grid feeding converter and its control

Modelling of the physical part of the converter

The equations modelling the RLC filter, the RL transformer and the DC/AC converter are given in the following. These equations are given in the DQ0 reference frame of the angular frequency ω_{PLL} of the PLL. It can be seen that the DC/AC converter is supposed to be perfect.

$$\frac{L_f}{\omega_b}\frac{di_{s_d}}{dt} = v_{m_d} - e_d - R_f i_{s_d} + \omega_{PLL} L_f i_{s_q} \tag{2.45}$$

$$\frac{L_f}{\omega_b}\frac{di_{s_q}}{dt} = v_{m_q} - e_q - R_f i_{s_q} - \omega_{PLL} L_f i_{s_d} \tag{2.46}$$

$$\frac{C_f}{\omega_b}\frac{de_d}{dt} = i_{s_d} - i_{g_d} + \omega_{PLL} C_f e_q \tag{2.47}$$

$$\frac{C_f}{\omega_b}\frac{de_q}{dt} = i_{s_q} - i_{g_q} - \omega_{PLL} C_f e_d \tag{2.48}$$

$$\frac{L_t}{\omega_b}\frac{di_{g_d}}{dt} = e_d - v_{g_d} - R_t i_{g_d} + \omega_{PLL} L_t i_{g_q} \tag{2.49}$$

$$\frac{L_t}{\omega_b}\frac{di_{g_q}}{dt} = e_q - v_{g_q} - R_t i_{g_q} - \omega_{PLL} L_t i_{g_d} \tag{2.50}$$

$$v^*_{m_d} = v_{m_d} \tag{2.51}$$

$$v^*_{m_q} = v_{m_q} \tag{2.52}$$

Modelling of the PLL

The grid feeding converter needs to measure the frequency and the angle of the voltage to inject a current at the same frequency. It is called the synchronisation. To do so, a PLL is used. Its equations are given in the following.

$$\frac{dM_{PLL}}{dt} = K_{i_{PLL}} e_q \tag{2.53}$$

$$\omega_{PLL} = \frac{K_{p_{PLL}} e_q + M_{PLL}}{\omega_b} + \omega_g \tag{2.54}$$

$$\frac{1}{\omega_b}\frac{d\theta_{PLL}}{dt} = \omega_{PLL} - \omega_g \tag{2.55}$$

These equations are summed up in the block diagram in Figure 2.10.

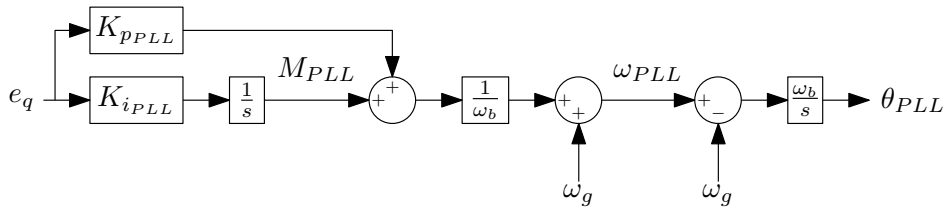

Figure 2.10: Structure of the PLL of the grid feeding converter

Modelling of the external loop

The external loop is made of two parts: one controlling the active power and one controlling the reactive power. Its equations are given in the following. The first two equations model the active and the reactive power, that are then controlled using two PI controllers.

$$p = e_d i_{g_d} + e_q i_{g_q} \tag{2.56}$$

$$q = e_q i_{g_d} - e_d i_{g_q} \tag{2.57}$$

$$\frac{dM_p}{dt} = K_{i_{pq}}(p^* - p) \tag{2.58}$$

$$\frac{dM_q}{dt} = K_{i_{pq}}(q^* - q) \tag{2.59}$$

$$i^*_{s_d} = K_{p_{pq}}(p^* - p) + M_p \tag{2.60}$$

$$i^*_{s_q} = K_{p_{pq}}(q^* - q) + M_q \tag{2.61}$$

These equations are summed up in the block diagram in Figure 2.11.

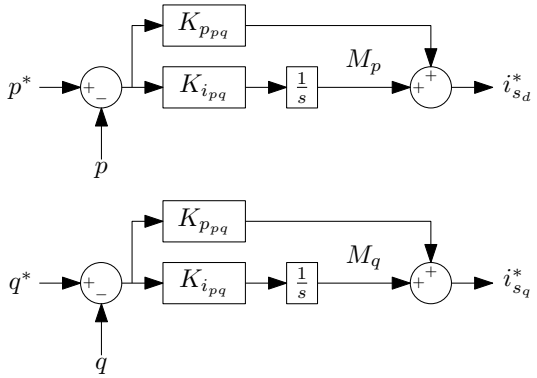

Figure 2.11: Structure of the external loop of the grid feeding converter

Modelling of the current loop

The equations of the current loop are given in the following. They use PI controllers to create the voltage reference of the DC/AC converter using the current reference given by the external loop.

$$\frac{dM_{CL_d}}{dt} = K_{i_{CL}}(i^*_{s_d} - i_{s_d}) \tag{2.62}$$

$$\frac{dM_{CL_q}}{dt} = K_{i_{CL}}(i^*_{s_q} - i_{s_q}) \tag{2.63}$$

$$\tau_f \frac{de_{d_f}}{dt} + e_{d_f} = e_d \tag{2.64}$$

$$\tau_f \frac{de_{q_f}}{dt} + e_{q_f} = e_q \tag{2.65}$$

$$v^*_{m_d} = e_{d_f} + K_{p_{CL}}(i^*_{s_d} - i_{s_d}) - \omega_{PLL} L_f i_{s_q} + M_{CL_d} \tag{2.66}$$

$$v^*_{m_q} = e_{q_f} + K_{p_{CL}}(i^*_{s_q} - i_{s_q}) + \omega_{PLL} L_f i_{s_d} + M_{CL_q} \tag{2.67}$$

These equations are summed up in the block diagram in Figure 2.12.

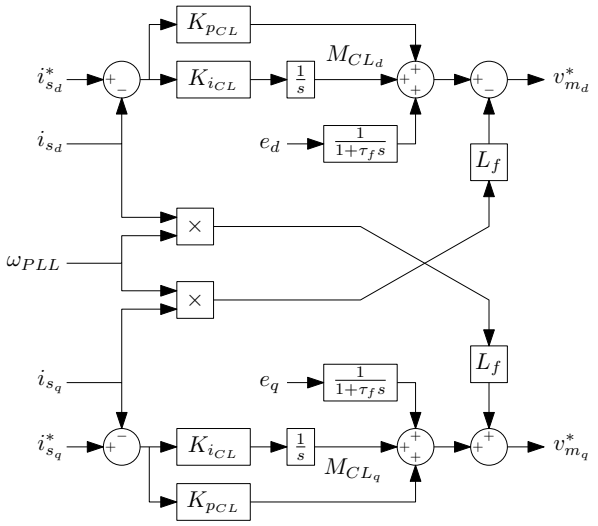

Figure 2.12: Structure of the current loop of the grid feeding converter

Parameters

The parameters are given in pu in the basis S_b, V_b corresponding to the nominal power and voltage of the converter. They are summed up in Table 2.2.

ω_b	314.159 rad/s	L_f	0.1	R_f	0.015	C_f	0.11
L_t	0.1	R_t	0.0075	τ_f	0.0003 s	ω_g	1
$K_{p_{PLL}}$	120	$K_{i_{PLL}}$	3603	$K_{p_{pq}}$	1.5	$K_{i_{pq}}$	150
$K_{p_{CL}}$	0.14	$K_{i_{CL}}$	60.87				

Table 2.2: Parameters of the grid feeding converter

Summary

In this subsection, the equations of the grid feeding converter are given. It leads to a DAE model with 14 differential equations/variables: it is thus an order 14 model.

2.2.2 Grid forming converter

Grid forming converter is the name given to the converters that form the voltage in a power system. They are designed to act as voltage sources instead of current sources (which is the case for the grid feeding converters) and therefore replace the SM (which create the voltage in today's power systems). They have been mainly developed for micro-grids [72, 73] at first but are now of particular interest in power systems [74] because of the fast increase in the PE penetration in transmission systems, which creates a need for grid forming capability.

General structure of grid forming converters

The structure of the grid forming converter studied in this thesis and its control is presented in Figure 2.13. It is a classical structure that can be found in [27] and [13].

This figure shows that the grid forming converter is made of the DC/AC converter itself (here the DC part is modelled as a perfect voltage source), an RLC filter, an RL transformer and the control part is made of an external loop, a voltage loop and a current loop (this structure is called a cascaded loops structure). All these parts are presented in the following.

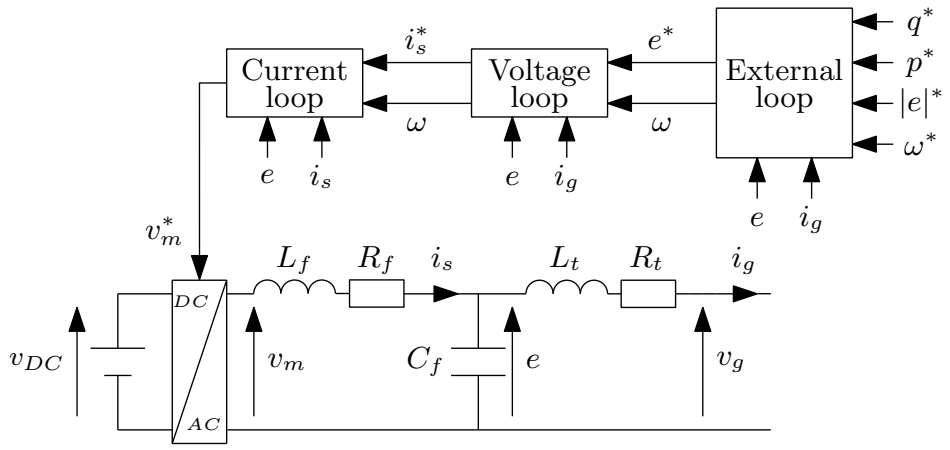

Figure 2.13: Structure of the grid forming converter and its control

Modelling of the physical part of the converter

The equations modelling the RLC filter, the RL transformer and the DC/AC converter are given in the following. These equations are given in the DQ0 reference frame

of the angular frequency ω given by the external loop. It can be seen that the DC/AC converter is supposed to be perfect.

$$\frac{L_f}{\omega_b}\frac{di_{s_d}}{dt} = v_{m_d} - e_d - R_f i_{s_d} + \omega L_f i_{s_q} \tag{2.68}$$

$$\frac{L_f}{\omega_b}\frac{di_{s_q}}{dt} = v_{m_q} - e_q - R_f i_{s_q} - \omega L_f i_{s_d} \tag{2.69}$$

$$\frac{C_f}{\omega_b}\frac{de_d}{dt} = i_{s_d} - i_{g_d} + \omega C_f e_q \tag{2.70}$$

$$\frac{C_f}{\omega_b}\frac{de_q}{dt} = i_{s_q} - i_{g_q} - \omega C_f e_d \tag{2.71}$$

$$\frac{L_t}{\omega_b}\frac{di_{g_d}}{dt} = e_d - v_{g_d} - R_t i_{g_d} + \omega L_t i_{g_q} \tag{2.72}$$

$$\frac{L_t}{\omega_b}\frac{di_{g_q}}{dt} = e_q - v_{g_q} - R_t i_{g_q} - \omega L_t i_{g_d} \tag{2.73}$$

$$v^*_{m_d} = v_{m_d} \tag{2.74}$$

$$v^*_{m_q} = v_{m_q} \tag{2.75}$$

Modelling of the external loop

The external loop is made of two parts: an active power droop control and a reactive power droop control.

The equations of the active power droop control are given in the following. It is made of a first equation modelling the active power injected by the converter, a second one modelling the measure of this power, a third one modelling the droop control and a fourth one modelling the angle of the converter.

$$p = e_d i_{g_d} + e_q i_{g_q} \tag{2.76}$$

$$\frac{dp_m}{dt} + \omega_f p_m = \omega_f p \tag{2.77}$$

$$\omega = \omega^* + m_p(p^* - p_m) \tag{2.78}$$

$$\frac{1}{\omega_b}\frac{d\theta}{dt} = \omega - \omega_g \tag{2.79}$$

These equations are summed up in the block diagram in Figure 2.14

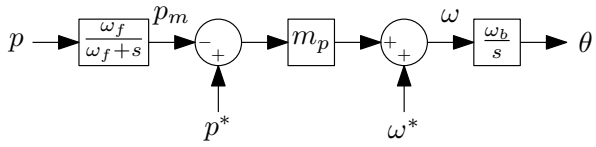

Figure 2.14: Structure of the active power droop control of the grid forming converter

The equations of the reactive power droop control are given in the following. It is a made of a first equation modelling the reactive power injected by the converter, a second one modelling the measure of this power, a third and a fourth one modelling an active damping and a fifth and a sixth one modelling the reactive power droop.

$$q = e_q i_{g_d} - e_d i_{g_q} \tag{2.80}$$

$$\frac{dq_m}{dt} + \omega_f q_m = \omega_f q \tag{2.81}$$

$$\frac{dM_{AD_d}}{dt} = \omega_{ff}(K_{ff} i_{g_d} - M_{AD_d}) \tag{2.82}$$

$$\frac{dM_{AD_q}}{dt} = \omega_{ff}(K_{ff} i_{g_q} - M_{AD_q}) \tag{2.83}$$

$$e_d^* = |e|^* + m_q(q^* - q_m) + M_{AD_d} - K_{ff} i_{g_d} \tag{2.84}$$

$$e_q^* = M_{AD_q} - K_{ff} i_{g_q} \tag{2.85}$$

These equations are summed up in the block diagram in Figure 2.15.

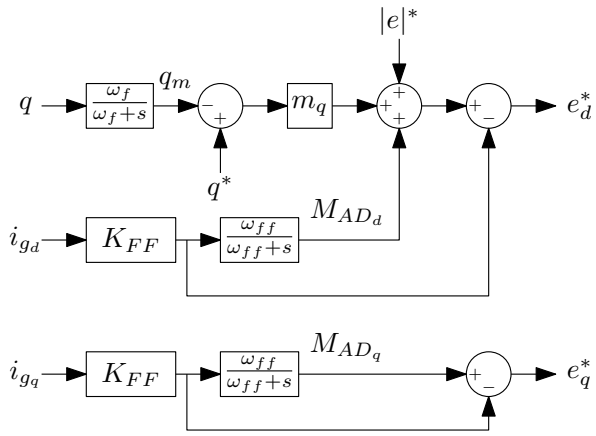

Figure 2.15: Structure of the reactive power droop control of the grid forming converter

One can note that instead of using an active power droop control, some authors use a Virtual Synchronous Machine (VSM) [75], which mimics the behaviour of a SM. Some comparisons have been made with the droop control [76] and equivalences can be found between the two methods [77].

Modelling of the voltage loop

The equations of the voltage loop are given in the following. It uses PI controllers to create the current reference for the current loop using the voltage reference as an input.

$$\frac{dM_{VL_d}}{dt} = K_{i_{VL}}(e_d^* - e_d) \tag{2.86}$$

$$\frac{dM_{VL_q}}{dt} = K_{i_{VL}}(e_q^* - e_q) \tag{2.87}$$

$$i_{s_d}^* = K_{FF_i} i_{g_d} + K_{p_{VL}}(e_d^* - e_d) - \omega C_f e_q + M_{VL_d} \tag{2.88}$$

$$i_{s_q}^* = K_{FF_i} i_{g_q} + K_{p_{VL}}(e_q^* - e_q) + \omega C_f e_d + M_{VL_q} \tag{2.89}$$

These equations are summed up in the block diagram in Figure 2.16.

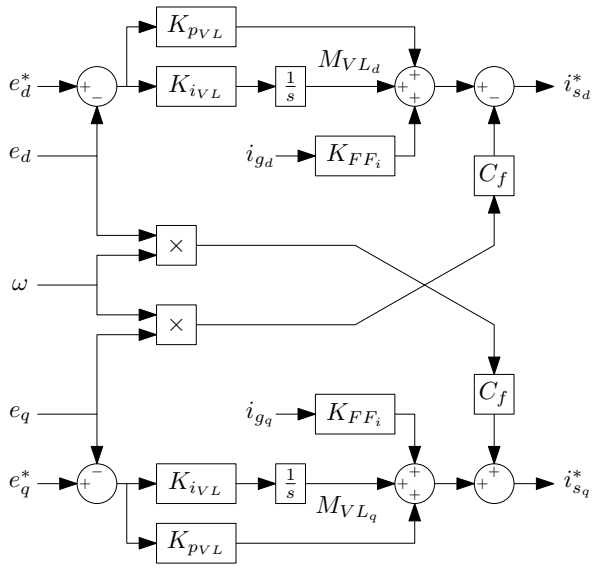

Figure 2.16: Structure of the voltage loop of the grid forming converter

Modelling of the current loop

The equations of the current loop are given in the following. It uses PI controllers to create the voltage reference of the DC/AC converter using the current reference given by the voltage loop.

$$\frac{dM_{CL_d}}{dt} = K_{i_{CL}}(i^*_{s_d} - i_{s_d}) \tag{2.90}$$

$$\frac{dM_{CL_q}}{dt} = K_{i_{CL}}(i^*_{s_q} - i_{s_q}) \tag{2.91}$$

$$v^*_{m_d} = K_{FF_v} e_d + K_{p_{CL}}(i^*_{s_d} - i_{s_d}) - \omega L_f i_{s_q} + M_{CL_d} \tag{2.92}$$

$$v^*_{m_q} = K_{FF_v} e_q + K_{p_{CL}}(i^*_{s_q} - i_{s_q}) + \omega L_f i_{s_d} + M_{CL_q} \tag{2.93}$$

These equations are summed up in the block diagram in Figure 2.17.

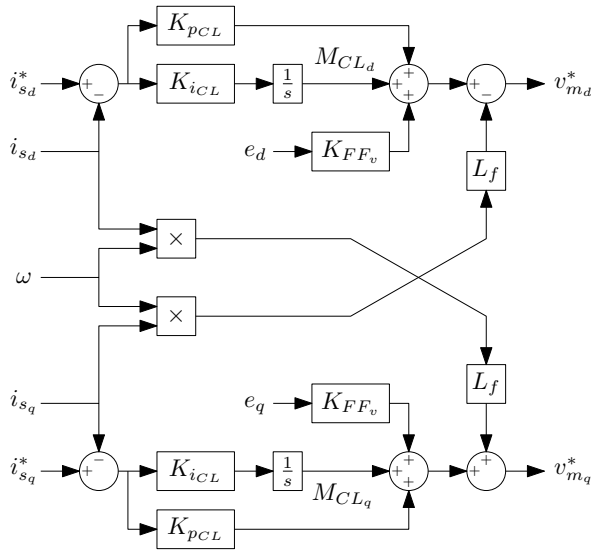

Figure 2.17: Structure of the current loop of the grid forming converter

Parameters

The parameters are given in pu in the basis S_b, V_b corresponding to the nominal power and voltage of the converter. They are summed up in Table 2.3 and are taken from [78].

ω_b	314.159 rad/s	L_f	0.15	R_f	0.005	C_f	0.066
L_t	0.15	R_t	0.005	m_p	0.03	m_q	0.0001
ω_f	31.4 rad/s	ω_{ff}	16.66 rad/s	K_{FF}	0.01	K_{FF_i}	1
$K_{p_{VL}}$	0.8	$K_{i_{VL}}$	1.16	K_{FF_v}	1	$K_{p_{CL}}$	0.7388
$K_{i_{CL}}$	1.19	ω_g	1				

Table 2.3: Parameters of the grid forming converter

Summary

In this subsection, the equations of the grid forming two-level voltage source converter are given. It leads to a DAE model with 15 differential equations/variables: it is an order 15 model.

One advantage of this model is that it has been validated with experimentations during the MIGRATE project [79]. It means that if the reduced models obtained with the developed methods are validated by a comparison with this detailed model, they are also validated with the experimentations.

2.2.3 Modular multilevel converter

The Modular Multilevel Converter (MMC) is a N-level voltage source converter. Because it has a lot of levels, there is less need to filter the output voltage which is a great advantage. However, the control is much more complex than with a 2-level VSC.

Several models exist for the MMC. Some are very detailed and therefore complex [80]. Other are averaged [81]. Some are adapted to unbalanced conditions [82]. Others are state-space model adapted to linear analysis [31]. In this report, a rather simple model taken from [83] is used.

General structure of the MMC

The structure of the MMC studied in this thesis and its control is presented in Figure 2.18. Exceptionally, the model presented here is not in pu for the sake of simplicity. When connected to another system, it is easy to put the output and input variables of the MMC in pu using the base voltages and power given in the parameters in Table 2.4.

The physical part of the converter is made of a DC part, an AC part, and a capacitor between them that stores energy. The DC control is made of an energy loop and a current loop. The AC control is made of an external loop, a PLL and a current loop.

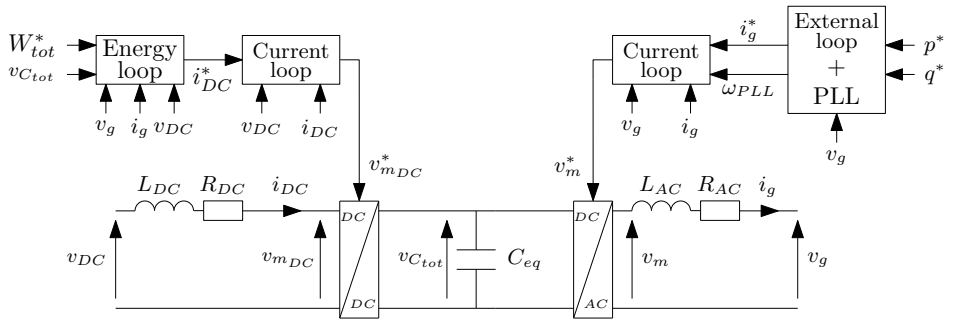

Figure 2.18: Structure of the MMC and its control

Modelling of the physical part of the converter

The equations modelling the physical part of the MMC are given in the following. The first two equations model the equivalent RL of the AC part. The third equation models the equivalent RL of the DC part and the fourth one models the storage of energy in the equivalent capacitor in the MMC.

$$L_{AC}\frac{di_{g_d}}{dt} = v_{m_d} - v_{g_d} - R_{AC}i_{g_d} + \omega_{PLL}L_{AC}i_{g_q} \tag{2.94}$$

$$L_{AC}\frac{di_{g_q}}{dt} = v_{m_q} - v_{g_q} - R_{AC}i_{g_q} - \omega_{PLL}L_{AC}i_{g_d} \tag{2.95}$$

$$L_{DC}\frac{di_{DC}}{dt} = v_{DC} - v_{m_{DC}} - R_{DC}i_{DC} \tag{2.96}$$

$$C_{eq}v_{C_{tot}}\frac{dv_{C_{tot}}}{dt} = v_{m_{DC}}i_{DC} - v_{m_d}i_{g_d} - v_{m_q}i_{g_q} \tag{2.97}$$

$$v^*_{m_{DC}} = v_{m_{DC}} \tag{2.98}$$

$$v^*_{m_d} = v_{m_d} \tag{2.99}$$

$$v^*_{m_q} = v_{m_q} \tag{2.100}$$

Modelling of the PLL

The equations modelling the PLL are given in the following.

$$\frac{dM_{PLL}}{dt} = K_{i_{PLL}}v_{g_q} \tag{2.101}$$

$$\omega_{PLL} = K_{p_{PLL}}v_{g_q} + M_{PLL} + \omega_g \tag{2.102}$$

$$\frac{d\theta_{PLL}}{dt} = \omega_{PLL} - \omega_g \tag{2.103}$$

These equations are summed up in the block diagram in Figure 2.19.

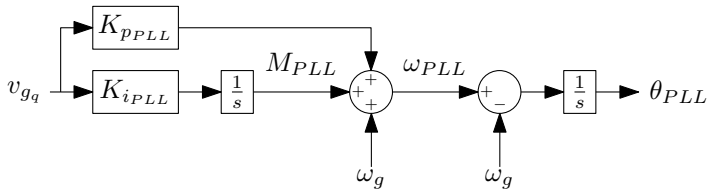

Figure 2.19: Structure of the MMC PLL

Modelling of the external loop

The equations modelling the external loop are given in the following. This loop gives the current reference using the active and reactive power references.

$$i_{g_d}^* = \frac{p^*}{v_{g_d}} \tag{2.104}$$

$$i_{g_q}^* = -\frac{q^*}{v_{g_d}} \tag{2.105}$$

These equations are summed up in the block diagram in Figure 2.20.

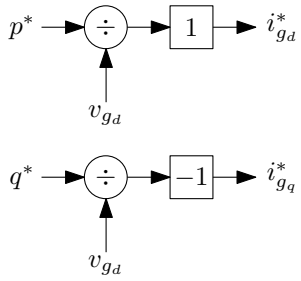

Figure 2.20: Structure of the external loop of the MMC

Modelling of the energy loop

The equations modelling the energy loop are given in the following. This loop uses a PI controller to give the DC current reference using the energy reference.

$$p_{AC} = v_{g_d} i_{g_d} + v_{g_q} i_{g_q} \tag{2.106}$$

$$W_{tot} = v_{c_{tot}}^2 \tag{2.107}$$

$$\tau_f \frac{dW_{tot_f}}{dt} + W_{tot_f} = W_{tot} \tag{2.108}$$

$$\frac{dM_W}{dt} = K_{i_W}(W^*_{tot} - W_{tot_f}) \tag{2.109}$$

$$i^*_{DC} = \frac{K_{p_W}(W^*_{tot} - W_{tot_f}) + M_W + p_{AC}}{v_{DC}} \tag{2.110}$$

These equations are summed up in the block diagram in Figure 2.21.

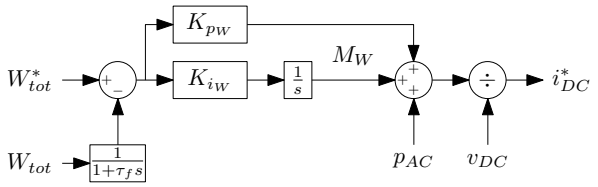

Figure 2.21: Structure of the energy loop of the MMC

Modelling of the AC current loop

The equations modelling the AC current loop are given in the following. This loop uses PI controllers to give the voltage reference of the DC/AC converter using the current references given by the external loop.

$$\frac{dM_{CL_d}}{dt} = K_{i_{CL}}(i^*_{g_d} - i_{g_d}) \tag{2.111}$$

$$\frac{dM_{CL_q}}{dt} = K_{i_{CL}}(i^*_{g_q} - i_{g_q}) \tag{2.112}$$

$$v^*_{m_d} = v_{g_d} + K_{p_{CL}}(i^*_{g_d} - i_{g_d}) - \omega_{PLL} L_{AC} i_{g_q} + M_{CL_d} \tag{2.113}$$

$$v^*_{m_q} = v_{g_d} + K_{p_{CL}}(i^*_{g_q} - i_{g_q}) + \omega_{PLL} L_{AC} i_{g_d} + M_{CL_q} \tag{2.114}$$

These equations are summed up in the block diagram in Figure 2.22.

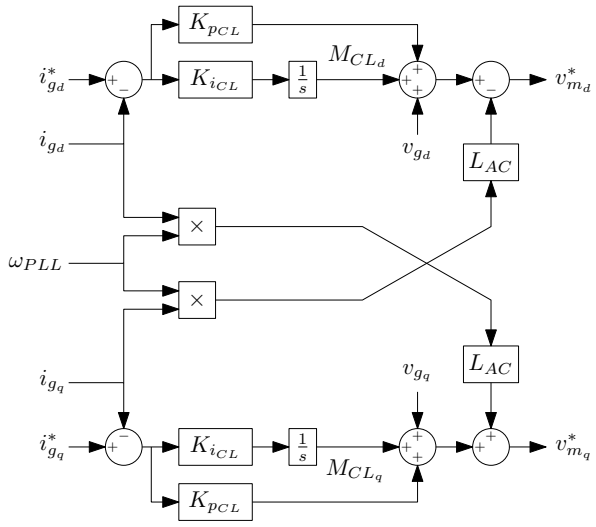

Figure 2.22: Structure of the AC current loop of the MMC

Modelling of the DC current loop

The equations modelling the DC current loop are presented hereafter. This loop uses a PI controller to give the DC voltage reference to the DC/DC converter using the DC current reference given by the energy loop.

$$\frac{dM_{DCCL}}{dt} = K_{i_{DCCL}}(i^*_{DC} - i_{DC}) \tag{2.115}$$

$$v^*_{m_{DC}} = v_{DC} - K_{p_{DCCL}}(i^*_{DC} - i_{DC}) - M_{DCCL} \tag{2.116}$$

These equations are summed up in the block diagram in Figure 2.23.

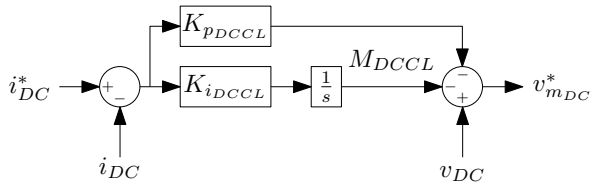

Figure 2.23: Structure of the DC current loop of the MMC

Parameters

As said before this MMC model is not given in pu for the sake of simplicity. Its parameters are given in Table 2.4.

L_{AC}	0.083 H	R_{AC}	1.024 Ω	L_{DC}	0.033 H	R_{DC}	0.683 Ω
$K_{p_{DCCL}}$	33.54	$K_{i_{DCCL}}$	$1.83e^{4}$	$K_{p_{CL}}$	68.8	$K_{i_{CL}}$	$2.99e^{4}$
$K_{p_{PLL}}$	$1.48e^{-3}$	$K_{i_{PLL}}$	$3.12e^{-6}$	K_{p_W}	0.0164	K_{i_W}	0.703
τ_f	0.001	ω_g	314.159 rad/s	C_{eq}	$1.95e^{-4}$ F	$V_{b_{AC}}$	320 kV
$V_{b_{DC}}$	640 kV	S_b	1 GVA	W^*_{tot}	$V^2_{b_{DC}}$		

Table 2.4: Parameters of the MMC

Summary

In this subsection, the equations of the MMC are given. It leads to a DAE model with 11 differential equations/variables: it is thus an order 11 model.

2.3 Modelling of a complete transmission system

The models for all the elements in the studied systems have been presented in this chapter. The only remaining thing to do is to connect them to each other and derive the connection equations. Two things need to be taken into account carefully:

- Each element is modelled either in pu in its own basis S_b, V_b or in SI (for the MMC). As a consequence, a proper basis change is needed to connect two elements whose models are expressed in different unit bases.
- Each model is derived in the DQ0 reference frame of a frequency ω which can be different for each element. To connect two elements whose models are expressed in different DQ0 representation, a proper basis change consisting in a rotation matrix is needed.

Once the adequate variables of two elements are expressed in the same unit basis and in the same DQ0 representation, the connection equations can be derived. Most of the time they consist in the Kirchhoff's laws.

For example, consider the system in Figure 2.24.

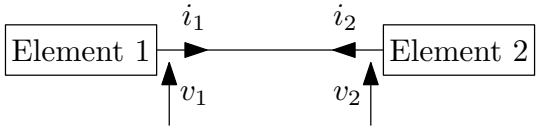

Figure 2.24: Connection of two elements in a power system

In this example, the model of the first element is expressed in the pu basis S_{b_1}, V_{b_1}, I_{b_1} (deduced from the two others) and in the DQ0 representation of a frequency ω_1 and an angle θ_1. The model of the second element is expressed in the pu basis S_{b_2}, V_{b_2}, I_{b_2} (deduced from the two others) and in the DQ0 representation of a frequency ω_2 and an angle θ_2. The two models output are then expressed in the same pu basis S_b, V_b, I_b and in the same DQ0 representation of a frequency ω and angle θ using the following basis changes.

$$\begin{pmatrix} v_{1_{d_g}} \\ v_{1_{q_g}} \end{pmatrix} = \frac{V_{b_1}}{V_b} \begin{pmatrix} cos(\theta_1 - \theta) & -sin(\theta_1 - \theta) \\ sin(\theta_1 - \theta) & cos(\theta_1 - \theta) \end{pmatrix} \begin{pmatrix} v_{1_d} \\ v_{1_q} \end{pmatrix} \tag{2.117}$$

$$\begin{pmatrix} i_{1_{d_g}} \\ i_{1_{q_g}} \end{pmatrix} = \frac{I_{b_1}}{I_b} \begin{pmatrix} cos(\theta_1 - \theta) & -sin(\theta_1 - \theta) \\ sin(\theta_1 - \theta) & cos(\theta_1 - \theta) \end{pmatrix} \begin{pmatrix} I_{1_d} \\ I_{1_q} \end{pmatrix} \tag{2.118}$$

$$\begin{pmatrix} v_{2_{d_g}} \\ v_{2_{q_g}} \end{pmatrix} = \frac{V_{b_2}}{V_b} \begin{pmatrix} cos(\theta_2 - \theta) & -sin(\theta_2 - \theta) \\ sin(\theta_2 - \theta) & cos(\theta_2 - \theta) \end{pmatrix} \begin{pmatrix} v_{2_d} \\ v_{2_q} \end{pmatrix} \tag{2.119}$$

$$\begin{pmatrix} i_{2_{d_g}} \\ i_{2_{q_g}} \end{pmatrix} = \frac{I_{b_2}}{I_b} \begin{pmatrix} cos(\theta_2 - \theta) & -sin(\theta_2 - \theta) \\ sin(\theta_2 - \theta) & cos(\theta_2 - \theta) \end{pmatrix} \begin{pmatrix} I_{2_d} \\ I_{2_q} \end{pmatrix} \tag{2.120}$$

That being done, the Kirchhoff's laws can be written:

$$v_{1_{d_g}} = v_{2_{d_g}} \tag{2.121}$$

$$v_{1_{q_g}} = v_{2_{q_g}} \tag{2.122}$$

$$i_{1_{d_g}} = -i_{2_{d_g}} \tag{2.123}$$

$$i_{1_{q_g}} = -i_{2_{q_g}} \tag{2.124}$$

In the case of a 100% PE power system, the frequency ω will be chosen as a weighted average of all the grid forming converters frequencies. One can note that in steady-state, all the grid forming converters frequencies are equal.

The system to model now consists of all the equations modelling each element of the transmission system plus the connection equations and the basis changes equations. This results in a DAE system that can be modelled as in (2.125).

$$\begin{cases} \dfrac{dx_{diff}}{dt} = f(x_{diff}, x_{alg}, u) \\ \qquad 0 = g(x_{diff}, x_{alg}, u) \\ \qquad y = h(x_{diff}, x_{alg}, u) \\ x_{diff} \in \mathbb{R}^{N_{diff}}, x_{alg} \in \mathbb{R}^{N_{alg}}, u \in \mathbb{R}^p, y \in \mathbb{R}^q \end{cases} \tag{2.125}$$

2.4 Chapter conclusion

In this chapter, the models of all the elements forming the studied transmission systems have been presented. Equations and block diagrams modelling grid forming converters, grid feeding converters, MMC, lines, transformers, loads, shunt capacitors and SM have been given, as well as a method to derive the connection equations. This results in a DAE system modelling the studied transmission system.

The idea now, as written in chapter 1, is to develop new MOR methods that will be applied on this model of a transmission system with a high PE penetration. And these new methods should respect some requirements deduced in chapter 1, that are not met by the usual MOR methods. This is the topic of chapter 3.

CHAPTER 3

Development of model order reduction methods

Contents

This chapter presents the developed MOR methods and how they meet the requirements deduced in chapter 1. It is recalled that these requirements are the preservation of the physical variables, the parameters and the most relevant dynamics of the system (i.e. the preservation of some poles), a guarantee that the operating point remains stable, as well as a simplicity of implementation in the most common nonlinear DAE solvers and of course a good trade-off between the accuracy and the order of the reduced model.

Because they keep the variables of the system during the MOR process, the developed methods simplify the analysis and the tuning of new controls. It is indeed easier to identify the critical variables during the stability analysis [84] and it is possible to add new control loops directly on the reduced model. The latter is illustrated in chapter 4.

The first section of this chapter presents the general principles that are common to all the methods: the residualization of some state variables [44] in the nonlinear model and the modal approach, so that this residualization discard some poles in the linearised model and keep the other poles almost unchanged. The second section presents three developed methods. For each one of them corresponds a strategy to choose the states to residualize in the nonlinear model and the poles to discard in the linearised one.

3.1 Common principles of the developed methods

As said in the chapter introduction, the general philosophy is the same for all the developed methods. It is presented in this section in details.

The first idea is the use of a state residualization [45]. It is explained in the first subsection. The second subsection presents the modal approach of the methods, which is used to preserve some poles of the system during the MOR and discard others.

3.1.1 The state residualization

In this subsection, the principles of the state residualization are presented. It is explained how this is an interesting MOR process and why it is chosen here for the development of the MOR methods.

Nonlinear differential algebraic system

A nonlinear DAE system is considered in (3.1). This is the model that is reduced with the developed methods as it can describe almost all the transmission systems. One can note that this is a continuous system. In case of discontinuities like a short-circuit or a line tripping, it is possible to switch from one continuous DAE system to another.

The size of this model is given by its number of differential variables/equations N_{diff} [85]. In this system x_{diff} represents the state variables, u the inputs, x_{alg} the algebraic variables and y the output.

$$\begin{cases} \dfrac{dx_{diff}}{dt} = f(x_{diff}, x_{alg}, u) \\ 0 = g(x_{diff}, x_{alg}, u) \\ y = h(x_{diff}, x_{alg}, u) \\ x_{diff} \in \mathbb{R}^{N_{diff}}, x_{alg} \in \mathbb{R}^{N_{alg}}, u \in \mathbb{R}^{p}, y \in \mathbb{R}^{q} \end{cases} \tag{3.1}$$

Residualization principle

The residualization of a state variable consists in changing this state variable into an algebraic variable by neglecting the derivative part in its associated differential equation, transforming it into an algebraic equation [45]. It is a well known process that is used today in the phasor approximation [11].

The reduced system obtained by state residualization can be written as in (3.2).

$$\begin{cases} E\dfrac{dx_{diff}}{dt} = f(x_{diff}, x_{alg}, u) \\ 0 = g(x_{diff}, x_{alg}, u) \\ y = h(x_{diff}, x_{alg}, u) \\ E = diag(\delta_i), \delta_i \in \{0; 1\}, \forall i, E \in \mathbb{R}^{N_{diff} \times N_{diff}} \\ x_{diff} \in \mathbb{R}^{N_{diff}}, x_{alg} \in \mathbb{R}^{N_{alg}}, u \in \mathbb{R}^{p}, y \in \mathbb{R}^{q} \end{cases} \tag{3.2}$$

The introduced E matrix before the derivative of x_{diff} is called the residualization matrix and has the following characteristics:

- It is a diagonal of 1 and 0.
- If $E = diag(1)$, the system is not reduced.
- If $E = diag(0)$ the reduced system is an algebraic system corresponding to the steady state equations.
- Each element $E(i,i)$ gives an indication on whether the state variable $x_{diff}(i)$ is residualized or not. If $E(i,i) = 0$ it is, if $E(i,i) = 1$ it is not.
- More generally, the size of the reduced system is given by $tr(E)$.

The idea is to choose E to have a trade-off between the order of the reduced model (to accelerate the simulation and simplify the analysis) and the accuracy.

Example of the phasor approximation using state residualization

As illustration, an R,L line is represented in Figure 3.1.

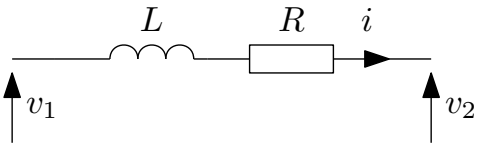

Figure 3.1: Model of an R,L line

The equations of this line, in the DQ0 reference frame of an angular frequency ω and in pu, are presented in (3.3).

$$\begin{cases} \frac{L}{\omega_b}\frac{di_d}{dt} = v_{1_d} - v_{2_d} - Ri_d + \omega L i_q \\ \frac{L}{\omega_b}\frac{di_q}{dt} = v_{1_q} - v_{2_q} - Ri_q - \omega L i_d \end{cases} \tag{3.3}$$

With the phasor approximation, these equations are changed into (3.4) by the residualization of the state variables i_d and i_q. In this case the line equations become algebraic.

$$\begin{cases} 0 = v_{1_d} - v_{2_d} - Ri_d + \omega L i_q \\ 0 = v_{1_q} - v_{2_q} - Ri_q - \omega L i_d \end{cases} \tag{3.4}$$

Remarks

One advantage of the state residualization is that it ensures that the steady state values of the full and the reduced models are the same. They are indeed the solution of the same system (3.5).

One can remark that for this to be true, the system needs to be steady state time invariant, which is possible if the DQ0 representation is deduced with the appropriate ω, the frequency of the system.

$$\begin{cases} 0 = f(x_{diff}, x_{alg}, u) \\ 0 = g(x_{diff}, x_{alg}, u) \\ y = h(x_{diff}, x_{alg}, u) \\ x_{diff} \in \mathbb{R}^{N_{diff}}, x_{alg} \in \mathbb{R}^{N_{alg}}, u \in \mathbb{R}^p, y \in \mathbb{R}^q \end{cases} \tag{3.5}$$

Another advantage is that the variables and the parameters of the full and the reduced model are exactly the same as no basis change, projection or truncation has been made. As a consequence, it is easily possible to directly work on the reduced system for the analysis or even the tuning of some controllers. In chapter 4 it is shown on an example that it is easily possible to add a new control loop directly on the reduced model without going back to the full model. Because of all that this method of state residualization is used for the development of the MOR methods in this thesis. Finally, the state residualization can easily be implemented in the classical DAE solvers as it simply consists in replacing some derivatives in the equations by 0.

Conclusion

The principle of the state residualization has been presented in this subsection. It has been shown that it can be a way to reduce the order of a system and it is used in the following because it meets the requirements presented in chapter 1: it keeps the variables and the parameters of the system during the MOR process and it can easily be implemented in the classical DAE solvers.

The next subsection presents the second common point between all the developed methods: the modal approach. It helps preserving some poles of the linearised system during the MOR in order to preserve some chosen physical dynamics, which is another requirements for the developed MOR methods. It is a first step in choosing the matrix E as it adds some constraints on it to preserve these poles.

3.1.2 The modal approach

The nonlinear DAE system to reduce is considered in (3.6).

$$\begin{cases} \dfrac{dx_{diff}}{dt} = f(x_{diff}, x_{alg}, u) \\ \qquad 0 = g(x_{diff}, x_{alg}, u) \\ \qquad y = h(x_{diff}, x_{alg}, u) \\ x_{diff} \in \mathbb{R}^{N_{diff}}, x_{alg} \in \mathbb{R}^{N_{alg}}, u \in \mathbb{R}^{p}, y \in \mathbb{R}^{q} \end{cases} \tag{3.6}$$

As explained in the previous subsection, the idea of the MOR by state residualization is to find a matrix E to reduce the order of the model like in (3.7).

$$\begin{cases} E\dfrac{dx_{diff}}{dt} = f(x_{diff}, x_{alg}, u) \\ \qquad 0 = g(x_{diff}, x_{alg}, u) \\ \qquad y = h(x_{diff}, x_{alg}, u) \\ \qquad E = diag(\delta_i), \delta_i \in \{0; 1\}, \forall i, E \in \mathbb{R}^{N_{diff} \times N_{diff}} \\ x_{diff} \in \mathbb{R}^{N_{diff}}, x_{alg} \in \mathbb{R}^{N_{alg}}, u \in \mathbb{R}^{p}, y \in \mathbb{R}^{q} \end{cases} \tag{3.7}$$

In this subsection, the residualization of state variables in the nonlinear model is linked to the discarding of poles in the linearised model around its operating point and the preservation of the others. Knowing the links between the states of the nonlinear model and the poles of the linearised system, it is indeed possible to choose which states to residualize in order to keep some poles of the system and discard others. This process, summed up in the synoptic in Figure 3.2 is described step by step in the following. It is inspired by [32] but unlike it it focuses on all the modes of the system and not only the inter-zone modes.

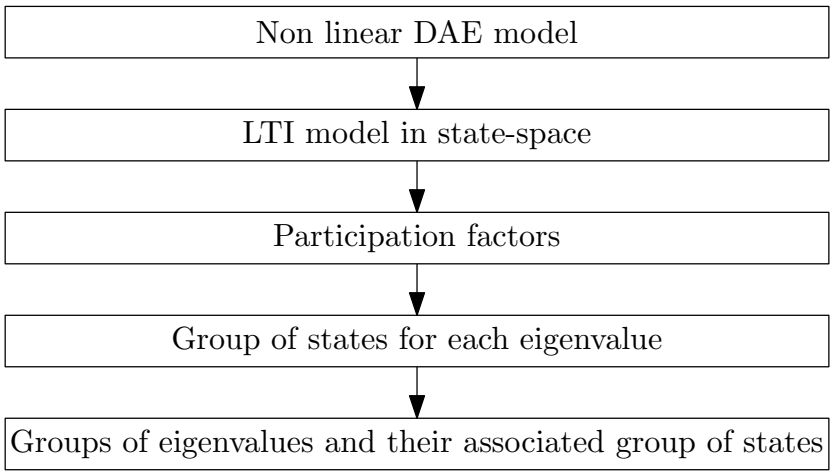

Figure 3.2: Synoptic describing the modal approach

Linearising the model

The system is first linearised around its operating point in steady state (the solution of (3.5)), which gives the simple LTI system represented in state-space in (3.8). More explanations can be found in chapter 1 for the linearisation process.

$$\begin{cases} \dfrac{dx}{dt} = Ax + Bu \\ \quad y = Cx + Du \\ \quad x \in \mathbb{R}^{N_{diff}}, u \in \mathbb{R}^{p}, y \in \mathbb{R}^{q} \end{cases} \tag{3.8}$$

Calculating the participation factors and forming the group of states that participate in an eigenvalue

The next step of the process consists in calculating the participation factors $p_{k,i}$ of the system using the method presented in chapter 1.

In the developed methods, the idea is to identify the states that participate the most in each eigenvalue in order to identify which one to residualize to discard some eigenvalues (and not the others).

To proceed, a participation criterion $\epsilon_{participation}$ is chosen. For each eigenvalue λ_i, the k state variables corresponding to the k largest participation factors (their modulus) are retained so that the sum of their participations is higher than $\epsilon_{participation}$ and the sum of the participations of the $k-1$ state variables corresponding to the $k-1$ largest participation factors is lower than $\epsilon_{participation}$. They form the group of states that participate in λ_i for the considered participation criterion $\epsilon_{participation}$. This group is noted $P_{\lambda_i,\epsilon_{participation}}$. The forming of this set $P_{\lambda_i,\epsilon_{participation}}$ is summed up in (3.9).

$$P_{\lambda_i,\epsilon_{participation}} = \{x_k / \forall x_m \notin P_{\lambda_i,\epsilon_{participation}}, |p_{k,i}| \geq |p_{m,i}| \\ \sum_{x_k} |p_{k,i}| \geq \epsilon_{participation} \\ \forall x_l \in P_{\lambda_i,\epsilon_{participation}}, \sum_{x_k \neq x_l} |p_{k,i}| < \epsilon_{participation}\} \tag{3.9}$$

The choice of the participation criterion $\epsilon_{participation}$ is important. If it is close to 1 the participation is very well taken into account but the result is that the considered eigenvalue depends on many state variables which can complicate the MOR. This indeed induces a lot of couplings, as shown in the next paragraph. If this criterion is lower, the participations are less taken into account but only the most important states are considered, which facilitates the MOR. A trade-off has to be made and this criterion must be chosen depending on how fast the participation factors decrease when ranked from the largest to the lowest.

This process is done for all the eigenvalues of the system. At the end, there should be N_{diff} groups $P_{\lambda_i,\epsilon_{participation}}$, one for each eigenvalue λ_i.

Forming the groups of eigenvalues in which the same states participate

When the system is coupled, each state variable participates in several eigenvalues and each eigenvalue depends on several state variables. This means that some of the previously created groups of states can be merged to form new groups of state variables, noted P_i, each group associated to one and only one group of eigenvalues in which they participate. A state variable can only be in one group and an eigenvalue can only be in one group as well. The state variables in a group only participate in the eigenvalues of the associated group of eigenvalues and not in the other eigenvalues (provided that the participation criterion is well chosen).

If the system is totally decoupled, there are as many groups as eigenvalues/state variables, with one eigenvalue/one state variable in each one of them. If the system is coupled, there are less groups, but with more states/eigenvalues. This also depends on the choice of the participation criterion $\epsilon_{participation}$. If it is low there are more groups than if it is high.

This process is done for all the eigenvalues until all the remaining groups are disjoint. At the end, there are between 1 and N_{diff} groups (the latter if the system is totally decoupled).

These groups can be seen as constraints on the states to residualize in the developed MOR methods. Residualizing all the states of a same group guarantees that the associated poles are discarded, and the other almost unmoved (the bigger the participation criterion, the less the remaining poles move). And keeping the poles in the linearised model brings a guarantee that the operating point remains stable during the MOR process. If no pole is moved, no pole becomes unstable.

A new set $\mathbb{E}_{\epsilon_{participation}}$ is created. It contains all the E matrices that are diagonal, made of 0 and 1 (see the previous subsection on the state residualization) and that

respect the constraint deduced from the participation factors analysis in this subsection. This constraint is explained in (3.10). It means that the states of a same group must be residualized (or not residualized) at the same time to discard (or keep) the associated poles and keep (or discard) the others. This also means that the order of the different possible reduced models is somehow imposed by these constraint. It is not possible to choose it completely freely.

$$\forall P_i, \forall x_k \in P_i, \forall x_l \in P_i, E(k,k) = E(l,l) \tag{3.10}$$

From now on, all the E matrices obtained from the MOR methods must be in $\mathbb{E}_{\epsilon_{participation}}$ so that the remaining poles in the reduced model are (almost) the same as in the full model (almost, because depending on the choice of $\epsilon_{participation}$ they can move more or less). This is what we call here a modal approach.

Illustration with an order 4 model

To illustrate this, an order 4 LTI model is considered in 3.11.

$$\begin{cases} \dfrac{dx}{dt} = Ax + Bu = \begin{pmatrix} -50 & -25 & 5 & 1 \\ -10 & -20 & 1 & 1 \\ 5 & 1 & -10 & -10 \\ 10 & 1 & 10 & -10 \end{pmatrix} x + \begin{pmatrix} 1 \\ 1 \\ 1 \\ 1 \end{pmatrix} u \\ \quad y = \begin{pmatrix} 0 & 0 & 0 & 0 \\ 0 & 1 & 0 & 0 \\ 0 & 0 & 0 & 0 \\ 0 & 0 & 0 & 0 \end{pmatrix} x \end{cases} \tag{3.11}$$

The participation factors of each state variable in each eigenvalue of A are calculated and their modulus are given in Table 3.1.

	x_1	x_2	x_3	x_4
$\lambda_1 = -57.8$	0.84	0.15	0.01	0.02
$\lambda_{2,3} = -9.4 \pm 10.5i$	0.03	0.04	0.48	0.46
$\lambda_4 = -13.4$	0.13	0.79	0.04	0.08

Table 3.1: Modulus of the participation factors of A

For each eigenvalue, a group is formed, containing the states that participate the most in it. This group depends on the choice of $\epsilon_{participation}$. Two examples are presented, $\epsilon_{participation} = 0.7$ and $\epsilon_{participation} = 0.9$. This gives Table 3.2 and 3.3.

	Eigenvalue	Group of states that participate in the eigenvalue
$P_{\lambda_1,\epsilon_{participation}}$	λ_1	x_1
$P_{\lambda_{2,3},\epsilon_{participation}}$	$\lambda_{2,3}$	x_3, x_4
$P_{\lambda_4,\epsilon_{participation}}$	λ_4	x_2

Table 3.2: Groups of states for $\epsilon_{participation} = 0.7$

	Eigenvalue	Group of states that participate in the eigenvalue
$P_{\lambda_1,\epsilon_{participation}}$	λ_1	x_1, x_2
$P_{\lambda_{2,3},\epsilon_{participation}}$	$\lambda_{2,3}$	x_3, x_4
$P_{\lambda_4,\epsilon_{participation}}$	λ_4	x_1, x_2

Table 3.3: Groups of states for $\epsilon_{participation} = 0.9$

For both cases, groups of eigenvalues are formed and the groups of states are merged if necessary. This gives Table 3.4 and 3.5.

	Group of eigenvalues	Associated group of states
P_1	λ_1	x_1
P_2	$\lambda_{2,3}$	x_3, x_4
P_3	λ_4	x_2

Table 3.4: Groups of eigenvalues for $\epsilon_{participation} = 0.7$

	Group of eigenvalues	Associated group of states
P_1	λ_1, λ_4	x_1, x_2
P_2	$\lambda_{2,3}$	x_3, x_4

Table 3.5: Groups of eigenvalues for $\epsilon_{participation} = 0.9$

In both cases, the remaining groups are disjoint. This means that the process is finished. The eigenvalues of a group only depend on the state variables of the associated group and the states of a group only participate in the eigenvalues of the associated group.

One can remark that the higher the participation criterion is, the less groups there are.

Now that the groups are formed, residualizing the states of a same group discards the associated poles and keeps the other almost unchanged.

3.1.3 Conclusion

In this section, two important aspects that are common to the developed MOR methods have been presented:

- The state residualization consists in neglecting the derivative of the considered state variable and thus transforming it into an algebraic variable, reducing the order of the model. This is the basis of all the MOR methods that are presented in the following. This approach has the advantage of keeping the variables of the system which simplifies the analysis and the tuning of new controllers if necessary (it is possible to add new loops directly on the reduced model, which is shown on an example in chapter 4).

- The modal approach analyses the participation factors of the linearised model to give the dependencies between the state variables and the poles of the system. Knowing that, groups of eigenvalues/state variables are formed. All the eigenvalues of a same group depend only on the states of the associated group and all the state variables of a same group participate only in the eigenvalues of the associated group. These groups add a constraint on the states to residualize: the states of a same group must be residualized together or not at all. This ensures a preservation of the poles of the system and thus that the operating point remains stable. This approach is close to the modal truncation [39]. But unlike it, it keeps the variables because there is no truncation and no basis change.

The two aspects can be summed up as follows: the developed MOR methods consist in finding a matrix E to reduce the model by state residualization. This matrix must be in $\mathbb{E}_{\epsilon_{participation}}$, which means that it should be diagonal, made of 0 and 1, and respect the constraints deduced from the participation factors analysis. The reduced model is presented in (3.12):

$$\begin{cases} E\dfrac{dx_{diff}}{dt} = f(x_{diff}, x_{alg}, u) \\ 0 = g(x_{diff}, x_{alg}, u) \\ y = h(x_{diff}, x_{alg}, u) \\ E = diag(\delta_i), \delta_i \in \{0; 1\}, \forall i \end{cases} \tag{3.12}$$

The following section presents different strategies to choose this E matrix in order to have an accurate and sufficiently reduced model that is adapted to the test case under consideration. In other words, these strategies help identifying the groups of states to residualize/the groups of poles to discard depending on the test case under consideration.

3.2 Developed strategies to choose the groups of states to residualize/the groups of poles to discard

This section presents the three developed strategies to choose the groups of states to residualize and the groups of poles to discard.

The first one consists in discarding the fastest poles, i.e. the one with the largest negative real part. It is inspired by the modal truncation [40].

The second one, inspired by the modal truncation like the first one but also by the balanced truncation [46], consists in discarding the poles that depend on the less observable and reachable states in the balanced realization.

The third one is based on an optimization to find a E matrix that minimizes an error criterion defined in advance.

The advantages and drawbacks of each method are presented here. In this chapter, each method is applied on a small order 4 example as illustration. Some application on realistic test cases are shown in chapter 4.

First, the DAE system to reduce is considered in (3.1). The process explained in the first section of this chapter is performed and N_{groups} groups P_i of state variables are formed, each one associated to a group L_i of eigenvalues in which they participate, for a given participation criterion $\epsilon_{participation}$.

3.2.1 Strategy 1: discarding the fastest poles

The synoptic in Figure 3.3 sums up the different steps of the first strategy. They are explained in details in the following.

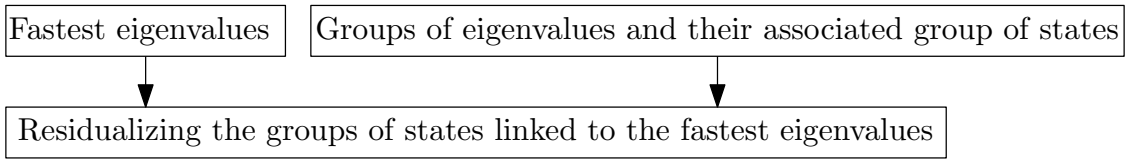

Figure 3.3: Synoptic describing the first strategy

Identifying the fastest poles

The first step in this strategy is to explain when a pole is considered faster than another. It is explained in (3.13) for two stable poles λ_i and λ_j. This time-scale separation between slow and fast poles is classical in the analysis of power systems [86]. The fast poles are linked to fast transients that quickly reach the steady-state and which can therefore be neglected in most cases (it is seen on test cases in chapter 4 that this is not true any more on certain cases when the PE penetration is high).

$$\forall \lambda_i \in \mathbb{C}, \forall \lambda_j \in \mathbb{C}, \lambda_i \text{ is faster than } \lambda_j \Leftrightarrow Re(\lambda_i) < Re(\lambda_j) < 0 \tag{3.13}$$

When represented on the complex plane, the fastest poles are the one that are the farther from the imaginary axis, i.e. on the left side of the plane.

Residualizing the groups of states linked to the fastest poles

The idea of this strategy is to residualize the groups of states that are linked to the fastest poles and keep the dynamics of the groups of states that are linked to the slowest poles. This approach is classical in the power system community. This is for example the idea of the phasor approximation.

To proceed, the groups of eigenvalues/state variables obtained with the modal approach are ranked so that the first group contains the slowest pole.

Then the states of the last groups are residualized to discard the fastest poles of the system.

With the developed method, based on the participation of the states in the eigenvalues, it is not possible to discard each pole separately and independently. It means that it is not possible to choose the order of the reduced model completely freely because of the constraints induced by the groups of poles/state variables deduced from the participation factors analysis.

Remarks on the strategy

This method is actually similar to the modal truncation [65]. The difference here is that, by avoiding a truncation, the modal reduction by residualization presented in this report, preserves the variables of the system, and thus its structure, making it easier to analyse and to add new control loops (see chapter 4 for an example).

One advantage of choosing to discard the fastest poles and keep the slow ones is that the process is direct. It is indeed very simple to identify the slow and the fast poles of the system.

Because it keeps the slow poles, the one that are close to the imaginary axis in the complex plane, this strategy is particularly adapted to stability analysis. The slow poles are indeed the most critical in terms of stability, because they can easily be moved to the right half of the complex plane if a parameter changes. This is why they need to be kept for this kind of analysis.

On the other hand, this method presents some drawbacks. First, for all observed variable (a current, a frequency or a voltage for instance) and for all considered event (a load step, a short-circuit or a line tripping for example), the reduced model, for a given order, is always the same. The poles are indeed the same in all those cases, so are their classification (fast/slow). This is not very flexible. One can indeed imagine that the reduced model should not be the same between a case where the current in a certain converter is observed during a short circuit close to it and a case where the frequency of the system is observed during a load step. This problem is solved with the two other

strategies that are presented in the next two subsections. Second, discarding fast poles means neglecting fast transients. These fast transients can be over-currents, that are quickly cleared but that can damage the device (it is especially the case with PE, more than wit SM). This is why they need to be taken into account when studying over-current capability. This problem is also solved with the two other strategies presented hereafter.

Illustration with an order 4 model

To illustrate the strategy, the order 4 LTI model in 3.14 is considered.

$$\begin{cases} \dfrac{dx}{dt} = Ax + Bu = \begin{pmatrix} -50 & -25 & 5 & 1 \\ -10 & -20 & 1 & 1 \\ 5 & 1 & -10 & -10 \\ 10 & 1 & 10 & -10 \end{pmatrix} x + \begin{pmatrix} 1 \\ 1 \\ 1 \\ 1 \end{pmatrix} u \\ \quad y = \begin{pmatrix} 0 & 0 & 0 & 0 \\ 0 & 1 & 0 & 0 \\ 0 & 0 & 0 & 0 \\ 0 & 0 & 0 & 0 \end{pmatrix} x \end{cases} \tag{3.14}$$

The previously formed groups of states and eigenvalues in 3.6 and 3.7, corresponding to this order 4 example, are considered.

	Group of eigenvalues	Associated group of states
P_1	$\lambda_1 = -57.8$	x_1
P_2	$\lambda_{2,3} = -9.4 \pm 10.5i$	x_3, x_4
P_3	$\lambda_4 = -13.4$	x_2

Table 3.6: Groups of eigenvalues for $\epsilon_{participation} = 0.7$

	Group of eigenvalues	Associated group of states
P_1	λ_1, λ_4	x_1, x_2
P_2	$\lambda_{2,3}$	x_3, x_4

Table 3.7: Groups of eigenvalues for $\epsilon_{participation} = 0.9$

The fastest pole is λ_1, followed by λ_4. Depending on the choice of $\epsilon_{participation}$, several reduced models can be deduced:

- if $\epsilon_{participation} = 0.7$:
  - an order 3 model that discards λ_1 by residualizing x_1;

- an order 2 model that discards λ_1 and λ_4 by residualizing x_1 and x_2;

- if $\epsilon_{participation} = 0.9$:

  - an order 2 model that discards λ_1 and λ_4 by residualizing x_1 and x_2;

3.2.2 Strategy 2: discarding the poles that depend on the less observable and reachable states in the balanced realization

The second strategy to choose the groups of poles to discard/the groups of state variables to residualize, is presented in this subsection. As said previously, it is inspired by the modal truncation and the balanced truncation. But unlike them, it does not truncate the system in order to maintain the physical structure and keep the variables during the MOR.

The synoptic in Figure 3.4 sums up the different steps of the second strategy. They are explained in details in the following.

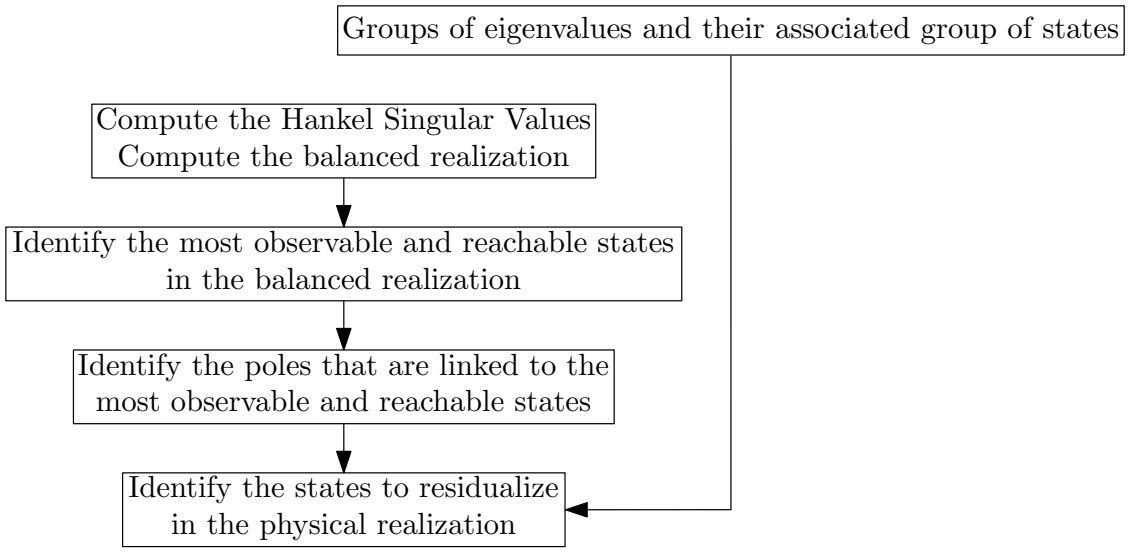

Figure 3.4: Synoptic describing the second strategy

Computing the Hankel Singular Values and the balanced realization

The DAE system to reduce is considered in (3.15).

$$\begin{cases} \dfrac{dx_{diff}}{dt} = f(x_{diff}, x_{alg}, u) \\ 0 = g(x_{diff}, x_{alg}, u) \\ y = h(x_{diff}, x_{alg}, u) \\ x_{diff} \in \mathbb{R}^{N_{diff}}, x_{alg} \in \mathbb{R}^{N_{alg}}, u \in \mathbb{R}^p, y \in \mathbb{R}^q \end{cases} \tag{3.15}$$

It is linearised around its operating point, which gives (3.16).

$$\begin{cases} \dfrac{dx}{dt} = Ax + Bu \\ y = Cx + Du \\ x \in \mathbb{R}^{N_{diff}}, u \in \mathbb{R}^p, y \in \mathbb{R}^q \end{cases} \tag{3.16}$$

This system is rewritten in the balanced realization as in (3.17). It is explained in chapter 1 how to obtain this balanced realization.

$$\begin{cases} \dfrac{dx_b}{dt} = A_b x_b + B_b u \\ y = C_b x_b + Du \\ x_b \in \mathbb{R}^{N_{diff}}, u \in \mathbb{R}^p, y \in \mathbb{R}^q \end{cases} \tag{3.17}$$

The gramians in the balanced realization are diagonal and equal. The HSV in their diagonal are written σ_i, as shown in (3.18). The HSV of the system are unique.

$$P_b = Q_b = diag(\sigma_1, ..., \sigma_{N_{diff}}), \text{ where } \sigma_1 > \sigma_2 > ... > \sigma_{N_{diff}} \tag{3.18}$$

One HSV is associated to each state in the balanced realization. It quantifies the degree of reachability and observability of each state in the balanced realization. The bigger it is, the more reachable and observable the state is. In this case x_{b_1} is the most observable and reachable state and $x_{b_{N_{diff}}}$ is the less observable and reachable state.

Identifying the group of the most observable and reachable states in the balanced realization

A criterion ϵ_{HSV} between 0 and 1 is chosen. The HSV are normalized so that their sum is equal to 1 (each HSV is just divided by the sum of the HSV). A set $P_{b,\epsilon_{HSV}}$ of the k most observable and reachable states is created as explained in (3.19).

$$P_{b,\epsilon_{HSV}} = \{x_{b_1}, ..., x_{b_k}\} / \sum_{i=1}^{k} \sigma_i \geq \epsilon_{HSV}, \sum_{i=1}^{k-1} \sigma_i < \epsilon_{HSV} \tag{3.19}$$

One can remark that, as the gramians and the HSV depend on the C matrix, this group depends on the observed variable. The most observable and reachable states are not the same when the observed variables y change.

Identifying the group of poles in which the most observable and reachable states participate

A participation factor analysis, made in the balanced realization, can tell in which poles the selected states participate (see the previous section for more information on how this is done). Groups of state variables P_{b_i}, each one with its associated group of eigenvalues L_{b_i} in which they participate, are created using the same process as the one explained in the last section, with the criterion $\epsilon_{participation}$. Two new sets $P_{b,\epsilon_{HSV},\epsilon_{participation}}$ and $L_{b,\epsilon_{HSV},\epsilon_{participation}}$ are created using (3.20).

$$\forall x_{b_j} \in P_{b,\epsilon_{HSV}}, \forall P_{b_i}, x_{b_j} \in P_{b_i} \Rightarrow \begin{cases} P_{b_i} \subset P_{b,\epsilon_{HSV},\epsilon_{participation}} \\ L_{b_i} \subset L_{b,\epsilon_{HSV},\epsilon_{participation}} \end{cases} \tag{3.20}$$

One can remark that $P_{b,\epsilon_{HSV}}$ is included in the new set $P_{b,\epsilon_{HSV},\epsilon_{participation}}$. The difference is that other state variables might be in the new set in order to respect the constraints deduced from the participation factor analysis. It is indeed possible that a state with a small HSV participate in the same eigenvalue as a state with a high HSV. This state needs to be put in the new set to respect the couplings. The new set $P_{b,\epsilon_{HSV},\epsilon_{participation}}$ contains not only the most observable and reachable states, but also the states that participate in the same group of eigenvalues. The set $L_{b,\epsilon_{HSV},\epsilon_{participation}}$ contains all these eigenvalues.

With this method, the poles to keep are in $L_{b,\epsilon_{HSV},\epsilon_{participation}}$, the other can be discarded. In [63], these poles are discarded by doing a modal truncation. In this report, another step, consisting in another participation factors analysis, is added to proceed to a residualization in the physical realization and thus keep the variables and the structure of the system.

Residualizing the states in the physical realization that participate in the poles that are linked to the less observable and reachable states in the balanced realization

The main idea here is that the eigenvalues of the system in the balanced and in the physical realization are the same. This way it is easy to identify the states in the physical realization that participate in the poles that depend on the less observable and reachable states in the balanced realization. And these poles have been identified previously, they are in $L_{b,\epsilon_{HSV},\epsilon_{participation}}$.

The two sets $P_{b,\epsilon_{HSV},\epsilon_{participation}}$ and $L_{b,\epsilon_{HSV},\epsilon_{participation}}$ are considered. The same $\epsilon_{participation}$ is considered here. A participation factors analysis in the physical realization gives sets P_i and L_i (just like in the balanced realization it gave P_{b_i} and L_{b_i}).

Two new sets $P_{\epsilon_{HSV},\epsilon_{participation}}$ and $L_{\epsilon_{HSV},\epsilon_{participation}}$ are created as in (3.21).

$$\forall \lambda_j \in L_{b,\epsilon_{HSV},\epsilon_{participation}}, \forall L_i, \lambda_j \in L_i \Rightarrow \begin{cases} P_i \subset P_{\epsilon_{HSV},\epsilon_{participation}} \\ L_i \subset L_{\epsilon_{HSV},\epsilon_{participation}} \end{cases} \tag{3.21}$$

The new set $P_{\epsilon_{HSV},\epsilon_{participation}}$ contains the state variables in the physical realization that participate in $L_{b,\epsilon_{HSV},\epsilon_{participation}}$ and that are not residualized. All the other states are. This way, the poles in $L_{\epsilon_{HSV},\epsilon_{participation}}$ are kept and all the other poles are discarded. One can remark that $L_{b,\epsilon_{HSV},\epsilon_{participation}}$ is included in the new set $L_{\epsilon_{HSV},\epsilon_{participation}}$.

The criterion ϵ_{HSV} is the one that defines the size of the reduced model. If it is close to 1, the model is less reduced than if it is close to 0.

The desired size for the reduced system can be chosen in advance and then the idea is to find the biggest ϵ_{HSV} that gives a reduced model with a size that is smaller or equal to it.

Summary

The strategy presented in this subsection can be summed up in Figure 3.5.

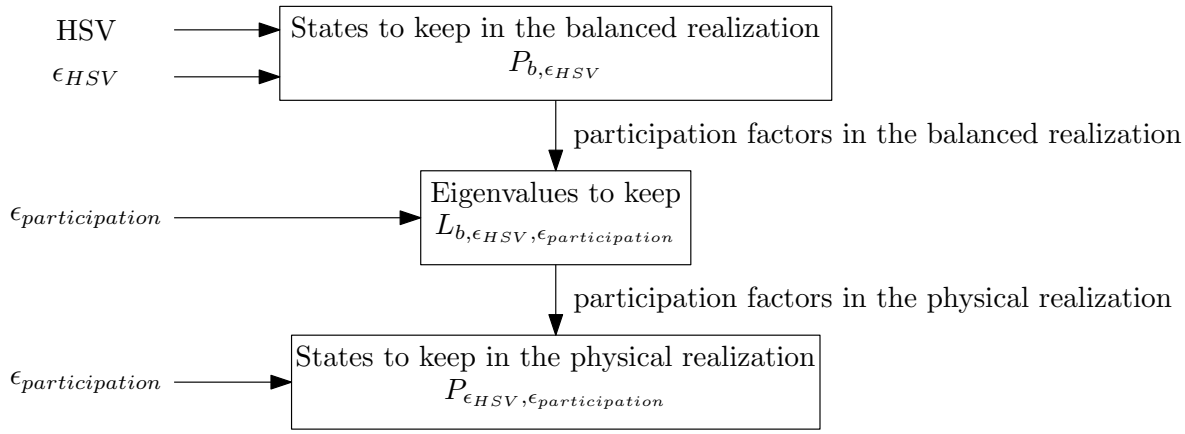

Figure 3.5: Summary of the second strategy

Remarks on the strategy

With this method, the poles that are discarded are not necessarily the fastest. Depending on what is observed (which variables), the given reduced model is not the same (see chapter 4 for some examples). This method proves to be flexible and adapts to the case under consideration.

Another advantage is that the process to identify the states to residualize/the poles to discard is quite straightforward and does not require a high computation time.

On the other hand, it is not possible to take into account each simulated event separately to deduce the reduced model. The B matrix that takes into account the inputs of the system can not be chosen freely, and is imposed by the model, unlike the C matrix for the observed variables.

Another remark is that, because it uses two participation factors analyses in a row, if the system is very coupled, it results in a not very reduced system. For example,

consider a 10^{th} order model. If the HSV analysis chooses 1 state to keep in the balanced realization (this is the minimum, with a low ϵ_{HSV}) and if this state participates in 4 different eigenvalues that each depend on 2 different state variables in the physical realization, this results in a 8^{th} order reduced model, which is not a good reduction. As a result, this method is powerful only when the system is well decoupled. A solution to solve this could be to reduce $\epsilon_{participation}$. But there is a risk that the participation is not enough taken into account any more, which induces a change in the remaining poles of the system (with the possibility for some of them to become unstable).

Some of these remarks are illustrated in chapter 4 with realistic test cases.

Illustration with an order 4 model

To illustrate the strategy, the order 4 LTI model in 3.22 is considered.

$$\begin{cases} \dfrac{dx}{dt} = Ax + Bu = \begin{pmatrix} -50 & -25 & 5 & 1 \\ -10 & -20 & 1 & 1 \\ 5 & 1 & -10 & -10 \\ 10 & 1 & 10 & -10 \end{pmatrix} x + \begin{pmatrix} 1 \\ 1 \\ 1 \\ 1 \end{pmatrix} u \\ \quad y = \begin{pmatrix} 0 & 0 & 0 & 0 \\ 0 & 1 & 0 & 0 \\ 0 & 0 & 0 & 0 \\ 0 & 0 & 0 & 0 \end{pmatrix} x \end{cases} \tag{3.22}$$

In this system, the observed variable is x_2.

The HSV are computed. One HSV is associated to each state in the balanced realization. It gives Table 3.8.

	x_{b_1}	x_{b_2}	x_{b_3}	x_{b_4}
HSV	0.95	0.04	0.01	0

Table 3.8: Hankel Singular Values of the order 4 system

ϵ_{HSV} is chosen to be equal to 0.9. It means that the only kept state in the balanced realization is x_{b_1} (with an HSV of 0.95).

The participation factors analysis forms the following groups of eigenvalues and states in Table 3.9 with $\epsilon_{participation} = 0.7$ and in the balanced realization.

Group of eigenvalues	Associated group of states
$\lambda_1 = -57.8$	x_{b_2}
$\lambda_{2,3} = -9.4 \pm 10.5i$	x_{b_3}, x_{b_4}
$\lambda_4 = -13.4$	x_{b_1}

Table 3.9: Groups of eigenvalues in the balanced realization for $\epsilon_{participation} = 0.7$

From this table, it is deduced that the only pole to keep is λ_4.

The previously formed groups of states and eigenvalues in the physical realization are considered in 3.10, with $\epsilon_{participation} = 0.7$.

Group of eigenvalues	Associated group of states
$\lambda_1 = -57.8$	x_1
$\lambda_{2,3} = -9.4 \pm 10.5i$	x_3, x_4
$\lambda_4 = -13.4$	x_2

Table 3.10: Groups of eigenvalues in the physical realization for $\epsilon_{participation} = 0.7$

From this table, it is deduced that the only state to keep is x_2. The other states can be residualized, which leads to an order 1 reduced model. As expected, the observed variable is the most important to keep.

3.2.3 Strategy 3: discarding some poles to minimize an error criterion

The last developed strategy is based on an optimization to find the residualization matrix E that minimizes an error criterion. The process is explained here step by step and summed up in the synoptic in Figure 3.6.

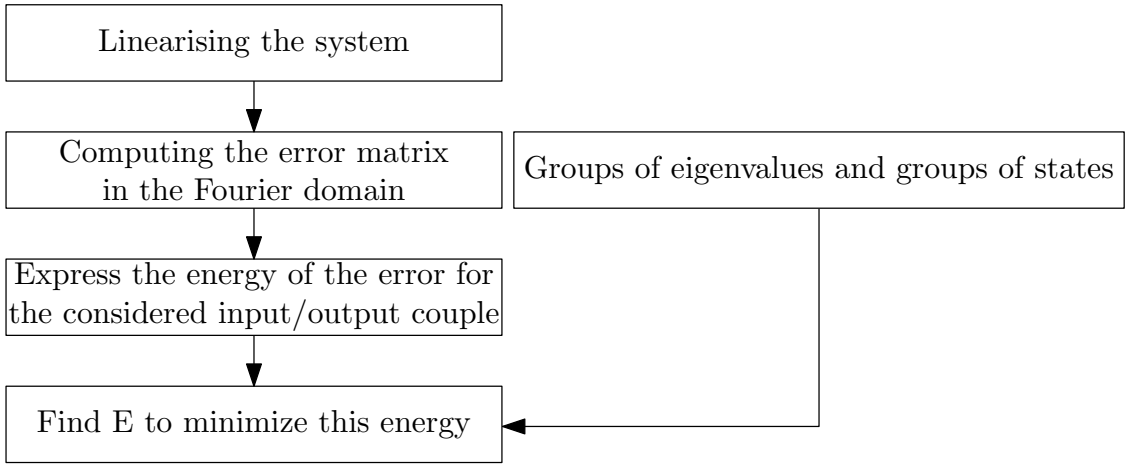

Figure 3.6: Synoptic describing the third strategy

Linearisation

Like the two other strategies, the residualization is done on the nonlinear DAE system in (3.1), but the process to find the residualization matrix E uses a linearisation of this model, like in (3.23).

$$\begin{cases} \dfrac{dx}{dt} = Ax + Bu \\ y = Cx + Du \\ x \in \mathbb{R}^{N_{diff}}, u \in \mathbb{R}^p, y \in \mathbb{R}^q \end{cases} \tag{3.23}$$

The reduced nonlinear DAE system is also linearised around the same operating point and it gives (3.24).

$$\begin{cases} E\dfrac{dx_r}{dt} = Ax_r + Bu \\ y_r = Cx_r + Du \\ x \in \mathbb{R}^{N_{diff}}, u \in \mathbb{R}^p, y \in \mathbb{R}^q \end{cases} \tag{3.24}$$

Error matrix in the Fourier representation

A Fourier transform is applied on the two systems. For (3.23), it leads to (3.25). For (3.24), it leads to (3.26).

$$\begin{cases} j\omega X = AX + BU \\ Y = CX + DU \end{cases} \tag{3.25}$$

$$\begin{cases} j\omega E X_r = AX_r + BU \\ Y_r = CX_r + DU \end{cases} \tag{3.26}$$

Some manipulations give the transfer functions in (3.27) and (3.28).

$$Y = (C(j\omega I_{N_{diff}} - A)^{-1}B + D)U \tag{3.27}$$

$$Y_r = (C(j\omega E - A)^{-1}B + D)U \tag{3.28}$$

The difference between these two transfer functions gives (3.29).

$$\begin{cases} Y - Y_r = \epsilon(\omega)U \\ \text{with } \epsilon(\omega) = C[(j\omega I_{N_{diff}} - A)^{-1} - (j\omega E - A)^{-1}]B \in \mathbb{C}^{q\times p} \end{cases} \tag{3.29}$$

The new matrix $\epsilon(\omega)$ is called the error matrix in this report.

One can remark that if $E = I_{N_{diff}}$, the system is not reduced and $\epsilon(\omega) = 0, \forall\omega$, as expected.

Energy of the error for a specific input-output couple

The error for the output Y_i with respect to the input U_j is a scalar given by $\epsilon_{i,j}(\omega)$, the element of $\epsilon(\omega)$ in the i^{th} row and j^{th} column. It corresponds to the error for a specific input/output couple, in other words for a specific simulated event/observed variable couple.

The energy of this error $\boldsymbol{\epsilon_{i,j}}$ is defined in (3.30). This is the error criterion to minimize in the rest of this subsection.

$$\boldsymbol{\epsilon_{i,j}} = \int_{-\infty}^{\infty} |\epsilon_{i,j}(\omega)|^2 d\omega \tag{3.30}$$

The Parseval's identity gives (3.31).

$$\int_{-\infty}^{\infty} |\epsilon_{i,j}(\omega)|^2 d\omega = 2\pi \int_{-\infty}^{\infty} |\epsilon_{i,j}(t)|^2 dt \tag{3.31}$$

This means that the energy of the error is the same in time-domain and in Fourier-domain.

This criterion to minimize is chosen as it allows to have a reduced model that is specific to each simulated event and observed variable, and because the Parseval identity proves that it also minimizes the energy error in time-domain.

Other criteria to minimize have been studied in the literature. For instance [87] studies another criterion that allows to take into account all the possible events and that is intrinsic to the model. This allows to obtain one model for all the simulated event.

However, in this thesis, a specific model for each simulated event is looked for and, for a given size, it should be the most adapted one for this simulation.

Minimization problem for a specific input-output couple

Knowing this, it is possible to choose the E matrix to minimize $\boldsymbol{\epsilon_{i,j}}$, which minimizes the energy of the error in time-domain. This E matrix is specific to the output-input couple (i,j). There is a different reduced model for each considered test case: observed variables-output/simulated event-input.

The deduced optimization problem is presented in (3.32). As always in the developed method, the E matrix must be in $\mathbb{E}_{\epsilon_{participation}}$ to respect the couplings of the system and discard some poles without moving too much the others (see previous section for more explanation). The desired size for the reduced model is written n.

$$\begin{cases} \underset{E}{\text{minimize}}\ \boldsymbol{\epsilon_{i,j}} = \int_{-\infty}^{\infty} |\epsilon_{i,j}(\omega)|^2 d\omega \\ \text{subject to } E \in \mathbb{E}_{\epsilon_{participation}},\ tr(E) \leq n \end{cases} \tag{3.32}$$

The minimization problem to solve is a discrete one. The E matrix to find is indeed a diagonal matrix made of 0 and 1. As a consequence, the classical optimization algorithms, like the Newton-Raphson algorithm cannot be used here.

One solution could be to list all the possible E matrices, test all of them, and choose the one that minimizes the error. This is what has been done in [88] and it is called brute-force method in this report. This works fine with small problems. However, if the size of the problem is N, there are 2^N possible E matrices, which can quickly become a problem in terms of computation time.

Therefore, a method using a genetic algorithm has been used for reducing large systems. A genetic algorithm is a search heuristic that is inspired by the theory of evolution. It reflects the process of natural selection where the most adapted individuals of a generation are selected for reproduction to produce offspring in the next generation. More information on the theory of this type of algorithm can be found in [89]. The use of this algorithm allows to have a low computation time compared to the brute-force method.

Remarks on the strategy

One advantage of this strategy is that it takes into account the observed variable (the output, here the i in the optimization) and the simulated event (the input, here the j in the optimization) to give a E matrix that minimizes the proposed error criterion for this specific input-output couple. This makes it flexible and adaptable.

As this strategy uses an optimization, it can take some time to find the optimal E matrix for large systems. However, in most cases, the gain in terms of simulation time with the reduced model compensates it. And the analysis is also simplified because the number of differential variables has decreased. This is illustrated in chapter 4.

Illustration with an order 4 model

To illustrate the strategy, the order 4 LTI model in 3.33 is considered.

$$\begin{cases} \dfrac{dx}{dt} = Ax + Bu = \begin{pmatrix} -50 & -25 & 5 & 1 \\ -10 & -20 & 1 & 1 \\ 5 & 1 & -10 & -10 \\ 10 & 1 & 10 & -10 \end{pmatrix} x + \begin{pmatrix} 1 \\ 1 \\ 1 \\ 1 \end{pmatrix} u \\ \quad y = \begin{pmatrix} 0 & 0 & 0 & 0 \\ 0 & 1 & 0 & 0 \\ 0 & 0 & 0 & 0 \\ 0 & 0 & 0 & 0 \end{pmatrix} x \end{cases} \tag{3.33}$$

The energy of the error $\boldsymbol{\epsilon_{i,j}}$ is minimized with a genetic algorithm for $i = 2$ (x_2 is observed), $j = 1$ (there is only one input in this example) and with a desired size of 1 for the reduced model. The result of this minimization is that the states to residualize are x_1, x_3 and x_4 just like with the previous strategy.

One can remark that with this method, as it is possible to choose the observed variables during the optimization, the choice of C has less influence than for the second strategy. For example, if it had been chosen to be equal to the identity matrix but still with $i = 2$ and $j = 1$ for the optimization, the result would have been the same; which is not the case with the second strategy.

3.2.4 Conclusion

This section has presented the three developed strategies to find the groups of poles to discard/the groups of state variables to residualize:

- The first one consists in residualizing in the nonlinear model the state variables that participate in the fastest poles of the linearised model.
- The second one consists in residualizing in the nonlinear model the state variables that participate in the poles in the linearised model that depend on the less observable and reachable states in the balanced realization.
- The third one consists in residualizing in the nonlinear model some state variables to minimize an error criterion.

A comparison of the characteristics of the three strategies is proposed in Table 3.11.

	Time to find the reduced model	Taking into account the observed variable	Taking into account the simulated event
Strategy 1	short	no	no
Strategy 2	short	yes	no
Strategy 3	long	yes	yes

Table 3.11: Comparison of the characteristics of the three developed strategies

The outcome of this comparison is that depending on the type of study and the knowledge of the test case, a strategy can be proposed:

- For a stability analysis, the first strategy is the most appropriate as it keeps the slow poles that are the most critical in terms of stability. Moreover, its application is straight-forward.
- When studying a particular variable (a current in a converter for example), two cases are possible:
  - if there is no information on the simulated events, the second strategy is recommended,
  - if the simulated event is known, the third strategy is the most appropriate.

This is illustrated in more details in chapter 4.

One need to notice that, although the residualization is made on the nonlinear system, which allows keeping the non linearities in the reduced model, the residualization matrix E is deduced, in each strategy, from an analysis of the linearised system.

3.3 Chapter conclusion

This chapter presented the methodologies of the developed MOR methods. The three methods are all based on the same two principles:

- The residualization: it consists in transforming differential variables (state variables) into algebraic variables to reduce the order of the model. Its advantage is that it keeps the variables of the system and thus its physical structure.
- The modal approach: it consists in choosing the variables that can be residualized in order to discard some poles of the system and keep the other almost unmoved. This approach guarantees that the operating point remains stable during the MOR. It adds a constraint on the variables to be residualized: some variables must be residualized (or kept) together and not independently.

Then each of the three strategies proposes a different way to choose the variables to residualize, while respecting the presented constraints at the same time:

- The first strategy proposes to residualize the state variables that participate in the fastest poles. It is well adapted to stability analysis.
- The second strategy proposes to residualize the state variables that participate in the poles that depend on the less observable and reachable states in the balanced realization. It is well adapted when a specific variable is observed.
- The third strategy proposes to residualize some state variables to minimize an error criterion. It is well adapted when a specific variable is observed and when the events to simulate are known.

After this theoretical presentation of the methods, the next chapter proposes some realistic test cases to which they are applied. Some comparisons are then made and the advantages and drawbacks of each method are illustrated. Moreover this gives some insights on how power systems with a high PE penetration should be modelled.

CHAPTER 4

Application of the methods for the simulation and analysis of transmission systems with a high power electronics penetration

Contents

In this chapter, the methods developed in chapter 3 are applied to several realistic test cases based on the models presented in chapter 2. The idea is to compare the different methods, present their advantages and drawbacks and validate them. Also one goal is to give some insights on how power systems with a high PE penetration should be modelled for accurate and fast simulations and analyses. All the test cases are simulated using the Modelica [90] language. This language indeed consists in writing all the equations directly, which makes the residualization, and therefore the MOR, very convenient.

4.1 Simple test cases

In this first section, the methods are applied to simple test cases. The aim of the first test case is to detail the process of each method in a didactic way to precisely understand how they work. The aim of the second test case is to show that depending on what is observed, a different reduced model should be used. The aim of the third test case is to show that depending on what is simulated (the event), a different reduced model should be used. Moreover, the phasor approximation is not always a good solution and it is proved with this third test case.

4.1.1 One grid forming converter connected to an infinite grid

The first test case to be studied consists in one grid forming converter connected to an infinite grid, as shown on Figure 4.1.

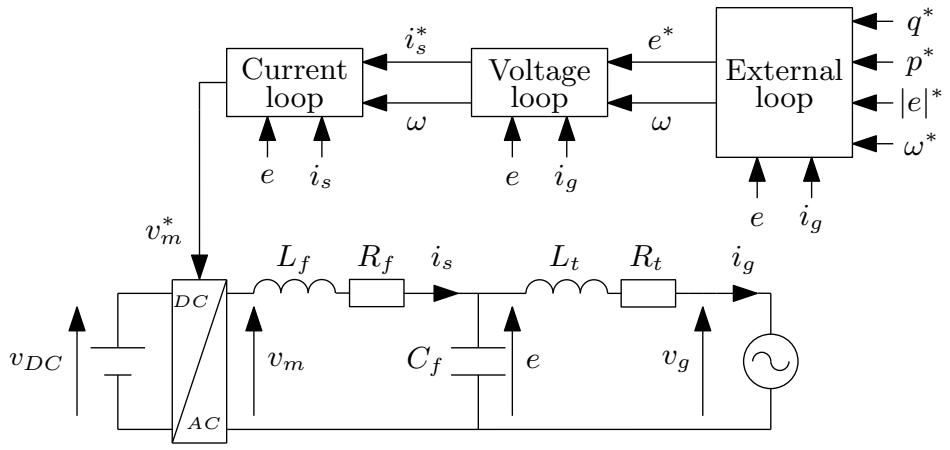

Figure 4.1: Structure of the system studied in the first test case

The converter in this system has been presented in the first section of chapter 2. As a consequence, the studied system here is a 15^{th} order DAE system presented in (4.1).

$$\begin{cases} \dfrac{dx_{diff}}{dt} = f(x_{diff}, x_{alg}, u) \\ 0 = g(x_{diff}, x_{alg}, u) \\ y = h(x_{diff}, x_{alg}, u) \\ x_{diff} = \left(i_{s_d}\ i_{s_q}\ e_d\ e_q\ i_{g_d}\ i_{g_q}\ p_m\ \theta\ q_m\ M_{CL_d}\ M_{CL_q}\ M_{VL_d}\ M_{VL_q}\ M_{AD_d}\ M_{AD_q}\right)^T \\ x_{alg} = \left(v_{m_d}\ v_{m_q}\ v^*_{m_d}\ v^*_{m_q}\ p\ \omega\ q\ e^*_d\ e^*_q\ i^*_{s_d}\ i^*_{s_q}\ v_{g_d}\ v_{g_d}\right)^T \\ u = \left(v_{g_{d_g}}\ v_{g_{q_g}}\ \omega^*\ p^*\ q^*\ |e|^*\right)^T \end{cases} \tag{4.1}$$

The corresponding equations can be found in chapter 2. Two relations have been added. They correspond to the grid voltage in the DQ0 reference frame of the converter v_{g_d} and v_{g_q} using the grid voltage in the DQ0 reference frame of the grid $v_{g_{d_g}}$ and $v_{g_{q_g}}$, which is an input here. They are given in (4.2), with θ the chosen angle for the transformation.

$$\begin{pmatrix} v_{g_d} \\ v_{g_q} \end{pmatrix} = \begin{pmatrix} cos(\theta) & sin(\theta) \\ -sin(\theta) & cos(\theta) \end{pmatrix} \begin{pmatrix} v_{g_{d_g}} \\ v_{g_{q_g}} \end{pmatrix} \tag{4.2}$$

The model of the system is now complete and ready to be simulated. For this test case, a short-circuit at the grid is simulated and cleared after $150ms$. The current in the converter is looked at. The process to find a reduced model with the three methods is detailed hereafter, starting with the participation factors analysis that is common to the three strategies.

Groups of states/eigenvalues

First, the system is linearised around its operating point, which gives the LTI system in (4.3).

$$\begin{cases} \dfrac{dx}{dt} = Ax + Bu \\ y = Cx + Du \\ x \in \mathbb{R}^{15}, u \in \mathbb{R}^6, y \in \mathbb{R}^q \end{cases} \tag{4.3}$$

The eigenvalues of A are computed, as well as the participation factors, which are given in Table 4.1.

	M_{CL_d}	M_{CL_q}	M_{VL_d}	M_{VL_q}	M_{AD_d}	M_{AD_q}	i_{s_d}	i_{s_q}	i_{g_d}	i_{g_q}	p_m	q_m	θ	e_d	e_q
$\lambda_1 = -1.4$	0.19	0.08	0.51	0.25	0	0	0	0	0	0	0	0	0	0	0
$\lambda_{2,3} = -1.5 \pm 0.11i$	0.17	0.35	0.16	0.34	0	0	0	0	0	0	0	0	0	0	0
$\lambda_4 = -1.7$	0.5	0.24	0.19	0.08	0	0	0	0	0	0	0	0	0	0	0
$\lambda_{5,6} = -15.5 \pm 28.2i$	0	0	0	0	0	0	0	0	0	0	0.51	0	0.52	0	0
$\lambda_7 = -16.2$	0	0	0	0	0.41	0.62	0	0	0	0	0	0	0	0	0
$\lambda_8 = -17.2$	0	0	0	0	0.62	0.42	0	0	0	0	0	0	0	0	0
$\lambda_9 = -31.4$	0	0	0	0	0	0	0	0	0	0	0	1	0	0	0
$\lambda_{10,11} = -21 \pm 134i$	0	0	0	0	0	0	0.25	0.25	0.25	0.25	0	0	0	0	0
$\lambda_{12,13} = -759 \pm 3330i$	0	0	0	0	0	0	0.13	0.13	0.13	0.12	0	0	0	0.26	0.25
$\lambda_{14,15} = -790 \pm 3820i$	0	0	0	0	0	0	0.13	0.12	0.13	0.14	0	0	0	0.25	0.25

Table 4.1: Modulus of the participation factors for the first test case

The participation criterion $\epsilon_{participation} = 0.99$ is chosen. It is then possible to identify the states that participate the most in each eigenvalue, in Table 4.2.

Eigenvalue	State variables
$\lambda_1 = -1.4$	M_{CL_d}, M_{CL_q}, M_{VL_d}, M_{VL_q}
$\lambda_{2,3} = -1.5 \pm 0.1i$	M_{CL_d}, M_{CL_q}, M_{VL_d}, M_{VL_q}
$\lambda_4 = -1.7$	M_{CL_d}, M_{CL_q}, M_{VL_d}, M_{VL_q}
$\lambda_{5,6} = -15.5 \pm 28.2i$	p_m, θ
$\lambda_7 = -16.2$	M_{AD_d}, M_{AD_q}
$\lambda_8 = -17.2$	M_{AD_d}, M_{AD_q}
$\lambda_9 = -31.4$	q_m
$\lambda_{10,11} = -21 \pm 134i$	i_{s_d}, i_{s_q}, i_{g_d}, i_{g_q}
$\lambda_{12,13} = -759 \pm 3330i$	i_{s_d}, i_{s_q}, i_{g_d}, i_{g_q}, e_d, e_q
$\lambda_{14,15} = -790 \pm 3820i$	i_{s_d}, i_{s_q}, i_{g_d}, i_{g_q}, e_d, e_q

Table 4.2: States that participate the most in each eigenvalue for the first test case

This table helps creating the groups of eigenvalues and their associated group of states that participate in them. This is shown in Table 4.3.

Eigenvalues	State variables	Group name
λ_1, $\lambda_{2,3}$, λ_4	M_{CL_d}, M_{CL_q}, M_{VL_d}, M_{VL_q}	P_1
$\lambda_{5,6}$	p_m, θ	P_2
λ_7, λ_8	M_{AD_d}, M_{AD_q}	P_3
λ_9	q_m	P_4
$\lambda_{10,11}$, $\lambda_{12,13}$, $\lambda_{14,15}$	i_{s_d}, i_{s_q}, i_{g_d}, i_{g_q}, e_d, e_q	P_5

Table 4.3: Groups of states and eigenvalues for the first test case

This table gives the possible reduced models, which are summed up in Table 4.4. If

N_{groups} is the number of groups created previously, there are $2^{N_{groups}}$ possible models. Here there are 32 possible reduced models.

Model order	Model name	Residualized groups	Kept groups
0	0	P_1, P_2, P_3, P_4, P_5	
1	1	P_1, P_2, P_3, P_5	P_4
2	2a	P_1, P_3, P_4, P_5	P_2
2	2b	P_1, P_2, P_4, P_5	P_3
3	3a	P_1, P_3, P_5	P_2, P_4
3	3b	P_1, P_2, P_5	P_3, P_4
4	4a	P_2, P_3, P_4, P_5	P_1
4	4b	P_1, P_4, P_5	P_2, P_3
5	5a	P_2, P_3, P_5	P_1, P_4
5	5b	P_1, P_5	P_2, P_3, P_4
6	6a	P_3, P_4, P_5	P_1, P_2
6	6b	P_2, P_4, P_5	P_1, P_3
6	6c	P_1, P_2, P_3, P_4	P_5
7	7a	P_3, P_5	P_1, P_2, P_4
7	7b	P_2, P_5	P_1, P_3, P_4
7	7c	P_1, P_2, P_3	P_4, P_5
8	8a	P_4, P_5	P_1, P_2, P_3
8	8b	P_1, P_3, P_4	P_2, P_5
8	8c	P_1, P_2, P_4	P_3, P_5
9	9a	P_5	P_1, P_2, P_3, P_4
9	9b	P_1, P_3	P_2, P_4, P_5
9	9c	P_1, P_2	P_3, P_4, P_5
10	10a	P_2, P_3, P_4	P_1, P_5
10	10b	P_1, P_4	P_2, P_3, P_5
11	11a	P_2, P_3	P_1, P_4, P_5
11	11b	P_1	P_2, P_3, P_4, P_5
12	12a	P_3, P_4	P_1, P_2, P_5
12	12b	P_2, P_4	P_1, P_3, P_5
13	13a	P_3	P_1, P_2, P_4, P_5
13	13b	P_2	P_1, P_3, P_4, P_5
14	14	P_4	P_1, P_2, P_3, P_5
15	15		P_1, P_2, P_3, P_4, P_5

Table 4.4: Possible reduced models for the first test case

Now that all the possible reduced models are known, the three developed strategies help choosing which one is the most adapted, depending on the observed variable, the simulated event and the desired size for the reduced model.

The desired size for the reduced model is here chosen arbitrarily as 6 (chosen as an example). The three methods are then applied to the test case to choose the reduced model between the models $6a$, $6b$ and $6c$.

It is a voluntary simple test case study to illustrate the proposed method. More complex examples are illustrated in the next sections.

First strategy

The application of the first strategy is quite direct. The slowest poles are indeed λ_1, $\lambda_{2,3}$, λ_4 and $\lambda_{5,6}$. As a result, the deduced reduced model is the model $6a$ that residualizes the groups P_3, P_4 and P_5, and keeps the dynamics of the states in the groups P_1 and P_2.

Second strategy

Before applying the second strategy, the h function is chosen so that the outputs of the system (the observed variables) are the currents i_{s_d} and i_{s_q}. This function (which gives the C matrix when the system is linearised) is necessary with this strategy as the observed variable is considered here (which is not the case with the first strategy).

To apply the second strategy, the HSV and the balanced realization of the model are computed. The HSV are given in Table 4.5.

	x_{b_1}	x_{b_2}	x_{b_3}	x_{b_4}	x_{b_5}	x_{b_6}	x_{b_7}	x_{b_8}	x_{b_9}	$x_{b_{10}}$	$x_{b_{11}}$	$x_{b_{12}}$	$x_{b_{13}}$	$x_{b_{14}}$	$x_{b_{15}}$
HSV (in %)	11.1	11	10.2	9.1	8.4	8.3	7.1	7	6.3	6.3	6.2	6.1	1.5	1	0.4

Table 4.5: HSV of the model for the first test case

A participation factors analysis in the balanced realization and in the physical realization helps creating the groups of state variables/eigenvalues. They are shown in Table 4.6, starting from the most observable and reachable states in the balanced realization.

State variables	Eigenvalues	State variables	Group name
x_{b_1}, x_{b_2}	$\lambda_{5,6}$	p_m, θ	P_2
x_{b_3}, x_{b_4}, x_{b_5}, x_{b_6}	λ_1, $\lambda_{2,3}$, λ_4	M_{CL_d}, M_{CL_q}, M_{VL_d}, M_{VL_q}	P_1
x_{b_7}, x_{b_8}, x_{b_9}, $x_{b_{10}}$, $x_{b_{11}}$, $x_{b_{12}}$	$\lambda_{10,11}$, $\lambda_{12,13}$, $\lambda_{14,15}$	i_{s_d}, i_{s_q}, i_{g_d}, i_{g_q}, e_d, e_q	P_5
$x_{b_{13}}$, $x_{b_{14}}$	λ_7, λ_8	M_{AD_d}, M_{AD_q}	P_3
$x_{b_{15}}$	λ_9	q_m	P_4

Table 4.6: Groups of states and eigenvalues for the first test case in the balanced and in the physical realization

In order to obtain a reduced model of order 6, the criterion $\epsilon_{HSV} = 50\%$ is chosen. The states to keep in the balanced realization are x_{b_1}, x_{b_2}, x_{b_3}, x_{b_4}, x_{b_5} and x_{b_6}, the poles to keep are λ_1, $\lambda_{2,3}$, λ_4 and $\lambda_{5,6}$ and the states to residualize in the physical realization are the states in P_3, P_4 and P_5.

One can remark that for this simple test case, the obtained reduced model is the same as with the first strategy.

Third strategy

To apply the third strategy, the following optimization problem is solved using a genetic algorithm (see chapter 3 for more information on how this optimization problem is obtained):

$$\begin{cases} \underset{E}{\text{minimize}}\ \boldsymbol{\epsilon_{i,j}} = \displaystyle\int_{-\infty}^{\infty} |\epsilon_{i,j}(\omega)|^2 d\omega \\ \text{subject to } E \in \mathbb{E}_{\epsilon_{participation}},\ tr(E) \leq 6 \end{cases} \tag{4.4}$$

In the considered test case, $i = 1$, which means that the observed variable is i_{s_d} (the same result applies for i_{s_q}) and $j = 1$, which means that the considered event is a change in the grid voltage $v_{g_{d_g}}$ (here a short-circuit in the simulations). Thanks to the participation factors analysis, $\mathbb{E}_{\epsilon_{participation}}$ is defined as follows:

$$\begin{aligned} \mathbb{E}_{\epsilon_{participation}} = \{ & E \in \mathbb{R}^{15\times15} / E = diag(\delta_i),\ \delta_i \in \{0;1\}, \\ & \forall (i,j) \in \{1,..,6\},\ E(i,i) = E(j,j), \\ & E(7,7) = E(8,8), \\ & \forall (i,j) \in \{10,..,13\},\ E(i,i) = E(j,j), \\ & E(14,14) = E(15,15) \} \end{aligned} \tag{4.5}$$

The optimization finds the following E as a solution:

$$E = \begin{pmatrix}
0&0&0&0&0&0&0&0&0&0&0&0&0&0&0\\
0&0&0&0&0&0&0&0&0&0&0&0&0&0&0\\
0&0&0&0&0&0&0&0&0&0&0&0&0&0&0\\
0&0&0&0&0&0&0&0&0&0&0&0&0&0&0\\
0&0&0&0&0&0&0&0&0&0&0&0&0&0&0\\
0&0&0&0&0&0&0&0&0&0&0&0&0&0&0\\
0&0&0&0&0&0&1&0&0&0&0&0&0&0&0\\
0&0&0&0&0&0&0&1&0&0&0&0&0&0&0\\
0&0&0&0&0&0&0&0&0&0&0&0&0&0&0\\
0&0&0&0&0&0&0&0&0&1&0&0&0&0&0\\
0&0&0&0&0&0&0&0&0&0&1&0&0&0&0\\
0&0&0&0&0&0&0&0&0&0&0&1&0&0&0\\
0&0&0&0&0&0&0&0&0&0&0&0&1&0&0\\
0&0&0&0&0&0&0&0&0&0&0&0&0&0&0\\
0&0&0&0&0&0&0&0&0&0&0&0&0&0&0
\end{pmatrix} \tag{4.6}$$

This residualization matrix corresponds to the residualization of the states in the groups P_3, P_4 and P_5. It gives a 6^{th} order model, which in this case, is the same as the ones obtained with the two other methods.

Simulation results

The full 15^{th} order model and the reduced 6^{th} order model obtained with the three MOR methods are considered.

First, a look at the poles of the linearised full model and of the linearised reduced model in Figure 4.2 shows that, as wanted, the slow poles of the system have been kept and have not moved much.

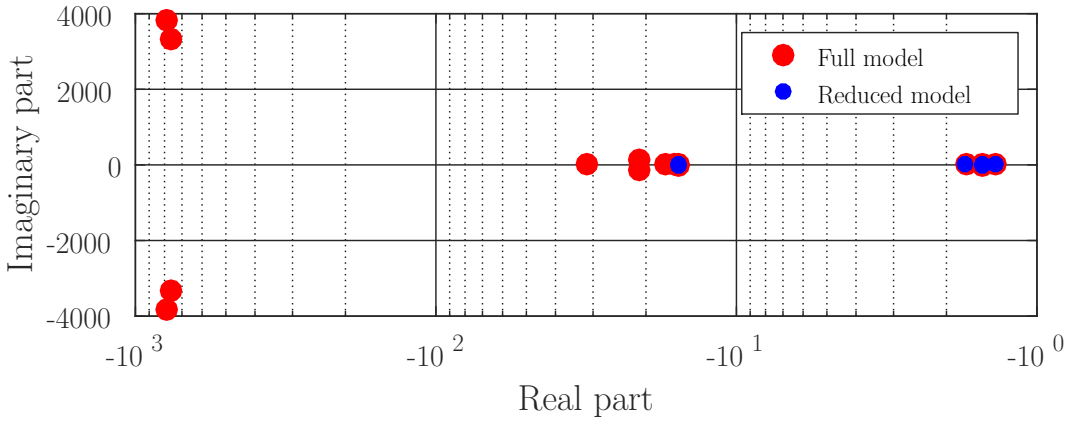

Figure 4.2: Comparison of the poles of the full and the reduced models for the first test case

Consider now the simulation of a short circuit at the grid at $t = 1s$ that is cleared after $150ms$. The current in the converter is observed in Figure 4.3.

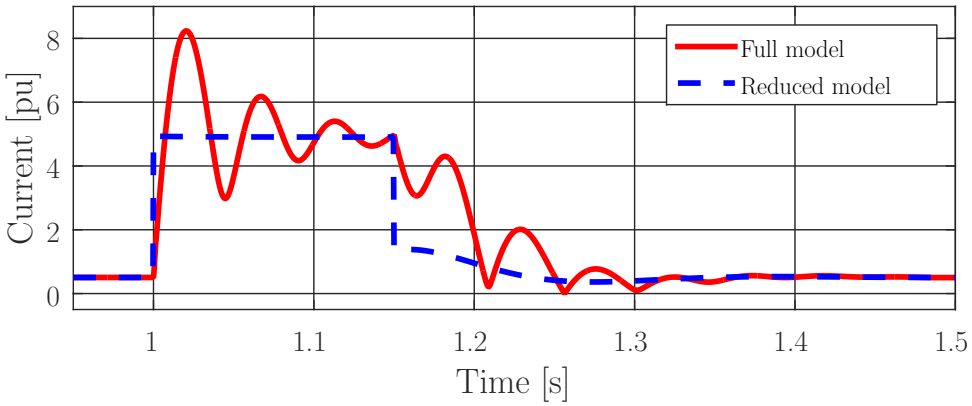

Figure 4.3: Comparison of the current in the converter for the full and the reduced models for the first test case

Several remarks can be made here. Although the peak current and the fast transient during the short-circuit are missed by the reduced model, the general shape of the current is captured by the reduced model and the poles are kept. This means that the order 6 model is good for stability studies. In both cases, the current during the short-circuit is way too high, which will damage the converter. This can be solved by adding a new control loop: the virtual impedance. It is shown hereafter that this loop can directly be added to the reduced model. This is an important feature as the control can be easily modified or updated with all the proposed methods.

Adding a new control loop

The virtual impedance, is a control loop that decreases the voltage reference of the converter when the current becomes too high. This way, it reduces the output current of the converter. Consider the following equations taken from chapter 2, giving the voltage reference to the converter using the external loop (reactive droop control here).

$$e_d^* = |e|^* + m_q(q^* - q_m) + M_{AD_d} - K_{ff} i_{g_d} \tag{4.7}$$

$$e_q^* = M_{AD_q} - K_{ff} i_{g_q} \tag{4.8}$$

When using a virtual impedance, these equations are replaced by the following four equations:

$$e_d^* = |e|^* + m_q(q^* - q_m) + M_{AD_d} - K_{ff} i_{g_d} - \Delta e_{VI_d} \tag{4.9}$$

$$e_q^* = M_{AD_q} - K_{ff} i_{g_q} - \Delta e_{VI_q} \tag{4.10}$$

$$\Delta e_{VI_d} = max(0, \sqrt{i_{s_d}^2 + i_{s_q}^2} - 1)(R_{VI} i_{s_d} - X_{VI} i_{s_q}) \tag{4.11}$$

$$\Delta e_{VI_q} = max(0, \sqrt{i_{s_d}^2 + i_{s_q}^2} - 1)(R_{VI} i_{s_q} + X_{VI} i_{s_d}) \tag{4.12}$$

In these equations, $R_{VI} = 0.67pu$ and $X_{VI} = 3.35pu$. These equations show that when the current in the converter is higher than $1pu$, the voltage reference is decreased to reduce this current. As the equations, variables and parameters are not changed during the MOR, these new equations can easily be added to the reduced model, without applying again a MOR method on the full model.

In Figure 4.4 the current in the converter is observed for the same test case as before.

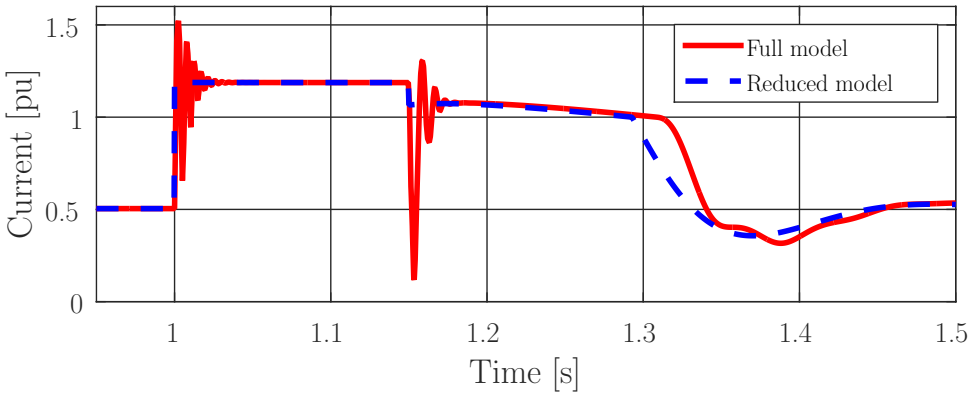

Figure 4.4: Comparison of the current in the converter for the full and the reduced models with a virtual impedance for the first test case

Now the current is limited during the short-circuit in both cases thanks to the virtual impedance.

Conclusion

In this subsection, the three developed MOR methods have been applied to a simple test case consisting in one converter connected to an infinite grid. The conclusions are the following. An order 6 model has been obtained with the three strategies and is adapted to stability studies. However, it is not accurate enough for sizing studies and more detailed models should be used. The modal approach works well and the remaining poles do not move much. The variables, parameters and equations are kept with the MOR, which allows to add new control loops directly on the reduced model. This is shown here with a virtual impedance example. This test case has been useful to illustrate the different methods but no method proves to be better than the others for this particular test case.

4.1.2 Two-converter system

As seen previously, it is not always possible to highly reduce the system when simulating events like short circuits (the important fast transients indeed need to be

captured by the simulation). But this applies to the considered converter. One can ask if it is possible, when looking at the current in one converter, to reduce the model of the other converters in the system. This is the topic of this subsection, and the question is answered using the three developed MOR methods.

The system in Figure 4.5 is considered. The two converters have exactly the same parameters, nominal power and power reference ($0.5pu$). The equations modelling them are the same as in the previous test case and a virtual impedance is used.

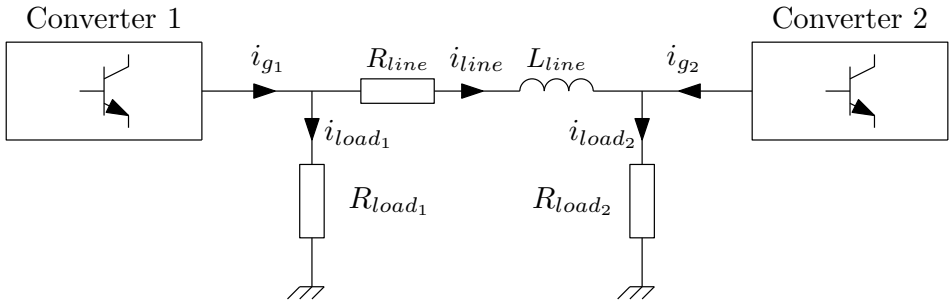

Figure 4.5: Structure of the system studied in the second test case

The line between the two converters is modelled as a simple RL line, which adds two state variables to the model. As a consequence, the system is modelled with a 32^{th} order model (15 for each converter and 2 for the line).

The parameters of the line and the loads are given in Table 4.7.

R_{line}	$0.02pu$	L_{line}	$0.2pu$
R_{load_1}	$2pu$	R_{load_2}	$2pu$

Table 4.7: Parameters of the line and the loads for the second test case

Groups of states/eigenvalues

The system is linearised around its operating point and a participation factors analysis is done for $\epsilon_{participation} = 0.7$. The same five groups as the test case with one converter (see Table 4.3) can be formed for each of the two converters. These groups are independent and there is no group formed that contains state variables of the two converters (in this particular test case and because $\epsilon_{participation}$ has been chosen small enough). This means that the two converters can be reduced independently with the developed methods. Another group made of the double eigenvalue $\lambda_{31,32}$ is formed and contains the state variables i_{line_d} and i_{line_q}. As a consequence, this two-converter system has 11 independent groups of state variables/eigenvalues, which means that there are $2^{11} = 2048$ possible models.

The three developed strategies help choosing which groups of states to residualize/groups of eigenvalues to discard, knowing that the observed variable is the current in the first converter.

For each of the three strategies, an 18^{th} order model is looked for (instead of 32 for the full model). The order of the reduced model is here chosen arbitrarily.

First strategy

The first strategy consists in residualizing some state variables to discard the fastest poles. As a consequence, the proposed 18^{th} order reduced model with this strategy consists in residualizing the states in the group P_5 for each converter and the group containing the state variables of the line between the two converters. As a result, each converter is modelled by the same 9^{th} order reduced model and the line between them is in phasor mode (quasi-static).

Second strategy

The second strategy, as it takes into account the C matrix in the linearised model and looks for the most observable and reachable states, gives a reduced model that is adapted to the observed variables (it is not the same whether the current in the first or in the second converter is observed).

In this study, the proposed reduced model consists in residualizing the states in the groups P_3 and P_4 for the first converter and the states in the groups P_3, P_4 and P_5 for the second converter. In other words, the dynamics of the filter and the transformer are kept in the model of the first converter (order 12 model) but not in the model of the second converter (order 6 model). The line between the two converters is in phasor mode.

Third strategy

As the second strategy, the third strategy takes into account the observed variable to give a specific reduced model.

For the studied test case, it gives the same reduced model as for the second strategy (an order 12 model for the first converter, an order 6 model for the second converter and a phasor line).

Simulation results

From the application of the three strategies, three models need to be compared:

- a reference order 32 model with an order 15 model for each converter and an order 2 model for the line between the two.

- an order 18 model with an order 12 model for the first converter, an order 6 for the second converter and a phasor line between the two converters. This model is given by the second and the third strategies.
- an order 18 model with an order 9 model for each converter and a phasor line between them. This model is given by the first strategy.

A short-circuit a the first load is simulated at $t = 1s$ and the current in the first converter is observed in Figure 4.6.

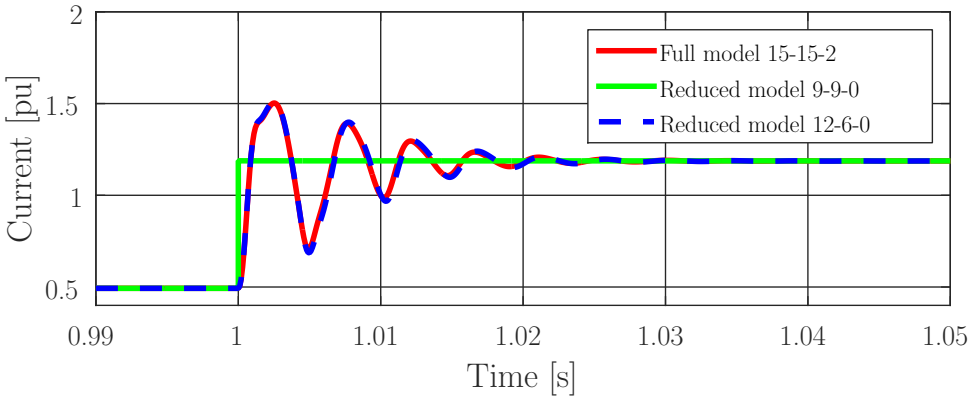

Figure 4.6: Comparison of the current in the first converter for the full and the reduced models for the second test case

In this figure, it can be seen that, although of the same size, the reduced models given by the second and the third strategies on one hand and the one given by the first strategy on the other hand give totally different simulation results. The latter misses the peak current and the fast transient induced by the short-circuit, which is an issue, whereas the other one captures them.

It seems like the first strategy is inadequate in this case to look at fast transients and peak currents. The conclusion here is that it shouldn't be used for over current capability studies.

Conclusion

With this second simple test case, it has been shown that the three developed methods don't give the same reduced model depending on what is observed (which variable). The first strategy is not adapted to studies where a specific variable is observed as it misses fast transients and peak currents that can damage the converters. For these cases, the second and the third strategies are better. As a consequence, the first strategy will only be used for stability studies.

This example has shown that, as one would expect, when a different part of the system is of interest, a different reduced model should be used. There is not one

reduced model that can be used for all the simulations. For example, in this test case, if the studied converter had been the second one and not the first one, the proposed reduced models wouldn't have been the same with the second and the third strategies. More generally, what is far from the observed converter can be more reduced than what is close. This is verified when studying larger systems like is shown in this report when studying the Irish transmission system.

The conclusion here is that a different model should be used for each converter in the system, depending on what is studied.

4.1.3 Three-converter system

In the last subsection, it has been shown that the reduced model should be adapted to the observed variables, which is possible with the second and the third strategy but not with the first one. In this subsection, it is shown that taking into account the simulated event is also important.

To do so, a simple system with three converters and one load is considered in Figure 4.7.

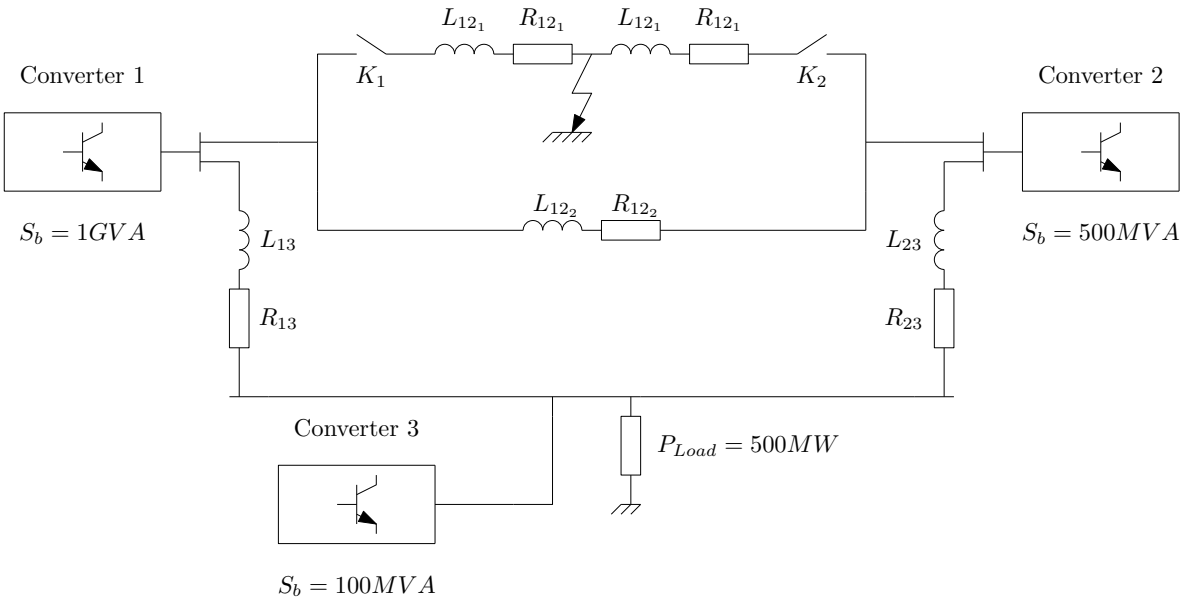

Figure 4.7: Structure of the system studied in the third test case

In this system, each converter has its own pu system associated to its S_b and V_b. For the grid between the converters and the load, $S_b = 100MVA$ and $V_b = 320kV$. The parameters of the grid are given in Table 4.8.

R_{12_1}	$1.5e^{-3}pu$	L_{12_1}	$1.5e^{-2}pu$	R_{12_2}	$1.5e^{-3}pu$	L_{12_2}	$1.5e^{-2}pu$
R_{13}	$7.3e^{-4}pu$	L_{13}	$7.4e^{-3}pu$	R_{23}	$3.7e^{-3}pu$	L_{23}	$3.7e^{-2}pu$

Table 4.8: Parameters of the grid for the third test case

Each converter has an order 15 model and the grid between them is of order 10 (2 per RL line). As a result, the whole system is modelled with an order 55 model.

For this test case, only the second and the third strategies are compared.

Two events are simulated and the strategies are applied to the system for each one of them:

- K_1 and K_2 are closed and a short-circuit happens in the middle of the line 12_1. For this event, the input that is considered in the third strategy is the resistor modelling the short-circuit.
- The line 12_1 is short-circuited and K_1 and K_2 are opened. For this event, the input that is considered in the third strategy is the resistor modelling the line-tripping (K_1 and K_2).

These two events lead to two different system topologies, which means that the MOR needs to be done separately to both cases to be accurate.

Groups of states/eigenvalues

As for the second test case, five groups for each converter can be independently formed (with a well chosen $\epsilon_{participation}$, here 0.5). A group containing the 10 state variables of the grid is also formed and is linked to the fastest eigenvalues. As a result, there are in total 16 groups, which leads to $2^{16} = 65536$ possible reduced models. To simplify, an order 36 model is looked for in the following. The order of the reduced model is here chosen arbitrarily.

Second strategy

The second strategy takes into account the observed variable but not the simulated event. It gives the same reduced model for both events (even though the topology is different in both cases): an order 12 first converter with the residualization of the states in P_3 and P_4, an order 7 second converter with the residualization of the states in P_3 and P_5, an order 7 third converter with the residualization of the states in P_3 and P_5 and the grid in EMT (order 10).

Third strategy

The third strategy can take into account the simulated event. As a result, it gives different reduced models for each event:

- For the short-circuit: an order 12 first converter with the residualization of the states in P_3 and P_4, an order 7 second converter with the residualization of the states in P_3 and P_5, an order 7 third converter with the residualization of the states in P_3 and P_5 and the grid in EMT (order 10).

- For the tripping of the line: an order 12 first converter with the residualization of the states in P_3 and P_4, an order 12 second converter with the residualization of the states in P_3 and P_4, an order 12 third converter with the residualization of the states in P_3 and P_4 and the grid in phasor (order 0).

Simulation results

Three models are compared with time simulations:

- a reference order 55 model (named 15-15-15-10).

- the order 36 model given by the second strategy and the third strategy during the short-circuit (named 15-7-7-10).

- the order 36 model given by the third strategy during the tripping of the line (named 12-12-12-0).

The short-circuit is simulated at $t = 1s$ and the tripping of the line $150ms$ after. The current in the first converter can be observed in Figure 4.8 during the short circuit and in Figure 4.9 during the tripping of the line.

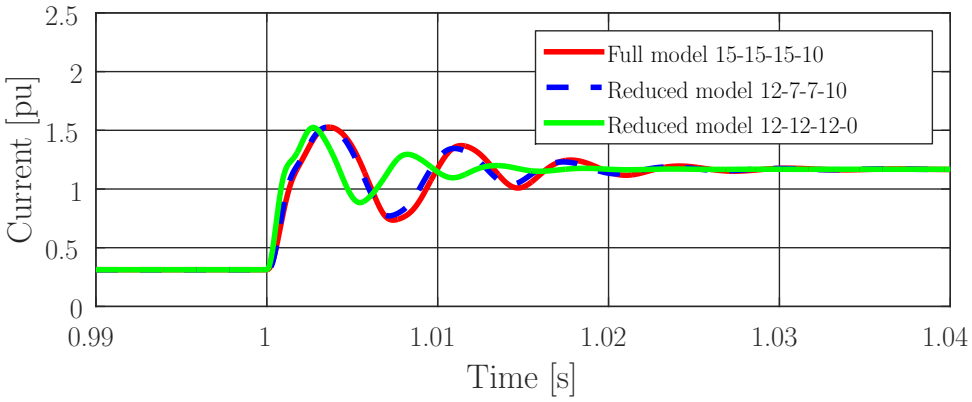

Figure 4.8: Comparison of the current in the first converter for the full and the reduced models for the third test case during the short-circuit

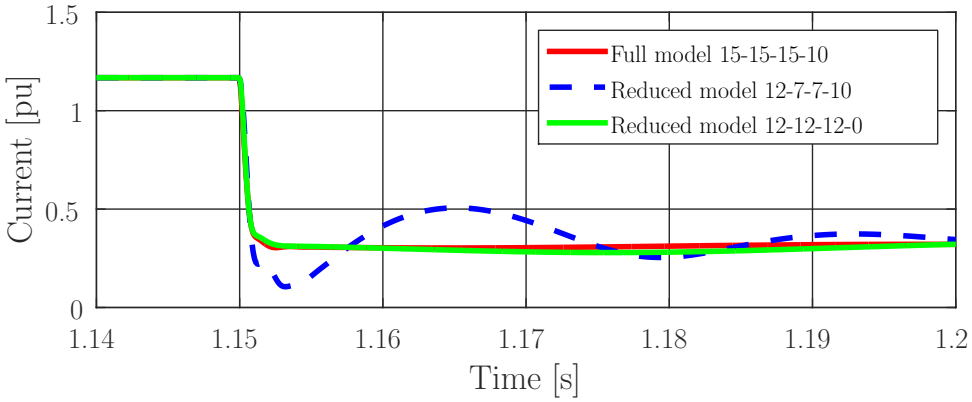

Figure 4.9: Comparison of the current in the first converter for the full and the reduced models for the third test case during the tripping of the line

These figures show that, as stated by the third strategy, a different reduced model should be used for each simulated event. During the short-circuit, reducing the second and third converter is indeed the best solution, while during the tripping of the line, reducing the grid and making the phasor approximation is the best solution. This is not the case with the second strategy, which misses this.

One can remark that instead of having a different reduced model for each simulated event, one could try to minimize a combination $\alpha\boldsymbol{\epsilon_{i,j_1}} + (1-\alpha)\boldsymbol{\epsilon_{i,j_2}}$ instead of only $\boldsymbol{\epsilon_{i,j_1}}$ or $\boldsymbol{\epsilon_{i,j_2}}$ separately, with α between 0 and 1. If $\alpha = 1$, the best reduced model is given for the short-circuit. If $\alpha = 0$, the best reduced model is given for the tripping of the line. By choosing $\alpha = 0.5$ a compromise could be found. When tested on this particular test case, this method doesn't give satisfying results. It indeed gives either the best model for the short-circuit or the best model for the line tripping but not an intermediate model, even when several values for α are tested, as can be seen on Table 4.9.

α	0	0.2	0.4	0.6	0.8	1
Model	12-12-12-0	12-12-12-0	12-12-12-0	12-7-7-10	12-7-7-10	12-7-7-10

Table 4.9: Reduced model depending on the value of α

Conclusion

With this test case, it has been shown that to reduce the model of a power system with a high PE penetration, taking into account the simulated event is of great importance. This is possible with the third developed MOR method in this thesis. As a conclusion, the third developed MOR method proves to be the best one to study this type of cases.

Moreover it has also been shown that for events like short-circuits, the phasor approximation should not be made to have a good accuracy.

4.1.4 Conclusion

This section has presented three simple test cases to which the developed MOR methods have been applied:

- a one-converter test case has been studied. The main idea here was to carefully explain the process of each one of the developed methods. For this particular test case, the reduced models proposed by the three strategies are the same.
- a two-converter test case has been studied to show that depending on which converter is of interest in the system, the reduced model should not be the same. This is what the second and the third strategies showed.
- a three-converter test case has been studied to show that depending on what event is simulated, the reduced model should not be the same. This is what the third strategy showed. Moreover it was a first example that showed that the phasor approximation can not always be made to preserve a good enough accuracy.

4.2 Transmission system test case

The developed MOR method now needs to be applied to larger systems. In this section, the Irish transmission system is taken as an example. All the data are given by the Irish TSO EirGrid [91]. In order to have a 100% PE power system, all the generators are replaced with grid forming converters. This system is made of 47 loads (actual loads and equivalent loads representing the distribution networks), 14 generators, 85 lines, 6 shunt capacitors and 40 transformers. Each generator is a grid forming converter modelled with a 15^{th} order model. Each transformer and shunt capacitor is modelled with its 2^{nd} order model. Each line is modelled with its 6^{th} order pi-line model and each load with its 2^{nd} order model. This leads to a system with 906 differential equations (the order of the whole system is actually less because some algebraic equations modelling the nodes reduce the number of state variables. For example, if two inductances are directly connected in series, there is actually only one state variable and not two). A representation of the structure of this transmission system is given in Figure 4.10. The red lines represent the $400kV$ branches and the green lines represent the $220kV$ branches [92].

Figure 4.10: Structure of the Irish transmission system

A short-circuit is simulated at a load at $t = 0.1s$ (Dunstown on the map). The

current in a converter close to this load (Shellybanks on the map) is observed. Only the third strategy is applied in this section as it has been shown in the last section that it is the most adapted one for this type of studies.

Usually, to reduce the model of such a system, the loads, shunt capacitors, transformers and lines are modelled with the phasor approximation. As a result, only the dynamics of the converters are taken into account and the system is of order 210. But it has been shown in the test case with three converters that the phasor approximation is not always valid with a high PE penetration. In this subsection, the developed MOR method is applied to the Irish transmission system modelled in EMT. The idea is to compare the phasor model to a reduced model of the same size obtained with the third strategy and to the full EMT model.

Third strategy

The participation factors analysis creates five groups of states for each converter, which can be reduced independently. For the lines, transformers, shunt capacitors and loads, it creates some groups as the dynamics of each one of these elements are not totally independent and participate in some common poles.

The third strategy is applied to obtain an order 210 model (same size as the phasor model) when observing the current in a converter (Shellybanks) when a short-circuit happens at a load (Dunstown) close to it. It gives a model where some converters are reduced, some are less reduced, some lines are in phasor (the one that are far from the converter) and some are in EMT (the one that are close to the converter). The optimisation that finds the reduced model takes 5 minutes and 21 seconds to be performed on an Intel(R) Core(TM) i7-6700HQ CPU @ 2.60GHz processor, which is not much compared to the gain in terms of simulation time as can be seen later when doing the simulations.

For instance, table 4.10 gives the order of the model for each of the 14 converters when the third strategy is applied. The observed converter is the second one (Shellybanks).

Converter	1	2	3	4	5	6	7	8	9	10	11	12	13	14
Order (strategy 3)	12	12	12	12	12	12	12	12	6	6	6	6	6	6

Table 4.10: Model order for each of the converter in the system

On Figure 4.11, the part of the grid that is in EMT and the part that is in Phasor mode are represented. One can see that the lines close to the observed converter and the simulated event are in EMT while the one that are far are in Phasor.

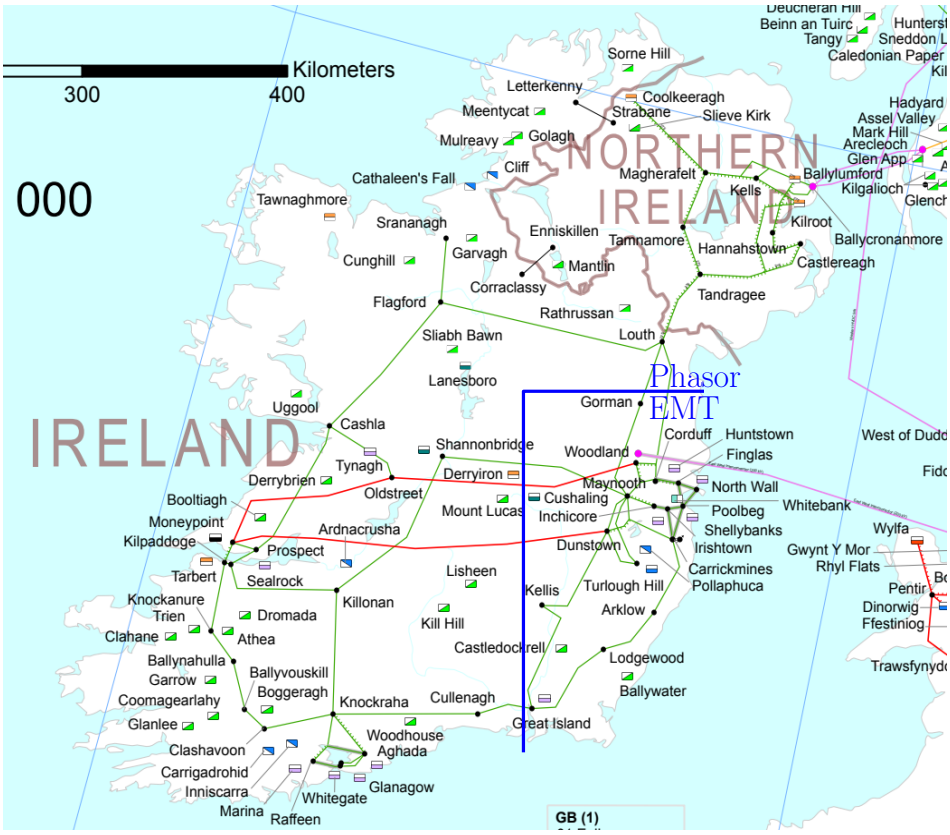

Figure 4.11: Structure of the Irish transmission system after the model order reduction

One can remark that the reduced model proposed by the third strategy makes a difference between the first 8 converters, that should be modelled with a quite detailed model, and the last 6 converters, that can be more reduced. When looking at the map of Ireland, it can be seen that the first group of converters actually corresponds to the converters in the Republic of Ireland while the converters of the second group are in Northern Ireland. And these two groups are only connected with one line, which makes them quite independent dynamically. The same kind of remarks applied when looking at the model of the lines. The one that are close to the event and the observed converter are in EMT while the other can be modelled in phasor.

One can also remark that if the observed variable is the current in another converter, the 12^{th} one for example, the proposed reduced model would have consisted in the first 8 converters (in the Republic of Ireland) more reduced than the last 6 converters (in Northern Ireland), which is the opposite of what is proposed here. It shows that the MOR method is flexible and adapts to the test case under consideration.

Simulation results

Figure 4.12 represents the current in the converter during the short-circuit for the three models: the full EMT model, the phasor model, and a reduced model of the same size obtained with the developed strategy.

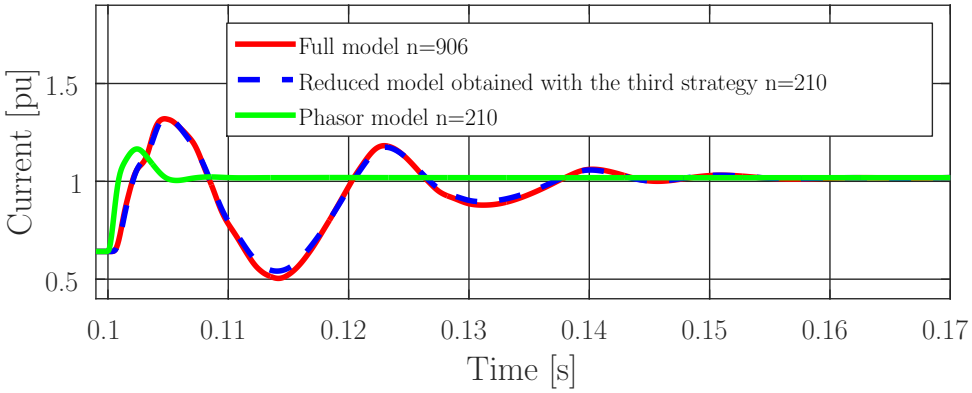

Figure 4.12: Comparison of the current in the converter for the full EMT model, the reduced model obtained with the 3^{rd} strategy and the phasor model during the short-circuit at the load

It can be seen that the phasor model misses the first peak of the current and the oscillations of the transient during the short-circuit, which can be dangerous for the device. On the other hand, the reduced model, as it keeps the most relevant dynamics, captures this transient with a very good accuracy and has the same simulation time as the phasor model. It is therefore a better model.

Moreover, the simulation time is reduced by more than four times (5 minutes and 39 seconds with the reduced model against approximately 21 minutes and 13 seconds with the full detailed model on an Intel(R) Core(TM) i7-6700HQ CPU @ 2.60GHz processor).

Conclusion

This section focused on the application of the developed MOR method to a real size transmission system. Several things have been presented. First, the phasor approximation is not always valid when studying fast transients and peak currents during events like short-circuits. It has been shown with the developed method that some lines must be modelled in EMT whereas others can be modelled using the phasor approximation. The developed strategy helps choosing which lines to simplify. It gives a reduced model from the full EMT model that is of the same size as the phasor model but that can capture the important dynamics during the transients. Then, the developed MOR applied to a transmission system allows to reduce the size of the model according to what is observed and what is simulated. This results in a reduced system that is adapted to

the test case under consideration. Finally, it is possible to use different models for each converter. The models of the converters that are far from the simulated event and the observed variable can be more reduced than the models of the other converters. The same thing applies for the lines and the process is automatic. Simulations have been made to validate the obtained reduced model. The reduced model is accurate and the simulation time has been reduced greatly.

4.3 Test case with one grid forming converter and one modular multilevel converter

To study the interactions between two different types of PE converters, this test case deals with a grid forming converter connected to an MMC. They both send power to a load and are connected to each other through two lines in parallel. A short-circuit is simulated in the middle of one line at $t = 1s$. Two cases are considered: in the first one the current in the grid forming converter is observed and in the second one the current in the MMC is observed. The models used for the two converters are the one presented in chapter 2. The system is represented in Figure 4.13. It has 32 state variables and is thus an order 32 model.

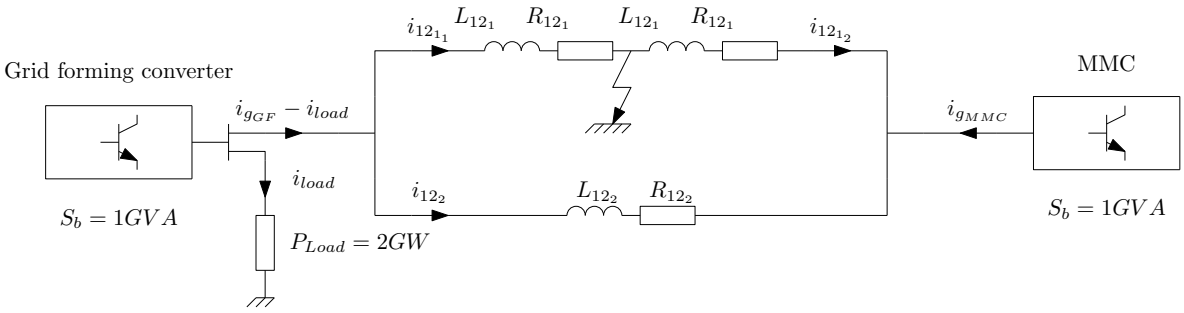

Figure 4.13: Structure of the system with one grid forming converter and one MMC

Groups of states/eigenvalues

The first step of the developed method consists in forming the groups of states and eigenvalues deduced from the participation factors analysis. It is done here with $\epsilon_{participation} = 0.8$. These groups are presented in Table 4.11.

This table presents 11 groups of states/eigenvalues. As a result, $2^{11} = 2048$ reduced models are possible.

Third strategy

To simplify, only the third strategy is applied to this system. Instead of choosing a size for the reduced model, a maximum tolerated error (for the energy of the error. See chapter 3 for more explanations) is chosen and the idea is to find the most reduced model that gives an error below this maximum tolerated error.

The strategy is applied to the two considered test cases:

- When the current in the grid forming converter is observed, the method proposes to residualize the state variables in the groups P_5, P_7 and P_9. It gives an order 24 model made of an order 6 MMC, an order 12 grid forming converter and the lines in EMT.

Eigenvalues	State variables	Group name
$\lambda_1 = 0$	θ_{GF}	P_1
$\lambda_{2,3} = -0.002 \pm 0.01i$	$M_{PLL_{MMC}}$, $\theta_{PLL_{MMC}}$	P_2
$\lambda_{4,5} = -1.45 \pm 0.04i$	$M_{VL_{d_{GF}}}$, $M_{VL_{q_{GF}}}$	P_3
$\lambda_{6,7} = -1.6 \pm 0.05i$	$M_{CL_{d_{GF}}}$, $M_{CL_{q_{GF}}}$	P_4
$\lambda_{8,9} = -16.6 \pm 0.07i$	$M_{AD_{d_{GF}}}$, $M_{AD_{q_{GF}}}$	P_5
$\lambda_{10} = -31$	$p_{m_{GF}}$	P_6
$\lambda_{11} = -31.4$	$q_{m_{GF}}$	P_7
$\lambda_{12,13} = -31.4 \pm 320i$	$i_{12_{1_d}}$, $i_{12_{1_q}}$	P_8
$\lambda_{29} = -2.3e^7$, $\lambda_{30} = -2.5e^7$	$i_{12_{2_d}}$, $i_{12_{2_q}}$	
$\lambda_{31} = -2.8e^7$, $\lambda_{32} = -8.1e^7$	$i_{12_{2_d}}$, $i_{12_{2_q}}$	
$\lambda_{14} = -73.6$, $\lambda_{15} = -113.3$	$M_{DCCL_{MMC}}$	P_9
$\lambda_{16,17} = -365 \pm 541i$	$v_{C_{tot_{MMC}}}$, $M_{W_{MMC}}$	
$\lambda_{26} = -1131$	$W_{tot_{f_{MMC}}}$, $i_{DC_{MMC}}$	
$\lambda_{18,19} = -420 \pm 428i$	$i_{g_{d_{MMC}}}$, $i_{g_{q_{MMC}}}$	P_{10}
$\lambda_{20,21} = -420 \pm 436i$	$M_{CL_{d_{MMC}}}$, $M_{CL_{q_{MMC}}}$	
$\lambda_{22,23} = -616 \pm 1374i$	$i_{s_{d_{GF}}}$, $i_{s_{q_{GF}}}$	P_{11}
$\lambda_{24,25} = -807 \pm 2795i$	$i_{g_{d_{GF}}}$, $i_{g_{q_{GF}}}$	
$\lambda_{27,28} = -1609 \pm 4409i$	$e_{d_{GF}}$, $e_{q_{GF}}$	

Table 4.11: Groups of states and eigenvalues for the test case with one grid forming converter and one MMC

- When the current in the MMC is observed, for the same accepted error, the method proposes to residualize the states in the groups P_5, P_7, P_8, P_9 and P_{11}. It gives an order 12 reduced model made of an order 6 MMC, an order 6 grid forming converter and the lines in phasor mode.

Simulation results

To validate the proposed reduced models, they are compared to the full EMT model with time simulations. Figure 4.14 presents the evolution of the current in the grid forming converter. One can see that the proposed order 24 model accurately captures the transient during the short-circuit while the order 12 model doesn't. This is why this is the model proposed by the developed strategy.

Figure 4.15 presents the evolution of the current in the MMC. One can see that the proposed order 12 and order 24 models accurately both capture the transient during the short-circuit. This is why the order 12 model is the one proposed by the developed strategy.

It can be seen that depending on what is looked at (the current in the grid forming converter or in the MMC), the MOR possibilities are not the same. In some cases it is

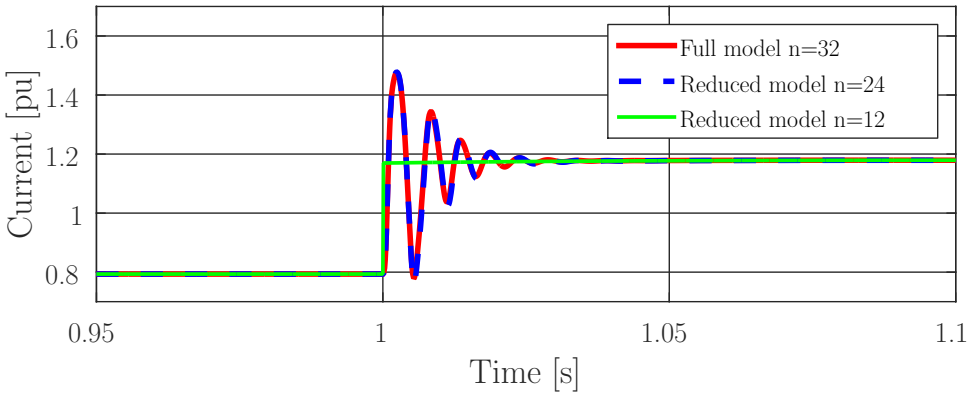

Figure 4.14: Comparison of the current in the grid forming converter for the full EMT model and the two reduced models obtained with the 3^{rd} strategy during the short-circuit in the middle of a line

possible to greatly reduce the model while in others it isn't.

Conclusion

This test case consisting in one grid forming converter and one MMC connected to the same load highlighted several points. When the current in the grid forming converter is observed during a short circuit, only the MMC can be reduced much and some fast poles of the grid forming converter must be kept. Moreover, the grid must be modelled in EMT. When the current in the MMC is observed there are more possibilities of reduction. Both the MMC and the grid forming converter can be highly reduced and the grid can be modelled in phasor mode. These two things are due to the fact that the grid forming converter, because it is a grid forming converter, handles the fast transient and the peak current induced by the fault. The MMC, as it is in grid feeding mode, keeps injecting its reference power/current without too much trouble (it is the same if it is not an MMC but a 2-level VSC in grid feeding mode). As a conclusion, the main outcome here is that the converters at risk when simulating are the grid forming converters and one should be careful when choosing how to model them.

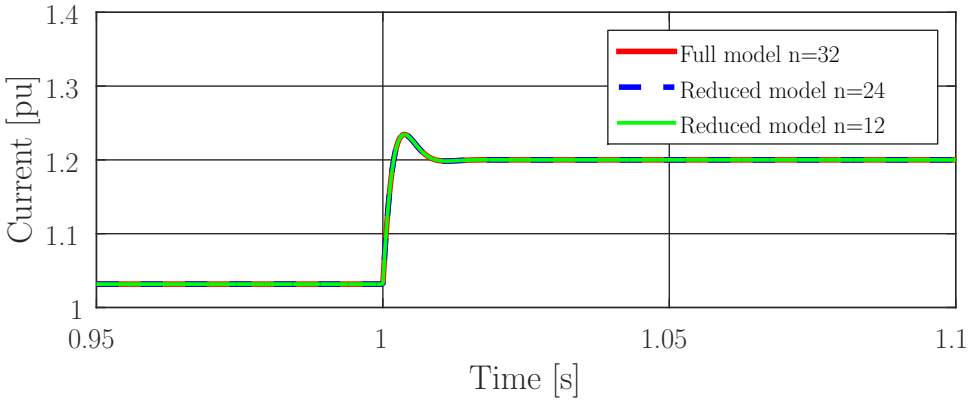

Figure 4.15: Comparison of the current in the MMC for the full EMT model and the two reduced models obtained with the 3^{rd} strategy during the short-circuit in the middle of a line

4.4 Test case with one grid feeding converter and one synchronous machine

Before being 100% PE, the transmission systems will go through a phase where PE devices and SM are both connected to the grid. To take this into account, a test case consisting in one SM connected to a grid feeding converter and a load is studied in this section. The system is represented in Figure 4.16. It has 32 state variables and is thus an order 32 model. The models used for the elements of this system are the one presented in chapter 2.

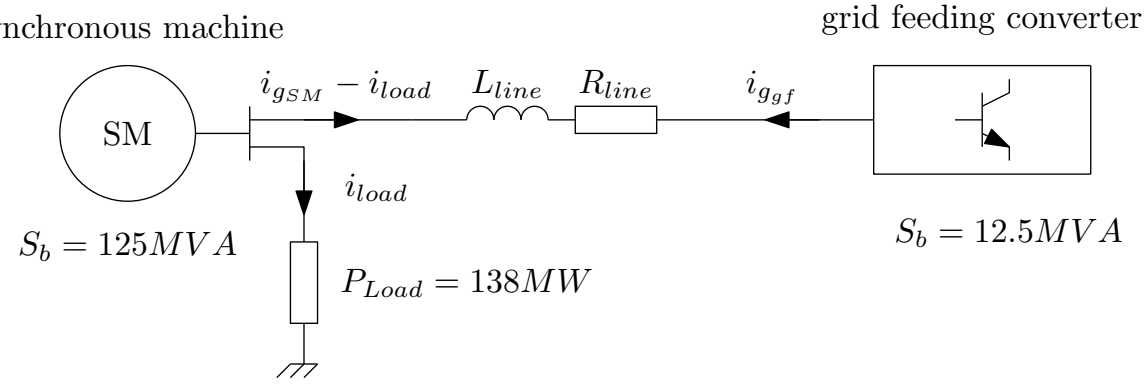

Figure 4.16: Structure of the system with one synchronous machine and one grid feeding converter

The simulated test case consists in a short-circuit at the load. Two cases are considered: in the first one, the current in the SM is observed and in the second one it is

the current in the converter. Again, only the third strategy is applied here. The idea is to find the most reduced model for a given maximum accepted error (like in the last test case with one grid forming converter and one MMC).

Groups of states/eigenvalues

The first step of the method consists as usual in forming the groups of states/eigenvalues based on the participation factors analysis. It is done here for $\epsilon_{participation} = 0.70$ and it gives Table 4.12. 12 groups are created, which means that there are $2^{12} = 4096$ possible reduced models. The developed MOR method helps us deciding which one is the most adequate to the test case.

Eigenvalues	State variables	Group name
$\lambda_1 = 0$	δ_{SM}	P_1
$\lambda_{2,3} = -0.13 \pm 0.87i$	$\phi_{f_{d_{SM}}}$, $V_{e_{SM}}$	P_2
$\lambda_{4,5} = -0.83 \pm 0.67i$	$\phi_{d_{SM}}$, $\phi_{q_{SM}}$	
$\lambda_6 = -1.77$, $\lambda_7 = -3.27$	ω_{SM}, $\Gamma_{m_{SM}}$	
$\lambda_{23,24} = -641 \pm 184i$	$\Delta P_{s_{SM}}$, $\phi_{1_{q_{SM}}}$	
$\lambda_{8,9} = -3.89 \pm 7.32i$	$V_{e_{f_{SM}}}$, $u^*_{f_{SM}}$	P_3
$\lambda_{10} = -13.23$	$\Delta P_{d_{SM}}$	P_4
$\lambda_{11} = -15.32$	$\phi_{2_{q_{SM}}}$	P_5
$\lambda_{12} = -16.62$	$V_{f_{SM}}$	P_6
$\lambda_{13} = -19.59$	$\Delta P_{a_{SM}}$	P_7
$\lambda_{14} = -30.81$	$\phi_{1_{d_{SM}}}$	P_8
$\lambda_{15,16} = -51.3 \pm 14i$	$M_{PLL_{gf}}$, $\theta_{PLL_{gf}}$	P_9
$\lambda_{18} = -73.04$	$M_{p_{gf}}$	
$\lambda_{17} = -58.5$	M_{qgf}	P_{10}
$\lambda_{19,20} = -516 \pm 804i$	$i_{s_{d_{gf}}}$, $i_{s_{q_{gf}}}$	P_{11}
$\lambda_{21,22} = -582 \pm 556i$	$i_{g_{d_{gf}}}$, $i_{g_{q_{gf}}}$	
$\lambda_{25,26} = -672 \pm 3982i$	$e_{d_{gf}}$, $e_{q_{gf}}$	
$\lambda_{27,28} = -893 \pm 3295i$	$e_{d_{f_{gf}}}$, $e_{q_{f_{gf}}}$	
$\lambda_{29,30} = -1604 \pm 119i$	$M_{CL_{d_{gf}}}$, $M_{CL_{q_{gf}}}$	
$\lambda_{31,32} = -2.2e^8 \pm 2.2e^8 i$	$i_{g_{d_{SM}}}$, $i_{g_{q_{SM}}}$	P_{12}

Table 4.12: Groups of states and eigenvalues for the test case with one synchronous machine and one grid feeding converter

Third strategy

The third strategy is applied in both cases and the idea is to find the most reduced model for a given accepted error:

- when considering the current in the SM, the method proposes to residualize the state variables in the groups P_4, P_6, P_7, P_{10}, P_{11} and P_{12}. It gives an order 16 model made of an order 3 grid feeding converter, an order 13 SM and a line in phasor mode.

- when considering the current in the grid feeding converter, the method proposes to residualize the states variables in the groups P_3, P_4, P_5, P_6, P_7, P_8 and P_{12}. It gives an order 23 model made of an order 14 grid feeding converter, an order 9 SM and a line in phasor mode.

One can remark that the states in the groups P_1, P_2 and P_9 are never residualized.

Simulation results

To validate the proposed reduced models, they are compared to the full EMT model with time simulations. Figure 4.17 presents the evolution of the current in the SM. One can see that the proposed order 16 model accurately captures the transient during the short-circuit while the order 23 model doesn't. This is why this is the model proposed by the developed strategy.

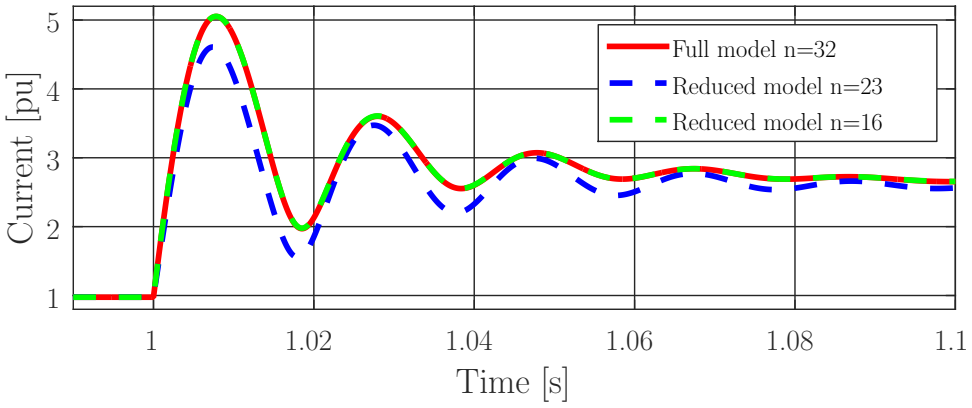

Figure 4.17: Comparison of the current in the synchronous machine for the full EMT model and the two reduced models obtained with the 3^{rd} strategy during the short-circuit at the load

Figure 4.18 presents the evolution of the current in the grid feeding converter. One can see that the proposed order 23 model and order 16 model both capture the transient during the short-circuit quite well. This is the same conclusion as with the MMC. The grid feeding converter can more easily be reduced than a grid forming converter or a SM.

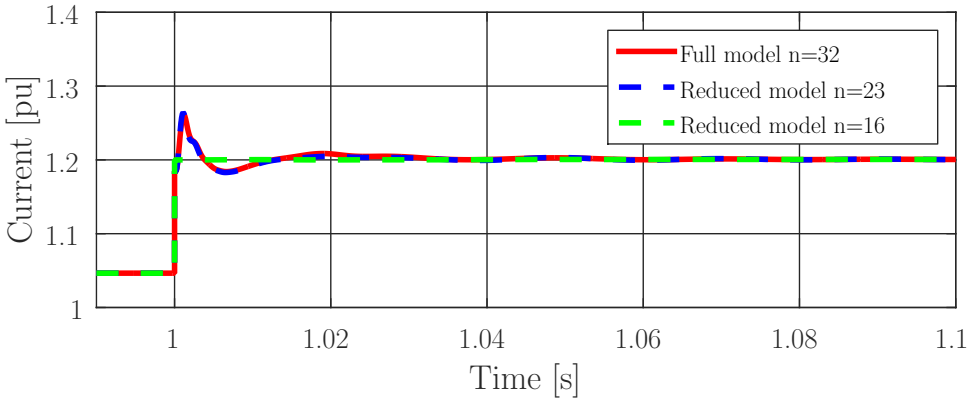

Figure 4.18: Comparison of the current in the grid feeding converter for the full EMT model and the two reduced models obtained with the 3^{rd} strategy during the short-circuit at the load

Conclusion

This section dealt with the case of a grid feeding converter and a SM connected to the same load. It highlighted several points. When the current in the SM is observed during a short-circuit, the grid feeding converter can be highly reduced to an order 3 model and the SM is reduced just a little bit. When the current in the grid feeding is observed, both can be quite reduced as the model of the grid feeding converter is less important than the one of a grid forming converter. In both cases, the line can be modelled in phasor mode. Time simulations validated the proposed reduced models .

4.5 Chapter conclusion

In this chapter, several test cases have been simulated and studied to validate the developed MOR and give some insights on how to model and simulate a transmission system with a high PE penetration. Several conclusions can be drawn from this.

The developed methods, as wanted, preserve the variables, parameters and some poles of the initial system.

Depending on what is observed (which variable, for example the current in a specific converter), the reduced model should not be the same.

Depending on what kind of event is simulated and where (for instance a short circuit or a load connection), the reduced model should not be the same.

These two points help the user identifying zones of the system that should be modelled in details and other zones where the models can be highly reduced. The developed methods identify the boundaries of these different zones. It is intuitive that what is close to the studied converter and the simulated event must be modelled with more details than what is far but the developed methods prove it and give the boundaries.

One consequence of this is that some lines of a transmission system can be modelled using the phasor approximation while other need to be modelled in EMT. Previously, either all the lines were in EMT or in phasor. This is now more flexible and the developed methods identify which lines must be in EMT.

Moreover, it has been shown that the simulation time and the number of variables have been reduced greatly thanks to the reduced models.

A last conclusion is that depending on the type of converter that is studied, the degree of the reduction is not the same. Grid forming converters, as they are voltage sources, are more subject to over current and therefore must be modelled with higher details than grid feeding converters.

Conclusion and perspectives

Contents

Conclusion

The context of this thesis was the search for technical solutions, such as new control laws, to ensure that the massive integration of power electronics in the transmission systems does not induce a decrease in the system stability and security. The main objective of the particular work of this thesis is reminded and has consisted in developing new tools and methods to simulate and analyse transmission systems with a high power electronics penetration. The different dynamic behaviour of power electronics compared to synchronous machines and the development of new grid forming capabilities for the converters indeed necessitate new simulation methods and analysis tools.

The first chapter has presented some common tools that are used today to simulate and analyse power systems. These tools are the EMT programs, the phasor approximation and the dynamic phasors for the simulation, and the small signal stability analysis, the sensitivity analysis and the participation factors for the analysis tools. Thanks to this state of the art, a need for model order reduction has been identified to accelerate the simulation and simplify the analysis. This is why the second part of this chapter was on the presentation of the classical model order reduction methods. The conclusion then was that the classical methods are not suitable for the simulation and analysis of power system because they use basis changes and truncations, which change the variables and the structure of the system. This is why the objective of this thesis was to develop model order reduction methods that preserve the variables and the physical structure of the system.

The second chapter has presented the models of the different elements of a transmission system with a high power electronics penetration: the converters (grid forming converters, grid feeding converters, MMC), the synchronous machines, the lines, the loads, the transformers and the shunt capacitors. For the sake of simplicity, these models are all balanced. For each model, its differential and algebraic equations are given, as well as block diagrams describing them when necessary. These models are used to create power systems models to which the developed model order reduction methods are applied later in the report.

The third chapter has theoretically presented the developed model order reduction methods. These three methods are based on state residualization, a modal approach and some features inspired by the classical methods presented in chapter 1. As wanted, the developed methods preserve the variables of the system, its physical structure, the stability of the operating point and have a limited error. Moreover, some of them give a reduced model that is specific to the test case under consideration, i.e. the observed variable and the simulated event. As the developed methods keep the physical structure and variables of the model, the analysis is simple, it is possible to add new control loops directly on the reduced model (this has been illustrated in this report by the addition to the reduced model of a virtual impedance) and it is easy to implement the reduced models in the classical simulation tools. Moreover, the computation time is highly reduced.

The fourth chapter has presented the results of the application of the three devel-

oped methods to realistic test cases. A first test case presented in details how the three developed methods are applied. Then several test cases, from simple ones to more complicated ones like the Irish transmission system, helped comparing the three developed methods. The conclusion is that the third one using an optimization is the most adapted to the test cases under consideration as it can at the same time take into account the simulated event and the observed variable. Recommendations on how to model, simulate and analyse transmission systems with a high power electronics penetration have also been given. Particularly, the case of the phasor approximation, which is largely used in power system studies today, has been addressed. It has been shown that it should not be used for all the lines in the system depending on the simulated event and the observed converter/variable. It has been proved with the developed method that, as expected, what is close to the simulated event and the observed converter should be modelled with more details than the rest of the system. The developed strategy identifies the boundaries between the detailed and the less detailed zones. Moreover, the gain in terms of computation time is important as a reduction by five has been observed.

Perspectives

Several possibilities of future work can be mentioned here.

Even though a real size transmission system has been studied in this report, the models used for the different elements (converters, lines, transformers and loads) are quite simple. More detailed models would make the use of model order reduction methods like the ones developed in this thesis even more relevant. This is why an application of the developed model order reduction method on more complex models would be interesting. For example, instead of Pi models, frequency dependent models could be used for the lines. More complex systems than the Irish transmission system could also be studied.

Moreover, all the test cases in this thesis focus on balanced systems. A work on unbalanced systems is an interesting perspective as there is a possibility that the most adapted reduced model is not the same when the system is unbalanced. Moreover, as unbalanced models are more complex than balanced ones, the need for model order reduction is even higher. This is why it should be investigated.

In all test cases, the desired size for the reduced model has been chosen arbitrarily. A work on the optimal reduced model size could be interesting. For now, the only solution is to test several sizes, compute the reduced model in each case and choose the best one. This solution demands a high computation time and should be greatly improved in the future.

The modal approach is based on the formation of groups of states and eigenvalues that depend on each other using a participation factors analysis. This approach needs a criterion $\epsilon_{participation}$ that defines the degree of participation that is taken into account when forming the groups. The choice of this criterion is based, in this report, on

several tests that lead to a specific value that gives a good trade-off between sufficiently taking into account the couplings and being able to enough reduce the model. A more systematic method to choose this criterion would be a good improvement of the developed methods.

Although reducing nonlinear models, the developed model order reduction methods are based on linear analyses. A study of the degree of validity of this approach could be done. To which extent a nonlinear reduced model given by a linear analysis is valid ? This is especially relevant when simulating large disturbances like short-circuits (which is the case in this work). A first perspective could be to study an extension of the participation factors to nonlinear models, which has been done in [25]. The nonlinear participation factors take into account the couplings induced by the non linearities. It is this way possible that an eigenvalue doesn't depend on a certain state variable when looking at the classical participation factors but this is not true any more when taking into account the nonlinear participation factors.

Other criteria to minimize could be tested for the third strategy and compared to each others. For example, an application of the criterion presented in [87] could be interesting.

As seen in this report, a different reduced model is given by the third method for each different simulated event. One perspective could be to work on how to change the model of the system during the simulation between two different events and how to do this change of model properly. It is indeed a scientific challenge to be able to initialize the new model using the data of the previous one. However, as the developed method keeps the variables of the system (which are the same for the full or any reduced model), the switching between two different models becomes easier than with the classical model order reduction methods, which change the variables of the system during the process.

The gain in computation time makes the developed methods interesting for an application to real time simulation test cases and it should be further investigated as a continuation of this work.

Finally, a toolbox could be developed to integrate the developed methods into the classical simulation software and make them more automatically applicable.

Bibliography

[1] MIGRATE, "https://www.h2020-migrate.eu/," 2016.

[2] H. Dommel, "Digital Computer Solution of Electromagnetic Transients in Single- and Multiphase Networks," *IEEE Transactions on Power Apparatus and Systems*, vol. PAS-88, no. 4, pp. 388–399, 1969.

[3] T. Demiray, *Simulation of Power System Dynamics using Dynamic Phasor Models*. PhD thesis, ETHZ, 2008.

[4] J. De Siqueira, B. Bonatto, M. J., J. Hollman, and H. Dommel, "A discussion about optimum time step size and maximum simulation time in EMTP-based programs," *International Journal of Electrical Power and Energy Systems*, vol. 72, pp. 24–32, 2015.

[5] A. Beddard, M. Barnes, and R. Preece, "Comparison of Detailed Modeling Techniques for MMC Employed on VSC-HVDC Schemes," *IEEE Transactions on Power Delivery*, vol. 30, no. 2, pp. 579–589, 2015.

[6] A. S. Trevisan, A. A. El-Deib, R. Gagnon, J. Mahseredjian, and M. Fecteau, "Field Validated Generic EMT-Type Model of a Full Converter Wind Turbine Based on a Gearless Externally Excited Synchronous Generator," *IEEE Transactions on Power Delivery*, vol. 33, pp. 2284–2293, oct 2018.

[7] M. Cervantes, I. Kocar, A. Montenegro, D. Goldsworthy, T. Tobin, J. Mahseredjian, R. Ramos, J. Marti, T. Noda, A. Ametani, and C. Martin, "Simulation of Switching Overvoltages and Validation With Field Tests," *IEEE Transactions on Power Delivery*, vol. 33, pp. 2884–2893, dec 2018.

[8] J. Mahseredjian, V. Dinavahi, and J. Martinez, "Simulation Tools for Electromagnetic Transients in Power Systems: Overview and Challenges," *IEEE Transactions on Power Delivery*, vol. 24, pp. 1657–1669, jul 2009.

[9] J. Mahseredjian, S. Dennetière, L. Dubé, B. Khodabakhchian, and L. Gérin-Lajoie, "On a new approach for the simulation of transients in power systems," *Electric Power Systems Research*, vol. 77, pp. 1514–1520, sep 2007.

[10] D. Woodford, A. Gole, and R. Menzies, "Digital Simulation of DC Links and AC Machines," *IEEE Transactions on Power Apparatus and Systems*, vol. PAS-102, pp. 1616–1623, jun 1983.

[11] P. Kundur, N. Balu, and M. Lauby, *Power system stability and control*. McGraw-Hill, 1994.

[12] J. Belikov and Y. Levron, "Comparison of time-varying phasor and dq0 dynamic models for large transmission networks," *International Journal of Electrical Power & Energy Systems*, vol. 93, pp. 65–74, dec 2017.

[13] N. Bottrell and T. Green, "Comparison of Current-Limiting Strategies During Fault Ride-Through of Inverters to Prevent Latch-Up and Wind-Up," *IEEE Transactions on Power Electronics*, vol. 29, pp. 3786–3797, jul 2014.

[14] M. Stubbe, A. Bihain, J. Deuse, and J. Baader, "STAG-a new unified software program for the study of the dynamic behaviour of electrical power systems," *IEEE Transactions on Power Systems*, vol. 4, no. 1, pp. 129–138, 1989.

[15] P. Aristidou, D. Fabozzi, and T. Van Cutsem, "Dynamic Simulation of Large-Scale Power Systems Using a Parallel Schur-Complement-Based Decomposition Method," *IEEE Transactions on Parallel and Distributed Systems*, vol. 25, pp. 2561–2570, oct 2014.

[16] P. Aristidou, S. Lebeau, and T. Van Cutsem, "Power System Dynamic Simulations Using a Parallel Two-Level Schur-Complement Decomposition," *IEEE Transactions on Power Systems*, vol. 31, pp. 3984–3995, sep 2016.

[17] D. Ramasubramanian, Z. Yu, R. Ayyanar, V. Vittal, and J. Undrill, "Converter Model for Representing Converter Interfaced Generation in Large Scale Grid Simulations," *IEEE Transactions on Power Systems*, vol. 32, pp. 765–773, jan 2017.

[18] H. Yang, J. Qin, S. Debnath, and M. Saeedifard, "Phasor domain steady-state modeling and design of the DC-DC modular multilevel converter," *IEEE Transactions on Power Delivery*, vol. 31, pp. 2054–2063, oct 2016.

[19] S. Sanders, J. Noworolski, X. Liu, and G. Verghese, "Generalized Averaging Method for Power Conversion Circuits," *IEEE Transactions on Power Electronics*, vol. 6, no. 2, pp. 251–259, 1991.

[20] A. Stanković and T. Aydin, "Analysis of asymmetrical faults in power systems using dynamic phasors," *IEEE Transactions on Power Systems*, vol. 15, no. 3, pp. 1062–1068, 2000.

[21] X. Guo, Z. Lu, B. Wang, X. Sun, L. Wang, and J. M. Guerrero, "Dynamic Phasors Based Modeling and Stablity Analysis of Droop-Controlled Inverters for Microgrid Applications," *IEEE Transactions on Smart Grid*, 2014.

[22] S. R. Deore, P. B. Darji, and A. M. Kulkarni, "Dynamic phasor modeling of Modular Multi-level Converters," in *2012 IEEE 7th International Conference on Industrial and Information Systems (ICIIS)*, pp. 1–6, IEEE, aug 2012.

[23] A. Stankovic, S. Sanders, and T. Aydin, "Dynamic phasors in modeling and analysis of unbalanced polyphase AC machines," *IEEE Transactions on Energy Conversion*, vol. 17, pp. 107–113, mar 2002.

[24] T. L. Vu and K. Turitsyn, "Lyapunov Functions Family Approach to Transient Stability Assessment," *IEEE Transactions on Power Systems*, vol. 31, pp. 1269–1277, mar 2016.

[25] M. Netto, Y. Susuki, and L. Mili, "Data-Driven Participation Factors for Nonlinear Systems Based on Koopman Mode Decomposition," *IEEE Control Systems Letters*, vol. 3, pp. 198–203, jan 2019.

[26] X.-F. Wang, Y. Song, and M. Irving, *Modern Power Systems Analysis*. Boston, MA: Springer US, 2008.

[27] S. D'Arco, J. Suul, and O. Fosso, "Automatic Tuning of Cascaded Controllers for Power Converters Using Eigenvalue Parametric Sensitivities," *IEEE Transactions on Industry Applications*, vol. 51, pp. 1743–1753, mar 2015.

[28] I. Perez-Arriaga, G. Verghese, and F. Schweppe, "Selective Modal Analysis with Applications to Electric Power Systems, Part I: Heuristic Introduction," *IEEE Power Engineering Review*, vol. PER-2, pp. 29–30, sep 1982.

[29] J. Quintero, V. Vittal, G. Heydt, and H. Zhang, "The impact of increased penetration of converter control-based generators on power system modes of oscillation," *IEEE Transactions on Power Systems*, vol. 29, pp. 2248–2256, sep 2014.

[30] J. Sancha and I. Perez-Arriaga, "Selective modal analysis of power system oscillatory instability," *IEEE Transactions on Power Systems*, vol. 3, pp. 429–438, may 1988.

[31] G. Bergna, J. Suul, and S. D'Arco, "Energy-Based State-Space Representation of Modular Multilevel Converters with a Constant Equilibrium Point in Steady-State Operation," *IEEE Transactions on Power Electronics*, pp. 1–1, 2017.

[32] B. Marinescu, B. Mallem, and L. Rouco, "Large-scale power system dynamic equivalents based on standard and border synchrony," *IEEE Transactions on Power Systems*, vol. 25, pp. 1873–1882, nov 2010.

[33] E. Abed, D. Lindsay, and W. Hashlamoun, "On participation factors for linear systems," *Automatica*, vol. 36, pp. 1489–1496, oct 2000.

[34] F. Garofalo, L. Iannelli, and F. Vasca, "Participation Factors and their Connections to Residues and Relative Gain Array," *IFAC Proceedings Volumes*, vol. 35, pp. 125–130, jan 2002.

[35] W. Hashlamoun, M. Hassouneh, and E. Abed, "New Results on Modal Participation Factors: Revealing a Previously Unknown Dichotomy," *IEEE Transactions on Automatic Control*, vol. 54, pp. 1439–1449, jul 2009.

[36] A. Varga, "Enhanced modal approach for model reduction," *Mathematical Modelling of Systems*, vol. 1, pp. 91–105, jan 1995.

[37] E. Davison, "A method for simplifying linear dynamic systems," *IEEE Transactions on Automatic Control*, vol. 11, pp. 93–101, jan 1966.

[38] J. Zhou, P. Shi, D. Gan, Y. Xu, H. Xin, C. Jiang, H. Xie, and T. Wu, "Large-Scale Power System Robust Stability Analysis Based on Value Set Approach," *IEEE Transactions on Power Systems*, vol. 32, pp. 4012–4023, sep 2017.

[39] A. López Ríos and A. Messina, "An optimal modal approximation method for model reduction of linear power system models," *International Journal of Electrical Power and Energy Systems*, vol. 44, no. 1, pp. 293–300, 2013.

[40] W. Schilders, H. Van der Vorst, and J. Rommes, *Model Order Reduction: Theory, Research Aspects and Applications*. Springer, 2008.

[41] B. Moore, "Principal component analysis in linear systems: Controllability, observability, and model reduction," *IEEE Transactions on Automatic Control*, vol. 26, no. 1, pp. 17–32, 1981.

[42] A. Ramirez, A. Mehrizi-Sani, D. Hussein, M. Matar, M. Abdel-Rahman, J. Jesus Chavez, A. Davoudi, and S. Kamalasadan, "Application of balanced realizations for model-order reduction of dynamic power system equivalents," *IEEE Transactions on Power Delivery*, vol. 31, pp. 2304–2312, oct 2016.

[43] S. Gugercin and A. Antoulas, "A Survey of Model Reduction by Balanced Truncation and Some New Results," *International Journal of Control*, vol. 77, no. 8, pp. 748–766, 2004.

[44] P. Kokotovic, R. O'Malley, and P. Sannuti, "Singular perturbations and order reduction in control theory — An overview," *Automatica*, vol. 12, pp. 123–132, mar 1976.

[45] A. Antoulas, *Approximation of Large-Scale Dynamical Systems*. Society for Industrial and Applied Mathematics, jan 2005.

[46] L. Pernebo and L. Silverman, "Model reduction via balanced state space representations," *IEEE Transactions on Automatic Control*, vol. 27, pp. 382–387, apr 1982.

[47] J. L. Lumley, *Stochastic tools in turbulence*. Academic press, 1970.

[48] G. Berkooz, P. Holmes, and J. L. Lumley, "The Proper Orthogonal Decomposition in the Analysis of Turbulent Flows," *Annual Review of Fluid Mechanics*, vol. 25, pp. 539–575, jan 1993.

[49] Y. Zhai and L. Vu-Quoc, "Analysis of Power Magnetic Components With Nonlinear Static Hysteresis: Proper Orthogonal Decomposition and Model Reduction," *IEEE Transactions on Magnetics*, vol. 43, pp. 1888–1897, may 2007.

[50] R. Venters, B. T. Helenbrook, Kun Zhang, and M.-C. Cheng, "Proper-Orthogonal-Decomposition Based Thermal Modeling of Semiconductor Structures," *IEEE Transactions on Electron Devices*, vol. 59, pp. 2924–2931, nov 2012.

[51] A. R. Messina and V. Vittal, "Extraction of Dynamic Patterns From Wide-Area Measurements Using Empirical Orthogonal Functions," *IEEE Transactions on Power Systems*, vol. 22, pp. 682–692, may 2007.

[52] Z. Bai, "Krylov subspace techniques for reduced-order modeling of large-scale dynamical systems," in *Applied Numerical Mathematics*, vol. 43, pp. 9–44, oct 2002.

[53] R. Freund, "Krylov-subspace methods for reduced-order modeling in circuit simulation," *Journal of Computational and Applied Mathematics*, vol. 123, no. 1-2, pp. 395–421, 2000.

[54] Z. Zhu, G. Geng, and Q. Jiang, "Power System Dynamic Model Reduction Based on Extended Krylov Subspace Method," *IEEE Transactions on Power Systems*, vol. 31, pp. 4483–4494, nov 2016.

[55] D. Chaniotis and M. A. Pai, "Model Reduction in Power Systems Using Krylov Subspace Methods," *IEEE Transactions on Power Systems*, vol. 20, no. 2, pp. 888–894, 2005.

[56] Z. Bai and Q. Ye, "Error Estimation of the Padé Approximation of Transfer Functions via the Lanczos Process," *Electronic Transactions on Numerical Analysis*, vol. 7, pp. 1–17, jan 1998.

[57] F. Chinesta, P. Ladeveze, and E. Cueto, "A Short Review on Model Order Reduction Based on Proper Generalized Decomposition," *Archives of Computational Methods in Engineering*, vol. 18, pp. 395–404, nov 2011.

[58] A. Ishchenko, J. Myrzik, and W. Kling, "Dynamic equivalencing of distribution networks with dispersed generation using Hankel norm approximation," *IET Generation, Transmission & Distribution*, vol. 1, no. 5, p. 818, 2007.

[59] S. Gugercin, "An iterative SVD-Krylov based method for model reduction of large-scale dynamical systems," *Linear Algebra and its Applications*, vol. 428, pp. 1964–1986, apr 2008.

[60] D. Osipov and K. Sun, "Adaptive Nonlinear Model Reduction for Fast Power System Simulation," *IEEE Transactions on Power Systems*, vol. 33, pp. 6746–6754, nov 2018.

[61] P. Vorobev, P. Huang, M. Al Hosani, J. Kirtley, and K. Turitsyn, "High-Fidelity Model Order Reduction for Microgrids Stability Assessment," *IEEE Transactions on Power Systems*, vol. 33, pp. 874–887, jan 2018.

[62] I. P. Nikolakakos, H. H. Zeineldin, M. S. El-Moursi, and N. D. Hatziargyriou, "Stability Evaluation of Interconnected Multi-Inverter Microgrids Through Critical Clusters," *IEEE Transactions on Power Systems*, vol. 31, pp. 3060–3072, jul 2016.

[63] M. Belhocine and B. Marinescu, "A mix balanced-modal truncations for power systems model reduction," in *2014 European Control Conference, ECC 2014*, pp. 2721–2726, IEEE, jun 2014.

[64] G. Scarciotti, "Low Computational Complexity Model Reduction of Power Systems With Preservation of Physical Characteristics," *IEEE Transactions on Power Systems*, vol. 32, pp. 743–752, jan 2017.

[65] Y. Gu, N. Bottrell, and T. Green, "Reduced-Order Models for Representing Converters in Power System Studies," *IEEE Transactions on Power Electronics*, pp. 1–1, 2017.

[66] Y. Levron and J. Belikov, "Reduction of Power System Dynamic Models Using Sparse Representations," *IEEE Transactions on Power Systems*, vol. 32, pp. 3893–3900, sep 2017.

[67] J. Marti, "Accurate Modelling of Frequency-Dependent Transmission Lines in Electromagnetic Transient Simulations," *IEEE Transactions on Power Apparatus and Systems*, vol. PAS-101, pp. 147–157, jan 1982.

[68] J. Marti and A. Tavighi, "Frequency-Dependent Multiconductor Transmission Line Model With Collocated Voltage and Current Propagation," *IEEE Transactions on Power Delivery*, vol. 33, pp. 71–81, feb 2018.

[69] S. Hosseini, M. Vakilian, and G. Gharehpetian, "Comparison of Transformer Detailed Models for Fast and Very Fast Transient Studies," *IEEE Transactions on Power Delivery*, vol. 23, pp. 733–741, apr 2008.

[70] J. Rocabert, A. Luna, F. Blaabjerg, and P. Rodríguez, "Control of Power Converters in AC Microgrids," *IEEE Transactions on Power Electronics*, vol. 27, pp. 4734–4749, nov 2012.

[71] T. Ackermann, *Wind power in power systems*. Wiley, 2005.

[72] J. Schiffer, D. Zonetti, R. Ortega, A. Stanković, T. Sezi, and J. Raisch, "A survey on modeling of microgrids—From fundamental physics to phasors and voltage sources," *Automatica*, vol. 74, pp. 135–150, dec 2016.

[73] A. Paquette, *Power Quality and Inverter-Generator Interactions in Microgrids*. PhD thesis, 2014.

[74] G. Denis, T. Prevost, M.-S. Debry, F. Xavier, X. Guillaud, and A. Menze, "The Migrate project: the challenges of operating a transmission grid with only inverter-based generation. A grid-forming control improvement with transient current-limiting control," *IET Renewable Power Generation*, 2017.

[75] O. Mo, S. D'Arco, and J. A. Suul, "Evaluation of Virtual Synchronous Machines With Dynamic or Quasi-Stationary Machine Models," *IEEE Transactions on Industrial Electronics*, vol. 64, pp. 5952–5962, jul 2017.

[76] J. Liu, Y. Miura, and T. Ise, "Comparison of Dynamic Characteristics Between Virtual Synchronous Generator and Droop Control in Inverter-Based Distributed Generators," *IEEE Transactions on Power Electronics*, vol. 31, pp. 3600–3611, may 2016.

[77] S. D'Arco and J. Suul, "Virtual synchronous machines — Classification of implementations and analysis of equivalence to droop controllers for microgrids," in *2013 IEEE Grenoble Conference*, pp. 1–7, IEEE, jun 2013.

[78] T. Qoria, F. Gruson, F. Colas, X. Guillaud, M.-S. Debry, and T. Prevost, "Tuning of cascaded controllers for robust grid-forming Voltage Source Converter," in *20th Power Systems Computation Conference, PSCC 2018*, (Dublin), 2018.

[79] T. Qoria, Q. Cossart, C. Li, X. Guillaud, F. Colas, F. Gruson, and X. Kestelyn, "WP3 - Control and Operation of a Grid with 100 % Converter-Based Devices : Deliverable 3 . 2 - Local control and simulation tools for large transmission systems," tech. rep., 2018.

[80] U. Gnanarathna, A. Gole, and R. Jayasinghe, "Efficient modeling of modular multilevel HVDC converters (MMC) on electromagnetic transient simulation programs," *IEEE Transactions on Power Delivery*, vol. 26, no. 1, pp. 316–324, 2011.

[81] H. Saad, S. Dennetiere, J. Mahseredjian, P. Delarue, X. Guillaud, J. Peralta, and S. Nguefeu, "Modular Multilevel Converter Models for Electromagnetic Transients," *IEEE Transactions on Power Delivery*, vol. 29, pp. 1481–1489, jun 2014.

[82] M. Guan and Z. Xu, "Modeling and Control of a Modular Multilevel Converter-Based HVDC System Under Unbalanced Grid Conditions," *IEEE Transactions on Power Electronics*, vol. 27, pp. 4858–4867, dec 2012.

[83] J. Freytes, L. Papangelis, H. Saad, P. Rault, T. Van Cutsem, and X. Guillaud, "On the modeling of MMC for use in large scale dynamic simulations," in *2016 Power Systems Computation Conference (PSCC)*, pp. 1–7, IEEE, jun 2016.

[84] P. Kundur, J. Paserba, V. Ajjarapu, G. Andersson, A. Bose, T. Van Cutsem, C. Canizares, N. Hatziargyriou, D. Hill, V. Vittal, A. Stanković, and C. Taylor, "Definition and Classification of Power System Stability IEEE/CIGRE Joint Task Force on Stability Terms and Definitions," *IEEE Transactions on Power Systems*, vol. 19, no. 3, pp. 1387–1401, 2004.

[85] G. Verghese, B. Levy, and T. Kailath, "A generalized state-space for singular systems," *IEEE Transactions on Automatic Control*, vol. 26, pp. 811–831, aug 1981.

[86] J. Winkelman, J. Chow, J. Allemong, and P. Kokotovic, "Multi-time-scale analysis of a power system," *Automatica*, vol. 16, pp. 35–43, jan 1980.

[87] M. Belhocine, *Modélisation et analyse structurelle du fonctionnement dynamique des systèmes électriques*. PhD thesis, 2016.

[88] Q. Cossart, F. Colas, and X. Kestelyn, "A priori error estimation of the structure-preserving modal model reduction by state residualization of a grid forming converter for use in 100% power electronics transmission systems," in *15th IET International Conference on AC and DC Power Transmission (ACDC 2019)*, (Coventry), pp. 67 (6 pp.)–67 (6 pp.), Institution of Engineering and Technology, 2019.

[89] K. Y. Lee and M. A. El-Sharkawi, *Modern heuristic optimization techniques : theory and applications to power systems*. Wiley, 2008.

[90] P. Fritzson, *Principles of object oriented modeling and simulation with Modelica 3.3 : a cyber-physical approach*. Wiley-IEEE Press, 2014.

[91] EirGrid, "http://www.eirgridgroup.com/," 2017.

[92] ENTSOE, "https://www.entsoe.eu/map/," 2017.

Appendices

Contents

The DQ0 transformation

The DQ0 (for Direct-Quadrature-Zero) transformation [11] is a basis change to represent the studied system in the DQ0 representation, which uses a rotating reference frame, instead of a fixed one, unlike the common ABC representation.

To illustrate it, consider a three-phase variable $\begin{pmatrix} x_a & x_b & x_c \end{pmatrix}^T$ in the ABC representation and an angle θ such as $\frac{d\theta}{dt} = \omega$. The expression of this variable $\begin{pmatrix} x_d & x_q & x_0 \end{pmatrix}^T$ in the DQ0 representation with the angle θ is obtained using the following transformation in (A.1).

$$\begin{pmatrix} x_d \\ x_q \\ x_0 \end{pmatrix} = \sqrt{\frac{2}{3}} \begin{pmatrix} cos(\theta) & cos(\theta - \frac{2\pi}{3}) & cos(\theta + \frac{2\pi}{3}) \\ -sin(\theta) & -sin(\theta - \frac{2\pi}{3}) & -sin(\theta + \frac{2\pi}{3}) \\ \frac{1}{\sqrt{2}} & \frac{1}{\sqrt{2}} & \frac{1}{\sqrt{2}} \end{pmatrix} \begin{pmatrix} x_a \\ x_b \\ x_c \end{pmatrix} = P(\theta) \begin{pmatrix} x_a \\ x_b \\ x_c \end{pmatrix} \tag{A.1}$$

The system is considered to be balanced. Several remarks can be made here. Proofs can be found in [11].

- The active and reactive power P and Q corresponding to a voltage v and a current i can be expressed as in (A.2) in the DQ0 representation.

$$\begin{cases} P = v_d i_d + v_q i_q \\ Q = v_q i_d - v_d i_q \end{cases} \tag{A.2}$$

- Applied to the derivative of $\begin{pmatrix} x_a & x_b & x_c \end{pmatrix}^T$, the transformation gives (A.3)

$$P(\theta) \frac{d}{dt} \begin{pmatrix} x_a \\ x_b \\ x_c \end{pmatrix} = \frac{d}{dt} \begin{pmatrix} x_d \\ x_q \\ x_0 \end{pmatrix} + \begin{pmatrix} 0 & -\omega & 0 \\ \omega & 0 & 0 \\ 0 & 0 & 0 \end{pmatrix} \begin{pmatrix} x_d \\ x_q \\ x_0 \end{pmatrix} \tag{A.3}$$

- The 0-axis value is always equal to 0 (if and only if the system is balanced, which is the case here). In the example, $x_0 = 0$ if the system is balanced. It means that only x_d and x_q are of interest in this case. It means that, without doing any approximation, the complexity of the model is reduced.

- If the variable $\begin{pmatrix} x_a & x_b & x_c \end{pmatrix}^T$ is sinusoidal at the frequency ω in steady-state, the variable $\begin{pmatrix} x_d & x_q & x_0 \end{pmatrix}^T$ is constant in steady-state. This is interesting because this simplifies the simulation (a larger time-step can be used in steady-state [3]) and it allows using the linear analysis tools (which are relevant only when the system is steady-state time-invariant) in the DQ0 representation, which is not possible in the ABC representation.

The eigenvalue decomposition

Consider a square matrix $A \in \mathbb{R}^{n \times n}$. The set of the eigenvalues of A is noted σ_A and is called its spectrum. The eigenvalues of A are complex values that can be defined as in (A.4).

$$\lambda_i \in \sigma_A \Leftrightarrow \exists y_i \in \mathbb{R}^n / A y_i = \lambda_i y_i \tag{A.4}$$

In (A.4), y_i is called a right eigenvector of A associated to the eigenvalue λ_i.

The matrix $P = \begin{pmatrix} y_1 & \dots & y_n \end{pmatrix}$ is defined. If P is not singular, the Eigenvalue Decomposition (EVD) of A is then done and presented in (A.5).

$$A = P \Lambda P^{-1} = P diag(\lambda_i) P^{-1} \tag{A.5}$$

The singular value decomposition

Consider a rectangular matrix $A \in \mathbb{R}^{n \times k}$. The singular value decomposition of A is defined in (A.6).

$$A = U \Sigma V^*,\ U \in \mathbb{R}^{n \times n},\ \Sigma \in \mathbb{R}^{n \times k},\ V \in \mathbb{R}^{k \times k} \tag{A.6}$$

In this equation, U and V are unitary ($U^*U = UU^* = I$ and $V^*V = VV^* = I$) and Σ is rectangular diagonal. The diagonal values of Σ are called the singular values of A.

One can note that the singular values of A are the square root of the eigenvalues of AA^* and A^*A.

Résumé étendu en français

Contents

Introduction

Contexte général

Pour lutter contre le réchauffement climatique et réduire les émissions de gaz à effet de serre, les gouvernements de la plupart des pays du monde ont décidé d'investir massivement dans les énergies renouvelables. En parallèle, de nombreuses lignes à courant continu haute tension sont construites pour connecter des réseaux asynchrones ou synchrones sur de longues distances. Ceci, ajouté à l'arrivé récente des véhicules électriques, entraîne une forte augmentation de la pénétration de l'électronique de puissance dans les réseaux de transport d'électricité.

Aujourd'hui, les convertisseurs d'électronique de puissance sont contrôlés comme de simples sources de courant (on parle de convertisseur « grid feeding »). S'ils viennent à remplacer les générateurs synchrones, ils devront être contrôlés comme des sources de tension pour créer la tension du réseau (on parle de convertisseur « grid forming »), et ces nouveaux types de contrôles restent à développer.

Pour anticiper, différents gestionnaires de réseaux de transport européens et des universités (voir figure B.1) se sont rassemblés au sein du projet européen MIGRATE (Massive InteGRATion of power Electronic devices). L'objectif principal du projet est de proposer des solutions innovantes pour progressivement ajuster les réseaux de transport à cette augmentation massive de la pénétration de l'électronique de puissance. Le projet est découpé en 8 groupes de travail présentés dans la figure B.2. Cette thèse fait partie du groupe 3 qui cherche à développer de nouveaux contrôles pour les réseaux 100% électronique de puissance.

Les objectifs de cette thèse sont la simulation et l'analyse de réseaux de transport 100% électronique de puissance. En effet, puisque les convertisseurs ont des comportements dynamiques très différents de celui des machines synchrones, rien ne garantit que les outils actuels ne soient encore valables. En conséquence, cette thèse développe de nouveaux outils d'analyse et de simulation et donne des conseils dans la manière avec laquelle un réseau 100% électronique de puissance doit être modélisé, simulé et analysé.

Plan de la thèse

Cette thèse est organisée en quatre chapitres.

Le premier chapitre passe en revue les outils et méthodes existants et utilisés actuellement pour simuler et analyser des réseaux de transport ainsi que les méthodes de réduction de modèles les plus couramment utilisées.

Le deuxième chapitre présente les modèles utilisés dans le reste de la thèse. Chaque élément d'un réseau de transport est modélisé: les convertisseurs, les lignes, les transformateurs, les machines synchrones et les charges.

Le troisième chapitre présente les trois méthodes de réduction de modèles développées. Le processus est détaillé pour chacune d'elles. Ces méthodes utilisent les outils d'analyse présentés dans le chapitre 1 et s'inspirent des méthodes existantes. Toutes les

méthodes préservent les variables, les paramètres, la structure physique et la stabilité du système.

Le quatrième et dernier chapitre applique les méthodes développées à des cas d'études réalistes en utilisant les modèles présentés dans le chapitre 2. Les conclusions pour chaque cas sont des recommandations pour modéliser, simuler et analyser un réseau de transport à forte pénétration d'électronique de puissance. Une des conclusions est que le meilleur modèle réduit à utiliser est différent selon la variable observée et l'événement simulé. Et ceci est pris en compte par les méthodes développées.

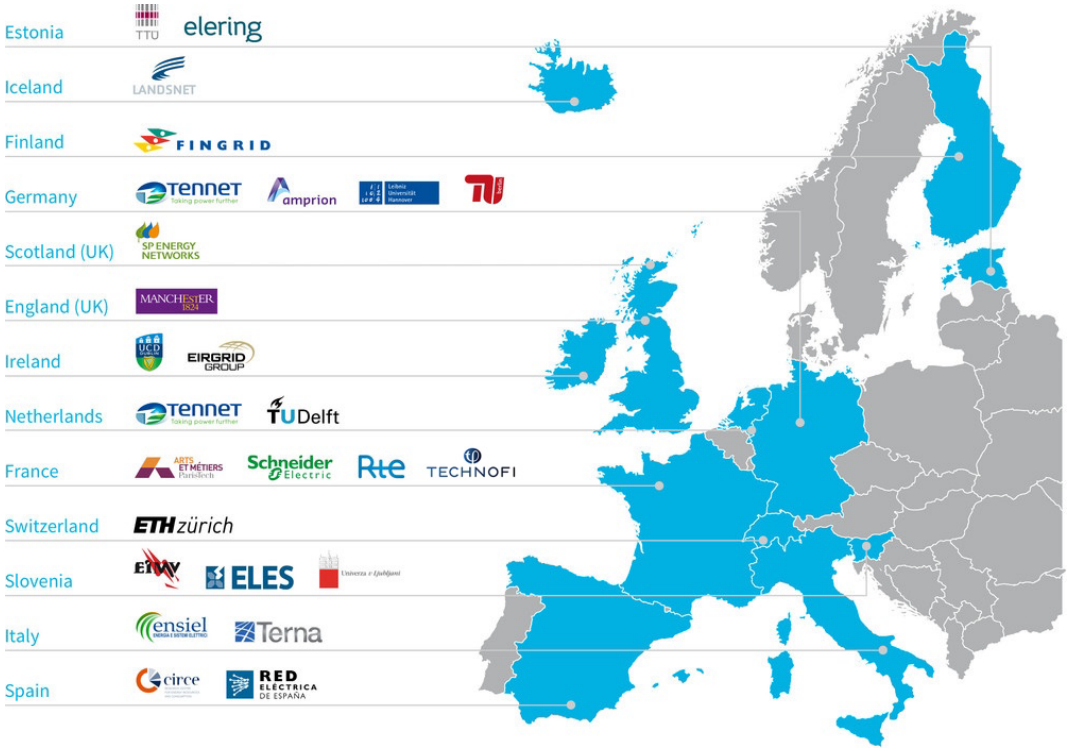

Figure B.1: Membres du projet MIGRATE

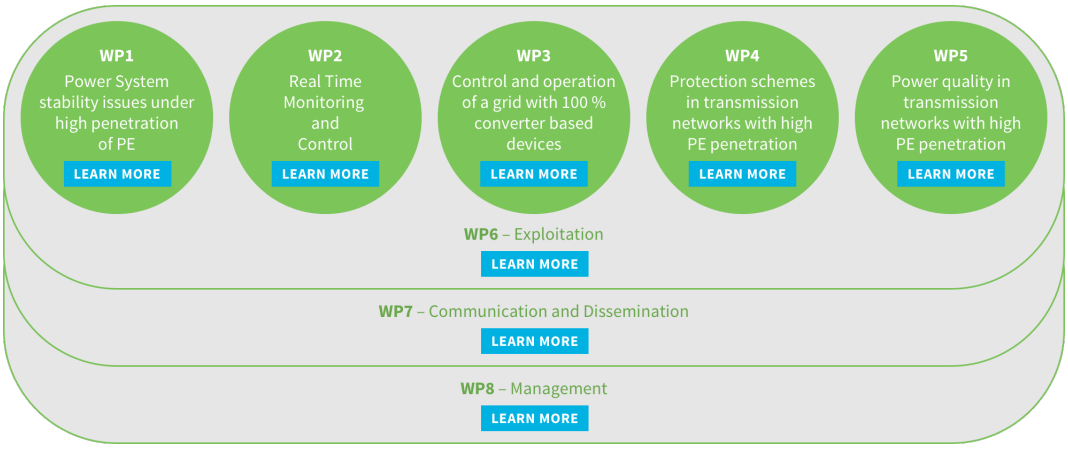

Figure B.2: Groupes de travail du projet MIGRATE

Chapitre 1: contexte scientifique

Ce chapitre présente le contexte scientifique de la thèse par le biais d'un travail bibliographique. La première section présente les outils existants pour simuler et analyser un réseau de transport tandis que la seconde section présente les méthodes classiques de réduction de modèles.

Outils et méthodes pour la simulation et l'analyse de réseaux de transport

Outils de simulation

Logiciels EMT Les logiciels EMT (Electromagnetic Transient) considèrent les transitoires électromagnétiques rapides en plus des transitoires électromécaniques lents (voir Figure B.3). Leur temps de simulation est élevé de par le niveau de détails des modèles utilisés et de par le fait que les pas de calculs utilisés doivent être petits (quelques dizaines de μs). De plus, le grand nombre de variables complique l'analyse. En conséquence, seules des parties locales du système sont simulées et sur une courte période.

Pour toutes ces raisons, ils sont particulièrement adaptés à la simulation de convertisseurs. Mais dans cette thèse, les systèmes simulés et analysés sont grands. Cela signifie qu'utiliser des logiciels EMT peut mener à des analyses trop complexes et des simulations trop longues.

L'approximation phaseurs L'approximation phaseurs consiste à négliger les dynamiques des lignes car elles sont plus rapides que les dynamiques des machines synchrones.

Par exemple, un modèle de ligne R,L est considéré dans la representation DQ dans l'équation (B.1).

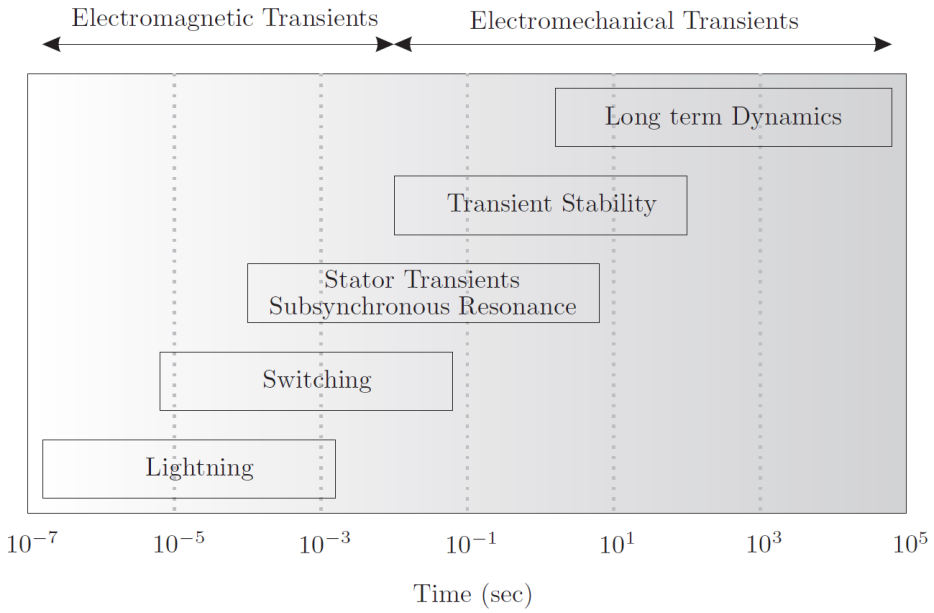

Figure B.3: Les transitoires dans les réseaux de transport

$$\begin{cases} \dfrac{L}{\omega_b}\dfrac{di_d}{dt} = v_{1_d} - v_{2_d} - Ri_d + \omega L i_q \\ \dfrac{L}{\omega_b}\dfrac{di_q}{dt} = v_{1_q} - v_{2_q} - Ri_q - \omega L i_d \end{cases} \tag{B.1}$$

Avec l'approximation phaseurs, cette équation devient (B.2).

$$\begin{cases} 0 = v_{1_d} - v_{2_d} - Ri_d + \omega L i_q \\ 0 = v_{1_q} - v_{2_q} - Ri_q - \omega L i_d \end{cases} \tag{B.2}$$

Le comportement de la ligne est désormais quasi-statique, ce qui simplifie le modèle et accélère la simulation. Il est maintenant possible d'utiliser des pas de calcul plus grands et l'analyse du système est simplifiée car le nombre de variables d'état a diminué. Mais cette approximation engendre des erreurs de simulation. La question est de décider si les transitoires non pris en compte sont importants pour l'étude ou non.

En revanche, l'hypothèse sur laquelle se base l'approximation phaseurs peut ne plus être vérifiée à l'avenir si la pénétration de l'électronique de puissance augmente et celle des machines synchrones diminue.

Phaseurs dynamiques Les phaseurs dynamiques sont basés sur une décomposition en série de Fourier. L'avantage est qu'ils peuvent prendre en compte les systèmes déséquilibrés, sont plus précis que les simulations phaseurs et moins couteux en temps de calcul que les logiciels EMT.

En revanche, ils augmentent le nombre de variables du système ce qui rend l'analyse compliquée. De plus ils ne sont pas facilement utilisables sur les logiciels de simulation classiques.

Outils d'analyse

Analyse petits signaux Tout d'abord, un système non linéaire algébro-différentiel est considéré dans l'équation (B.3).

$$\begin{cases} \dfrac{dx_{diff}}{dt} = f(x_{diff}, x_{alg}, u) \\ \qquad 0 = g(x_{diff}, x_{alg}, u) \\ \qquad y = h(x_{diff}, x_{alg}, u) \\ x_{diff} \in \mathbb{R}^{N_{diff}}, x_{alg} \in \mathbb{R}^{N_{alg}}, u \in \mathbb{R}^p, y \in \mathbb{R}^q \end{cases} \tag{B.3}$$

Ce système est linéarisé, ce qui donne l'équation (B.4).

$$\begin{cases} \dfrac{dx}{dt} = Ax + Bu \\ \quad y = Cx + Du \\ \quad x \in \mathbb{R}^{N_{diff}}, u \in \mathbb{R}^p, y \in \mathbb{R}^q \end{cases} \tag{B.4}$$

Les pôles de ce système sont les valeurs propres de la matrice A. L'ensemble des valeurs propres de A est noté σ_A et appelé spectre de A. Les valeurs propres de A sont les racines du polynôme caractéristique de A, comme présenté dans (B.5).

$$\lambda_i \in \sigma_A \Leftrightarrow det(A - \lambda_i I_{n_{diff}}) = 0 \tag{B.5}$$

Un système linéaire est exponentiellement stable si tous ses pôles ont une partie réelle strictement négative, comme expliqué dans (B.6).

$$\text{Le système est stable} \Leftrightarrow \forall \lambda_i \in \sigma_A, Re(\lambda_i) < 0 \tag{B.6}$$

Analyse de sensibilité La sensibilité $s_{r_{i,j}}$ de la partie réelle du pôle λ_i en fonction du paramètre p_j est définie dans (B.7).

$$s_{r_{i,j}} = \frac{\partial Re(\lambda_i)}{\partial p_j} \tag{B.7}$$

Elle donne l'évolution du pôle considéré lorsque le paramètre en question change.

Facteurs de participation Les valeurs propres de A, définies dans (B.5) peuvent aussi être définies dans (B.8).

$$\lambda_i \in \sigma_A \Leftrightarrow \exists y_i \in \mathbb{R}^{N_{diff}} / Ay_i = \lambda_i y_i \tag{B.8}$$

Dans (B.8), y_i est appelé vecteur propre à droite de A associé à la valeur propre λ_i. De la même façon, la définition dans (B.8) peut être réécrite avec un vecteur propre à gauche comme dans (B.9).

$$\lambda_i \in \sigma_A \Leftrightarrow \exists u_i \in \mathbb{R}^{N_{diff}} / u_i^T A = \lambda_i u_i^T \tag{B.9}$$

Le facteurs de participation $p_{k,i}$ est un nombre complexe qui donne la participation de la variable d'état x_k dans la valeur propre λ_i. Il est calculé dans (B.10).

$$p_{k,i} = u_i(k) y_i(k) \tag{B.10}$$

Réduction de modèles

Une réduction de modèles est un processus qui trouve un modèle avec une sortie proche de celle du modèle initial mais de taille réduite. Par example, considérons les modèle dans (B.11) et (B.12).

$$\begin{cases} \dfrac{dx_{diff}}{dt} = f(x_{diff}, x_{alg}, u) \\ 0 = g(x_{diff}, x_{alg}, u) \\ y = h(x_{diff}, x_{alg}, u) \\ x_{diff} \in \mathbb{R}^{N_{diff}}, x_{alg} \in \mathbb{R}^{N_{alg}}, u \in \mathbb{R}^p, y \in \mathbb{R}^q \end{cases} \tag{B.11}$$

$$\begin{cases} \dfrac{dx_{diff_r}}{dt} = f_r(x_{diff_r}, x_{alg_r}, u) \\ 0 = g_r(x_{diff_r}, x_{alg_r}, u) \\ y_r = h_r(x_{diff_r}, x_{alg_r}, u) \\ x_{diff_r} \in \mathbb{R}^{N_{diff_r}}, x_{alg_r} \in \mathbb{R}^{N_{alg_r}}, u \in \mathbb{R}^p, y_r \in \mathbb{R}^q \end{cases} \tag{B.12}$$

Le système dans (B.12) est une réduction du système dans (B.11) si l'équation (B.13) est respectée, pour une erreur acceptée ϵ donnée.

$$\begin{cases} ||y - y_r|| < \epsilon \\ N_{diff_r} << N_{diff} \end{cases} \tag{B.13}$$

Les méthodes de réduction de modèles les plus courantes sont présentées ici.

Troncature modale

La troncatures modale est basée sur la suppression de certains pôles du système et la préservation d'autres, assurant ainsi la préservation de la stabilité.

Pour illustrer, la méthode est appliquée au système dans (B.14).

$$\begin{cases} \dfrac{dx}{dt} = Ax + Bu \\ y = Cx + Du \\ x \in \mathbb{R}^{N_{diff}}, u \in \mathbb{R}^p, y \in \mathbb{R}^q \end{cases} \tag{B.14}$$

Décomposition en valeurs propres et changements de base La décomposition en valeurs propres de A est effectuée dans (B.15).

$$A = P^{-1}\Lambda P = P^{-1} diag(\lambda_i) P \tag{B.15}$$

En écrivant $x_m = Px$, $B_m = PB$, $C_m = CP^{-1}$, le système peut être réécrit dans (B.16).

$$\begin{cases} \dfrac{dx_m}{dt} = \Lambda x_m + B_m u \\ y = C_m x_m + Du \\ x_m \in \mathbb{R}^{N_{diff}}, u \in \mathbb{R}^p, y \in \mathbb{R}^q \end{cases} \tag{B.16}$$

Pôles rapides/pôles lents Le système est organisé comme suit dans (B.17). Dans ces équations, Λ_1 contient les pôles à garder et Λ_2 les pôles à supprimer. En général les pôles les plus lents sont gardés (ceux proches de l'axe imaginaire).

$$\begin{cases} \dfrac{d}{dt}\begin{pmatrix} x_{m_1} \\ x_{m_2} \end{pmatrix} = \begin{pmatrix} \Lambda_1 & 0 \\ 0 & \Lambda_2 \end{pmatrix}\begin{pmatrix} x_{m_1} \\ x_{m_2} \end{pmatrix} + \begin{pmatrix} B_{m_1} \\ B_{m_2} \end{pmatrix} u \\ y = \begin{pmatrix} C_{m_1} & C_{m_2} \end{pmatrix}\begin{pmatrix} x_{m_1} \\ x_{m_2} \end{pmatrix} + Du \\ x_{m_1} \in \mathbb{R}^{N_{diff_1}}, x_{m_2} \in \mathbb{R}^{N_{diff_2}}, u \in \mathbb{R}^p, y \in \mathbb{R}^q \end{cases} \tag{B.17}$$

Le choix de N_{diff_1} détermine la taille du modèle réduit.

La troncature modale consiste à tronquer le modèle dans (B.17) pour ne garder que x_{m_1}. Cela donne le modèle réduit dans (B.18)

$$\begin{cases} \dfrac{dx_{m_{1_r}}}{dt} = \Lambda_1 x_{m_{1_r}} + B_{m_1} u \\ y_r = C_{m_1} x_{m_{1_r}} + Du \\ x_{m_{1_r}} \in \mathbb{R}^{N_{diff_1}}, u \in \mathbb{R}^p, y_r \in \mathbb{R}^q \end{cases} \tag{B.18}$$

Cependant, les variables d'état du modèle complet et du modèle réduit ne sont plus les mêmes à cause du changement de base et de la troncature, ce qui complique l'analyse.

Troncature équilibrée

Le système à réduire est celui dans (B.19).

$$\begin{cases} \dfrac{dx}{dt} = Ax + Bu \\ \quad y = Cx + Du \\ \quad x \in \mathbb{R}^{N_{diff}}, u \in \mathbb{R}^p, y \in \mathbb{R}^q \end{cases} \tag{B.19}$$

Gramiens d'observabilité et de commandabilité Les Gramiens de commandabilité P et d'observabilité Q sont définis dans (B.20).

$$\begin{cases} P = \displaystyle\int_0^{+\infty} e^{At} B B^T e^{A^T t} dt \\ Q = \displaystyle\int_0^{+\infty} e^{A^T t} C^T C e^{At} dt \end{cases} \tag{B.20}$$

Ils peuvent être calculés en résolvant les équations de Lyapunov dans (B.21).

$$\begin{cases} AP + PA^T + BB^T = 0 \\ A^T Q + QA + C^T C = 0 \end{cases} \tag{B.21}$$

Le système est considéré dans une nouvelle base b dans (B.22).

$$\begin{cases} \dfrac{dx_b}{dt} = A_b x_b + B_b u \\ \quad y = C_b x_b + Du \end{cases} \tag{B.22}$$

Les variables et matrices dans cette nouvelle base sont calculées en utilisant la matrice T_b comme dans (B.23).

$$\begin{cases} x_b = T_b x \\ A_b = T_b A T_b^{-1} \\ B_b = T_b B \\ C_b = C T_b^{-1} \end{cases} \tag{B.23}$$

Les Gramiens dans cette nouvelle base sont alors exprimés comme suit dans (B.24).

$$\begin{cases} P_b = T_b P T_b^T \\ Q_b = T_b^{-T} Q T_b^{-1} \end{cases} \tag{B.24}$$

Valeurs singulières de Hankel Les valeurs singulières de Hankel (HSV) sont la racine carrée des valeurs propres du produit PQ et sont notées σ_i comme dans (B.25).

$$\sigma_i = \sqrt{\lambda_i(PQ)} \tag{B.25}$$

Transformation d'équilibrage Considérons une matrice triangulaire supérieure U et inférieure L telles que $P = UU^T$ et $Q = LL^T$.

Une decomposition en valeurs singulières du produit $U^T L$ est faite dans (B.26).

$$U^T L = Z\Sigma Y^T \tag{B.26}$$

La transformation d'équilibrage T_b est alors définie dans (B.27).

$$T_b = \Sigma^{\frac{1}{2}} Z^T U^{-1} \tag{B.27}$$

Dans la nouvelle base b, les Gramiens sont alors égaux et diagonaux comme dans (B.28). Les valeurs dans la diagonales sont les valeurs singulières de Hankel.

$$P_b = Q_b = diag(\sigma_i) \tag{B.28}$$

États les plus commandables et observables Dans ces conditions, une HSV est associée à chaque état dans la réalisation équilibrée x_{b_i}. C'est un réel positif qui donne le degré d'observabilité et de commandabilité de l'état en question.

Le système est réarrangé de façon à ce que x_{b_1} soit l'état le plus commandable et observable et $x_{b_{N_{diff}}}$ le moins.

Dans ces conditions, le modèle peut être exprimé comme dans (B.29).

$$\begin{cases} \dfrac{d}{dt}\begin{pmatrix} x_{b_1} \\ x_{b_2} \end{pmatrix} = \begin{pmatrix} A_{b_{11}} & A_{b_{12}} \\ A_{b_{21}} & A_{b_{22}} \end{pmatrix}\begin{pmatrix} x_{b_1} \\ x_{b_2} \end{pmatrix} + \begin{pmatrix} B_{b_1} \\ B_{b_2} \end{pmatrix} u \\ y = \begin{pmatrix} C_{b_1} & C_{b_2} \end{pmatrix}\begin{pmatrix} x_{b_1} \\ x_{b_2} \end{pmatrix} + Du \\ x_{b_1} \in \mathbb{R}^{N_{diff_1}}, x_{b_2} \in \mathbb{R}^{N_{diff_2}}, u \in \mathbb{R}^p, y \in \mathbb{R}^q \end{cases} \tag{B.29}$$

Troncature équilibrée La troncatures équilibrée consiste à tronquer le modèle dans (B.29) pour ne garder que les états les plus commandables et observables x_{b_1}. Cela donne le modèle réduit dans (B.30).

$$\begin{cases} \dfrac{dx_r}{dt} = A_{b_{11}} x_r + B_{b_1} u \\ y_r = C_{b_1} x_r + Du \end{cases} \tag{B.30}$$

POD

La POD (Proper Orthogonal Decomposition) est appliquée à système différentiel ordinaire non linéaire dans (B.31).

$$\begin{cases} \dfrac{dx}{dt} = f(x,u) \\ \quad y = g(x,u) \\ \quad x \in \mathbb{R}^N, u \in \mathbb{R}^p, y \in \mathbb{R}^q \end{cases} \tag{B.31}$$

Matrice de snapshots, decomposition en valeurs propres et approximation La première étape de la méthode consiste à collecter des snapshots d'une simulation précédente. Cela donne la matrice X dans (B.32).

$$X = \begin{pmatrix} x_1(t_1) & \dots & x_1(t_{N_{time}}) \\ \vdots & \ddots & \vdots \\ x_N(t_1) & \dots & x_N(t_{N_{time}}) \end{pmatrix} \tag{B.32}$$

Une decomposition en valeurs propres de la matrice XX^T est effectuée dans (B.33).

$$\begin{cases} XX^T = U\Sigma V \\ XX^T \in \mathbb{R}^{N\times N}, \Sigma \in \mathbb{R}^{N\times N}, U \in \mathbb{R}^{N\times N}, V \in \mathbb{R}^{N\times N} \end{cases} \tag{B.33}$$

L'équation (B.33) est réorganisée dans (B.34) de façon à ce que σ_1 soit la valeur propre la plus grande et σ_N la plus petite. Dans cette équation $\Sigma_k = diag(\sigma_1, ..., \sigma_k)$ contient les k valeurs propres les plus grandes de XX^T.

$$\begin{cases} XX^T = \begin{pmatrix} U_k & U_{rest} \end{pmatrix} \begin{pmatrix} \Sigma_k & 0 \\ 0 & \Sigma_{rest} \end{pmatrix} \begin{pmatrix} V_k \\ V_{rest} \end{pmatrix} \\ \qquad = U_k\Sigma_k V_k + U_{rest}\Sigma_{rest}V_{rest} \end{cases} \tag{B.34}$$

La matrice XX^T peut être approximée dans (B.35).

$$XX^T \approx U_k\Sigma_k V_k \tag{B.35}$$

Réduction de modèle La réduction de modèle par POD consiste à définir le système réduit dans (B.36).

$$\begin{cases} \dfrac{dx_r}{dt} = V_k f(U_k x_r, u) \\ \quad y_r = g(U_k x_r, u) \\ \quad x_r \in \mathbb{R}^k, u \in \mathbb{R}^p, y_r \in \mathbb{R}^q \end{cases} \tag{B.36}$$

Les fonctions f_r et g_r sont définies dans (B.37).

$$\begin{cases} f_r(x_r, u) = V_k f(U_k x_r, u) \\ g_r(x_r, u) = g(U_k x_r, u) \end{cases} \tag{B.37}$$

Cela permet d'écrire le nouveau système réduit dans (B.38).

$$\begin{cases} \dfrac{dx_r}{dt} = f_r(x_r, u) \\ y_r = g_r(x_r, u) \\ x_r \in \mathbb{R}^k, u \in \mathbb{R}^p, y_r \in \mathbb{R}^q \end{cases} \tag{B.38}$$

Comparaison des méthodes et applicabilité à des réseaux de transport à forte pénétration d'électronique de puissance

Le tableau B.13 résume les différentes caractéristiques des méthodes présentées ainsi que les caractéristiques désirées pour la méthode recherchée. Ce tableau montre que les méthodes classiques ne remplissent pas les critères recherchées.

	Applicabilité à des modèles non linéaires	Préservation des variables	Préservation des pôles	Préservation de la stabilité
Modale	Non	Non	Oui	Oui
Équilibrée	Non	Non	No	Oui
POD	Oui	Non	Non	Non
Attendue	Oui	Oui	Oui	Oui

Table B.13: Comparaison des caractéristiques des méthodes de réduction de modèles classiques

Conclusion du chapitre

Au vu de l'étude bibliographique effectuée dans ce chapitre, cette thèse se concentre sur le développement de nouvelles méthodes de réduction de modèles. Ces méthodes devront préserver les variables, les pôles et la stabilité du système de départ.

Chapitre 2: modélisation de réseaux de transport à forte pénétration d'électronique de puissance

Ce chapitre présente les différents modèles utilisés dans cette thèse.

Modélisation des éléments basiques d'un réseau de transport

Lignes

Modèle en Pi Les équations d'une ligne en modèle en Pi sont données ici.

$$\frac{L}{\omega_b}\frac{di_d}{dt} = v_{1_d} - v_{2_d} - Ri_d + \omega L i_q \tag{B.39}$$

$$\frac{L}{\omega_b}\frac{di_q}{dt} = v_{1_q} - v_{2_q} - Ri_q - \omega L i_d \tag{B.40}$$

$$\frac{C}{2\omega_b}\frac{dv_{1_d}}{dt} = i_{i_d} - i_d + \omega\frac{C}{2}v_{1_q} \tag{B.41}$$

$$\frac{C}{2\omega_b}\frac{dv_{1_q}}{dt} = i_{i_q} - i_q - \omega\frac{C}{2}v_{1_d} \tag{B.42}$$

$$\frac{C}{2\omega_b}\frac{dv_{2_d}}{dt} = i_d - i_{j_d} + \omega\frac{C}{2}v_{2_q} \tag{B.43}$$

$$\frac{C}{2\omega_b}\frac{dv_{2_q}}{dt} = i_q - i_{j_q} - \omega\frac{C}{2}v_{2_d} \tag{B.44}$$

Modèle RL Les équations d'une ligne en modèle RL sont données ici.

$$\frac{L}{\omega_b}\frac{di_d}{dt} = v_{1_d} - v_{2_d} - Ri_d + \omega L i_q \tag{B.45}$$

$$\frac{L}{\omega_b}\frac{di_q}{dt} = v_{1_q} - v_{2_q} - Ri_q - \omega L i_d \tag{B.46}$$

Transformateurs

Les équations du modèle utilisé pour les transformateurs sont données ici.

$$\frac{L}{\omega_b}\frac{di_d}{dt} = v'_{1_d} - v'_{2_d} - Ri_d + \omega L i_q \tag{B.47}$$

$$\frac{L}{\omega_b}\frac{di_q}{dt} = v'_{1_q} - v'_{2_q} - Ri_q - \omega L i_d \tag{B.48}$$

$$\begin{pmatrix} v'_{1_d} \\ v'_{1_q} \end{pmatrix} = \frac{1}{r}\begin{pmatrix} v_{1_d} \\ v_{1_q} \end{pmatrix} \tag{B.49}$$

$$\begin{pmatrix} v'_{2_d} \\ v'_{2_q} \end{pmatrix} = \begin{pmatrix} cos(\delta) & -sin(\delta) \\ sin(\delta) & cos(\delta) \end{pmatrix}\begin{pmatrix} v_{2_d} \\ v_{2_q} \end{pmatrix} = R(\delta)\begin{pmatrix} v_{2_d} \\ v_{2_q} \end{pmatrix} \tag{B.50}$$

Charges

Les équations du modèle des charges sont données ici.

$$\frac{L}{\omega_b}\frac{di_d}{dt} = v_d - Ri_d + \omega L i_q \tag{B.51}$$

$$\frac{L}{\omega_b}\frac{di_q}{dt} = v_q - Ri_q - \omega L i_d \tag{B.52}$$

Condensateurs shunt

Les équations du modèle des condensateurs shunt sont données ici.

$$\frac{C}{\omega_b}\frac{dv_d}{dt} = i_d + \omega C v_q \tag{B.53}$$

$$\frac{C}{\omega_b}\frac{dv_q}{dt} = i_q - \omega C v_d \tag{B.54}$$

Machines synchrones

Les équations du modèle de la machine synchrone utilisé sont données ici.

$$\frac{1}{\omega_b}\frac{d\phi_d}{dt} = v_d + R_s i_d + \omega \phi_q \tag{B.55}$$

$$\frac{1}{\omega_b}\frac{d\phi_q}{dt} = v_q + R_s i_q - \omega \phi_d \tag{B.56}$$

$$\frac{1}{\omega_b}\frac{d\phi_{f_d}}{dt} = V_e - R_f i_{f_d} \tag{B.57}$$

$$\frac{1}{\omega_b}\frac{d\phi_{1_d}}{dt} = -R_{1_d} i_{1_d} \tag{B.58}$$

$$\frac{1}{\omega_b}\frac{d\phi_{1_q}}{dt} = -R_{1_q} i_{1_q} \tag{B.59}$$

$$\frac{1}{\omega_b}\frac{d\phi_{2_q}}{dt} = -R_{2_q} i_{2_q} \tag{B.60}$$

$$\phi_d = -L_d i_d + L_{a_d} i_{f_d} + L_{a_d} i_{1_d} \tag{B.61}$$

$$\phi_q = -L_q i_q + L_{a_q} i_{1_q} + L_{a_q} i_{2_q} \tag{B.62}$$

$$\phi_{f_d} = -L_{a_d} i_d + L_{f_d} i_{f_d} + L_{a_d} i_{1_d} \tag{B.63}$$

$$\phi_{1_d} = -L_{a_d} i_d + L_{a_d} i_{f_d} + L_{1_d} i_{1_d} \tag{B.64}$$

$$\phi_{1_q} = -L_{a_q} i_q + L_{1_q} i_{1_q} + L_{a_q} i_{2_q} \tag{B.65}$$

$$\phi_{2_q} = -L_{a_q} i_q + L_{a_q} i_{1_q} + L_{2_q} i_{2_q} \tag{B.66}$$

$$\Gamma_e = \phi_d i_q - \phi_q i_d \tag{B.67}$$

$$\frac{L_g}{\omega_b}\frac{di_d}{dt} = v_d - v_{g_d} - R_g i_d + \omega L_g i_q \tag{B.68}$$

$$\frac{L_g}{\omega_b}\frac{di_q}{dt} = v_q - v_{g_q} - R_g i_q - \omega L_g i_d \tag{B.69}$$

$$2J\frac{d\omega}{dt} = \Gamma_m - \Gamma_e - k_d(\omega - \omega_g) \tag{B.70}$$

$$\frac{1}{\omega_b}\frac{d\delta}{dt} = \omega - \omega_g \tag{B.71}$$

$$m_d \Delta P^* = \omega^* - \omega \tag{B.72}$$

$$T_d\frac{d\Delta P_d}{dt} = \Delta P^* - \Delta P_d \tag{B.73}$$

$$T_{se}\frac{d\Delta P_s}{dt} = P^* - \Delta P_s - \Delta P_d \tag{B.74}$$

$$T_{ac}\frac{d\Delta P_a}{dt} = \Delta P_s - \Delta P_a \tag{B.75}$$

$$T_1\frac{d\Delta P_a}{dt} + \Delta P_a = T_2\frac{d\Gamma_m}{dt} + \Gamma_m \tag{B.76}$$

$$V = \sqrt{v_d^2 + v_q^2} \tag{B.77}$$

$$T_r\frac{dV_f}{dt} = V - V_f \tag{B.78}$$

$$u^* = V^* - V_f - V_{e_f} \tag{B.79}$$

$$T_a\frac{du_f^*}{dt} = K_a u^* - u_f^* \tag{B.80}$$

$$T_e\frac{dV_e}{dt} = K_e u_f^* - V_e \tag{B.81}$$

$$K_f\frac{dV_e}{dt} = V_{e_f} + T_f\frac{dV_{e_f}}{dt} \tag{B.82}$$

Modèles des convertisseurs

Convertisseurs grid feeding

Les équations du modèle des convertisseurs grid feeding sont données ici.

$$\frac{L_f}{\omega_b}\frac{di_{s_d}}{dt} = v_{m_d} - e_d - R_f i_{s_d} + \omega_{PLL} L_f i_{s_q} \tag{B.83}$$

$$\frac{L_f}{\omega_b}\frac{di_{s_q}}{dt} = v_{m_q} - e_q - R_f i_{s_q} - \omega_{PLL} L_f i_{s_d} \tag{B.84}$$

$$\frac{C_f}{\omega_b}\frac{de_d}{dt} = i_{s_d} - i_{g_d} + \omega_{PLL} C_f e_q \tag{B.85}$$

$$\frac{C_f}{\omega_b}\frac{de_q}{dt} = i_{s_q} - i_{g_q} - \omega_{PLL} C_f e_d \tag{B.86}$$

$$\frac{L_t}{\omega_b}\frac{di_{g_d}}{dt} = e_d - v_{g_d} - R_t i_{g_d} + \omega_{PLL} L_t i_{g_q} \tag{B.87}$$

$$\frac{L_t}{\omega_b}\frac{di_{g_q}}{dt} = e_q - v_{g_q} - R_t i_{g_q} - \omega_{PLL} L_t i_{g_d} \tag{B.88}$$

$$v^*_{m_d} = v_{m_d} \tag{B.89}$$

$$v^*_{m_q} = v_{m_q} \tag{B.90}$$

$$\frac{dM_{PLL}}{dt} = K_{i_{PLL}} e_q \tag{B.91}$$

$$\omega_{PLL} = \frac{K_{p_{PLL}} e_q + M_{PLL}}{\omega_b} + \omega_g \tag{B.92}$$

$$\frac{1}{\omega_b}\frac{d\theta_{PLL}}{dt} = \omega_{PLL} - \omega_g \tag{B.93}$$

$$p = e_d i_{g_d} + e_q i_{g_q} \tag{B.94}$$

$$q = e_q i_{g_d} - e_d i_{g_q} \tag{B.95}$$

$$\frac{dM_p}{dt} = K_{i_{pq}}(p^* - p) \tag{B.96}$$

$$\frac{dM_q}{dt} = K_{i_{pq}}(q^* - q) \tag{B.97}$$

$$i^*_{s_d} = K_{p_{pq}}(p^* - p) + M_p \tag{B.98}$$

$$i^*_{s_q} = K_{p_{pq}}(q^* - q) + M_q \tag{B.99}$$

$$\frac{dM_{CL_d}}{dt} = K_{i_{CL}}(i^*_{s_d} - i_{s_d}) \tag{B.100}$$

$$\frac{dM_{CL_q}}{dt} = K_{i_{CL}}(i^*_{s_q} - i_{s_q}) \tag{B.101}$$

$$\tau_f \frac{de_{d_f}}{dt} + e_{d_f} = e_d \tag{B.102}$$

$$\tau_f \frac{de_{q_f}}{dt} + e_{q_f} = e_q \tag{B.103}$$

$$v^*_{m_d} = e_{d_f} + K_{p_{CL}}(i^*_{s_d} - i_{s_d}) - \omega_{PLL} L_f i_{s_q} + M_{CL_d} \tag{B.104}$$

$$v^*_{m_q} = e_{q_f} + K_{p_{CL}}(i^*_{s_q} - i_{s_q}) + \omega_{PLL} L_f i_{s_d} + M_{CL_q} \tag{B.105}$$

Convertisseurs grid forming

Les équations du modèle des convertisseurs grid forming sont données ici.

$$\frac{L_f}{\omega_b}\frac{di_{s_d}}{dt} = v_{m_d} - e_d - R_f i_{s_d} + \omega L_f i_{s_q} \tag{B.106}$$

$$\frac{L_f}{\omega_b}\frac{di_{s_q}}{dt} = v_{m_q} - e_q - R_f i_{s_q} - \omega L_f i_{s_d} \tag{B.107}$$

$$\frac{C_f}{\omega_b}\frac{de_d}{dt} = i_{s_d} - i_{g_d} + \omega C_f e_q \tag{B.108}$$

$$\frac{C_f}{\omega_b}\frac{de_q}{dt} = i_{s_q} - i_{g_q} - \omega C_f e_d \tag{B.109}$$

$$\frac{L_t}{\omega_b}\frac{di_{g_d}}{dt} = e_d - v_{g_d} - R_t i_{g_d} + \omega L_t i_{g_q} \tag{B.110}$$

$$\frac{L_t}{\omega_b}\frac{di_{g_q}}{dt} = e_q - v_{g_q} - R_t i_{g_q} - \omega L_t i_{g_d} \tag{B.111}$$

$$v^*_{m_d} = v_{m_d} \tag{B.112}$$

$$v^*_{m_q} = v_{m_q} \tag{B.113}$$

$$p = e_d i_{g_d} + e_q i_{g_q} \tag{B.114}$$

$$\frac{dp_m}{dt} + \omega_f p_m = \omega_f p \tag{B.115}$$

$$\omega = \omega^* + m_p(p^* - p_m) \tag{B.116}$$

$$\frac{1}{\omega_b}\frac{d\theta}{dt} = \omega - \omega_g \tag{B.117}$$

$$q = e_q i_{g_d} - e_d i_{g_q} \tag{B.118}$$

$$\frac{dq_m}{dt} + \omega_f q_m = \omega_f q \tag{B.119}$$

$$\frac{dM_{AD_d}}{dt} = \omega_{ff}(K_{ff} i_{g_d} - M_{AD_d}) \tag{B.120}$$

$$\frac{dM_{AD_q}}{dt} = \omega_{ff}(K_{ff} i_{g_q} - M_{AD_q}) \tag{B.121}$$

$$e^*_d = |e|^* + m_q(q^* - q_m) + M_{AD_d} - K_{ff} i_{g_d} \tag{B.122}$$

$$e^*_q = M_{AD_q} - K_{ff} i_{g_q} \tag{B.123}$$

$$\frac{dM_{VL_d}}{dt} = K_{i_{VL}}(e^*_d - e_d) \tag{B.124}$$

$$\frac{dM_{VL_q}}{dt} = K_{i_{VL}}(e^*_q - e_q) \tag{B.125}$$

$$i^*_{s_d} = K_{FF_i} i_{g_d} + K_{p_{VL}}(e^*_d - e_d) - \omega C_f e_q + M_{VL_d} \tag{B.126}$$

$$i^*_{s_q} = K_{FF_i} i_{g_q} + K_{p_{VL}}(e^*_q - e_q) + \omega C_f e_d + M_{VL_q} \tag{B.127}$$

$$\frac{dM_{CL_d}}{dt} = K_{i_{CL}}(i^*_{s_d} - i_{s_d}) \tag{B.128}$$

$$\frac{dM_{CL_q}}{dt} = K_{i_{CL}}(i^*_{s_q} - i_{s_q}) \tag{B.129}$$

$$v^*_{m_d} = K_{FF_v} e_d + K_{p_{CL}}(i^*_{s_d} - i_{s_d}) - \omega L_f i_{s_q} + M_{CL_d} \tag{B.130}$$

$$v^*_{m_q} = K_{FF_v} e_q + K_{p_{CL}}(i^*_{s_q} - i_{s_q}) + \omega L_f i_{s_d} + M_{CL_q} \tag{B.131}$$

Modular multilevel converter

Les équations du MMC sont données ici.

$$L_{AC}\frac{di_{g_d}}{dt} = v_{m_d} - v_{g_d} - R_{AC} i_{g_d} + \omega_{PLL} L_{AC} i_{g_q} \tag{B.132}$$

$$L_{AC}\frac{di_{g_q}}{dt} = v_{m_q} - v_{g_q} - R_{AC} i_{g_q} - \omega_{PLL} L_{AC} i_{g_d} \tag{B.133}$$

$$L_{DC}\frac{di_{DC}}{dt} = v_{DC} - v_{m_{DC}} - R_{DC} i_{DC} \tag{B.134}$$

$$C_{eq} v_{C_{tot}} \frac{dv_{C_{tot}}}{dt} = v_{m_{DC}} i_{DC} - v_{m_d} i_{g_d} - v_{m_q} i_{g_q} \tag{B.135}$$

$$v^*_{m_{DC}} = v_{m_{DC}} \tag{B.136}$$

$$v^*_{m_d} = v_{m_d} \tag{B.137}$$

$$v^*_{m_q} = v_{m_q} \tag{B.138}$$

$$\frac{dM_{PLL}}{dt} = K_{i_{PLL}} v_{g_q} \tag{B.139}$$

$$\omega_{PLL} = K_{p_{PLL}} v_{g_q} + M_{PLL} + \omega_g \tag{B.140}$$

$$\frac{d\theta_{PLL}}{dt} = \omega_{PLL} - \omega_g \tag{B.141}$$

$$i^*_{g_d} = \frac{p^*}{v_{g_d}} \tag{B.142}$$

$$i^*_{g_q} = -\frac{q^*}{v_{g_d}} \tag{B.143}$$

$$p_{AC} = v_{g_d} i_{g_d} + v_{g_q} i_{g_q} \tag{B.144}$$

$$W_{tot} = v^2_{c_{tot}} \tag{B.145}$$

$$\tau_f \frac{dW_{tot_f}}{dt} + W_{tot_f} = W_{tot} \tag{B.146}$$

$$\frac{dM_W}{dt} = K_{i_W}(W^*_{tot} - W_{tot_f}) \tag{B.147}$$

$$i^*_{DC} = \frac{K_{p_W}(W^*_{tot} - W_{tot_f}) + M_W + p_{AC}}{v_{DC}} \tag{B.148}$$

$$\frac{dM_{CL_d}}{dt} = K_{i_{CL}}(i^*_{g_d} - i_{g_d}) \tag{B.149}$$

$$\frac{dM_{CL_q}}{dt} = K_{i_{CL}}(i^*_{g_q} - i_{g_q}) \tag{B.150}$$

$$v^*_{m_d} = v_{g_d} + K_{p_{CL}}(i^*_{g_d} - i_{g_d}) - \omega_{PLL} L_{AC} i_{g_q} + M_{CL_d} \tag{B.151}$$

$$v^*_{m_q} = v_{g_d} + K_{p_{CL}}(i^*_{g_q} - i_{g_q}) + \omega_{PLL} L_{AC} i_{g_d} + M_{CL_q} \tag{B.152}$$

$$\frac{dM_{DCCL}}{dt} = K_{i_{DCCL}}(i^*_{DC} - i_{DC}) \tag{B.153}$$

$$v^*_{m_{DC}} = v_{DC} - K_{p_{DCCL}}(i^*_{DC} - i_{DC}) - M_{DCCL} \tag{B.154}$$

Conclusion du chapitre

Dans ce chapitre, les modèles des éléments d'un réseau de transport ont été présentés. Cela donne, pour le réseau complet, un système algébro différentiel non linéaire qui sera réduit grâce aux méthodes de réduction de modèles présentées dans le chapitre 3.

Chapitre 3: développement de méthodes de réduction de modèles

Ce chapitre présente les méthodes de réduction de modèles développées.

Principes communs aux méthodes

Résidualisation d'état

Système algébro différentiel non linéaire Un système algébro différentiel non linéaire est considéré dans (B.155). La taille de ce modèle est donnée par N_{diff}. x_{diff} représente les variables d'état, u les entrées, x_{alg} les variables algébriques et y les sorties.

$$\begin{cases} \dfrac{dx_{diff}}{dt} = f(x_{diff}, x_{alg}, u) \\ 0 = g(x_{diff}, x_{alg}, u) \\ y = h(x_{diff}, x_{alg}, u) \\ x_{diff} \in \mathbb{R}^{N_{diff}}, x_{alg} \in \mathbb{R}^{N_{alg}}, u \in \mathbb{R}^{p}, y \in \mathbb{R}^{q} \end{cases} \tag{B.155}$$

Principe de la résidualisation La résidualisation d'une variable d'état consiste à transformer cette variable en une variable algébrique en négligeant la partie dérivée dans l'équation différentielle correspondante, ce qui la transforme en une équation algébrique.

Le modèle réduit obtenu par résidualisation d'état peut être écrit comme dans (B.156).

$$\begin{cases} E\dfrac{dx_{diff}}{dt} = f(x_{diff}, x_{alg}, u) \\ 0 = g(x_{diff}, x_{alg}, u) \\ y = h(x_{diff}, x_{alg}, u) \\ E = diag(\delta_i), \delta_i \in \{0; 1\}, \forall i, E \in \mathbb{R}^{N_{diff} \times N_{diff}} \\ x_{diff} \in \mathbb{R}^{N_{diff}}, x_{alg} \in \mathbb{R}^{N_{alg}}, u \in \mathbb{R}^{p}, y \in \mathbb{R}^{q} \end{cases} \tag{B.156}$$

La taille du modèle réduit est donnée par $tr(E)$.

L'avantage de la résidualisation est qu'elle préserve les variables et la structure physique du système.

L'approche modale

Le système dans (B.155) est considéré.

Ici, on cherche à relier les états du système à ses pôles de façon à ce que la résidualisation entraine une suppression de pôles tout en gardant les autres pratiquement inchangés. Cela est résumé dans B.4.

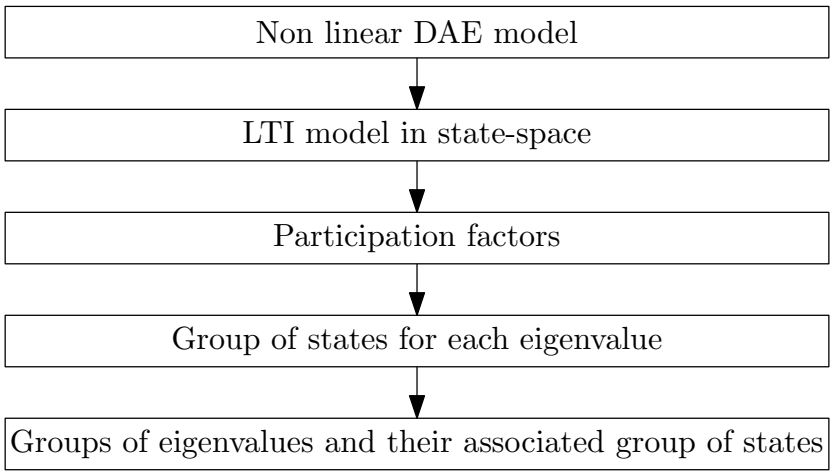

Figure B.4: Synoptique décrivant l'approche modale

Linéarisation du modèle Le modèle est dans un premier temps linéarisé dans (B.157).

$$\begin{cases} \dfrac{dx}{dt} = Ax + Bu \\ \quad y = Cx + Du \\ \quad x \in \mathbb{R}^{N_{diff}}, u \in \mathbb{R}^p, y \in \mathbb{R}^q \end{cases} \tag{B.157}$$

Calcul des facteurs de participation et formation de groupes d'états qui participent dans une valeur propre La seconde étape consiste à calculer les facteurs de participation $p_{k,i}$.

Un critère $\epsilon_{participation}$ entre 0 et 1 est choisi. Pour chaque valeur propre λ_i, les k variables d'état correspondant au k plus grands facteurs de participation sont gardées de façon à ce que la somme de leur participation soit supérieure à $\epsilon_{participation}$. Elles forment le groupe des états qui participe dans λ_i. Ce groupe est noté $P_{\lambda_i,\epsilon_{participation}}$. Tout ceci est résumé dans (B.158).

$$\begin{aligned} P_{\lambda_i,\epsilon_{participation}} = \{x_k / \forall x_m \notin P_{\lambda_i,\epsilon_{participation}}, |p_{k,i}| \geq |p_{m,i}| \\ \sum_{x_k} |p_{k,i}| \geq \epsilon_{participation} \\ \forall x_l \in P_{\lambda_i,\epsilon_{participation}}, \sum_{x_k \neq x_l} |p_{k,i}| < \epsilon_{participation}\} \end{aligned} \tag{B.158}$$

Ce processus est effectué pour toutes les valeurs propres du système.

Formation de groupes de valeurs propres dans lesquelles les mêmes états participent Quand le système est couplé, chaque état participe dans plusieurs valeurs

propres et chaque valeur propre dépend de plusieurs états. De cette façon, certains des groupes formés précédemment sont fusionnés pour former P_i. Chaque groupe P_i est associé à un unique groupe de valeurs propres dans lesquelles les états de P_i participent. Tous les groupes sont disjoints.

Ces groupes ajoutent une contrainte sur la matrice E recherchée. Cela est formalisé dans $\mathbb{E}_{\epsilon_{participation}}$ qui contient toutes les matrices E respectant les couplages identifiés auparavant. Cela est résumé dans (B.159). Cela signifie que les états d'un même groupe doivent être résidualisés en même temps.

$$\forall P_i, \forall x_k \in P_i, \forall x_l \in P_i, E(k,k) = E(l,l) \tag{B.159}$$

Stratégies développées pour choisir les groupes d'états à résidualiser/les groupes de valeurs propres à supprimer

Les groupes P_i d'états sont formés et chacun est associé à un groupe de pôles L_i.

Stratégie 1: supprimer les pôles les plus rapides

Le synoptique dans la figure B.5 résume cette stratégie.

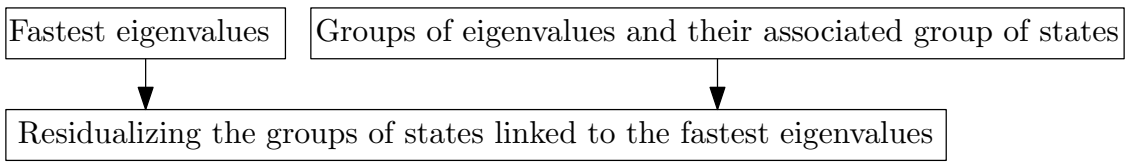

Figure B.5: Synoptique décrivant la stratégie 1

Stratégie 2: supprimer les pôles qui dépendent des états les moins observables et commandables dans la réalisation équilibrée

Le synoptique dans la figure B.6 résume cette stratégie

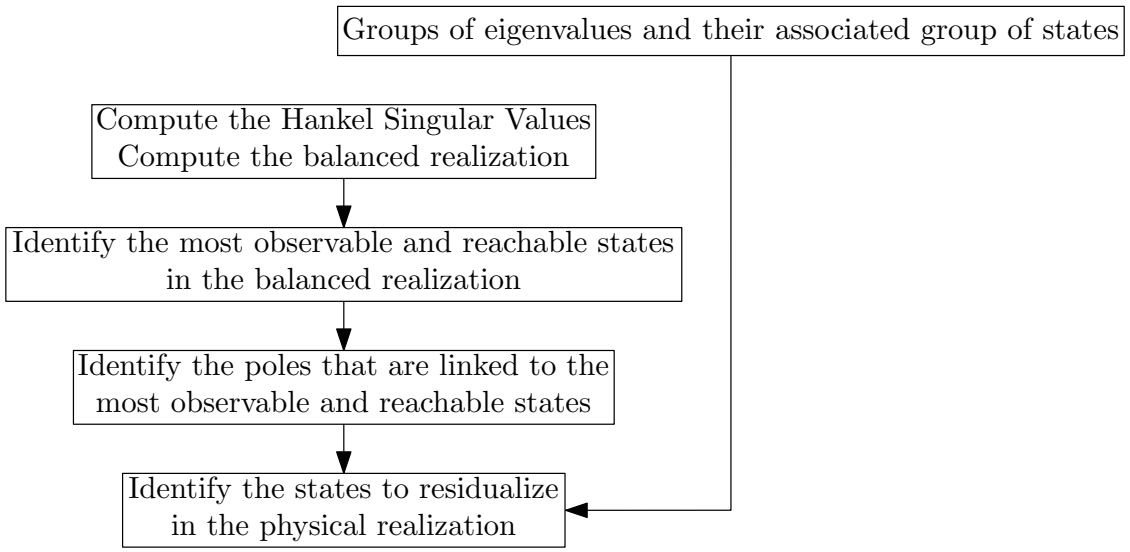

Figure B.6: Synoptic décrivant la stratégie 2

Stratégie 3: supprimer les pôles qui minimisent un critère d'erreur

Le synoptique dans la figure B.7 résume cette stratégie.

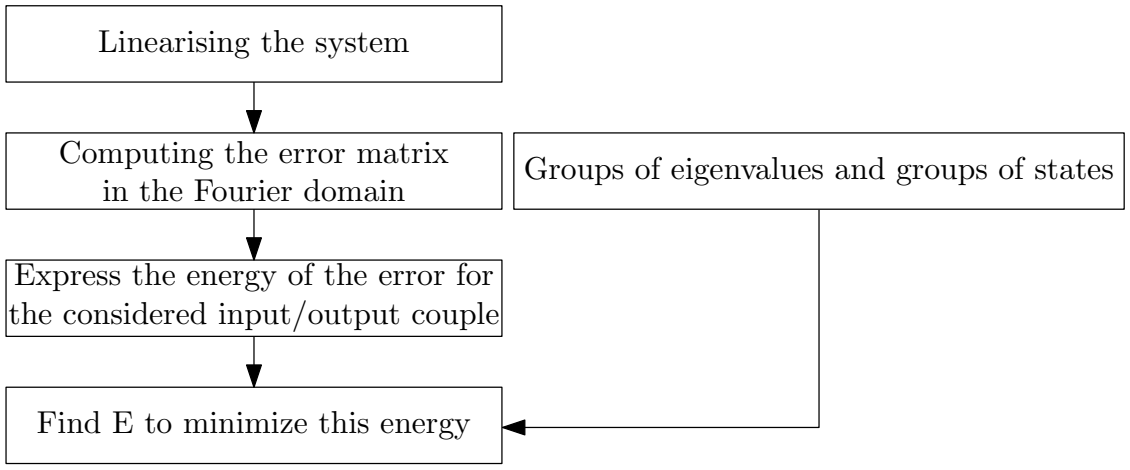

Figure B.7: synoptique décrivant la stratégie 3

Linéarisation Les modèles complets et réduits sont linéarisés dans (B.160) et (B.161).

$$\begin{cases} \dfrac{dx}{dt} = Ax + Bu \\ \quad y = Cx + Du \\ \quad x \in \mathbb{R}^{N_{diff}}, u \in \mathbb{R}^p, y \in \mathbb{R}^q \end{cases} \tag{B.160}$$

$$\begin{cases} E\dfrac{dx_r}{dt} = Ax_r + Bu \\ y_r = Cx_r + Du \\ x \in \mathbb{R}^{N_{diff}}, u \in \mathbb{R}^p, y \in \mathbb{R}^q \end{cases} \tag{B.161}$$

Matrice d'erreur dans la representation de Fourier Une transformation de Fourier et quelques operations mathématiques aboutissent à (B.162).

$$\begin{cases} Y - Y_r = \epsilon(\omega)U \\ \text{avec } \epsilon(\omega) = C[(j\omega I_{N_{diff}} - A)^{-1} - (j\omega E - A)^{-1}]B \in \mathbb{C}^{q\times p} \end{cases} \tag{B.162}$$

La nouvelle matrice $\epsilon(\omega)$ est appelée matrice d'erreur.

Énergie de l'erreur pour un couple entrée-sortie spécifique L'erreur pour la sortie Y_i par rapport à l'entrée U_j est un scalaire donné par $\epsilon_{i,j}(\omega)$.

L'énergie de cette erreur $\boldsymbol{\epsilon_{i,j}}$ est définie dans B.163).

$$\boldsymbol{\epsilon_{i,j}} = \int_{-\infty}^{\infty} |\epsilon_{i,j}(\omega)|^2 d\omega \tag{B.163}$$

L'identité de Parseval dans (B.164) nous indique que les énergies dans la representation de Fourier et en temporel sont égales.

$$\int_{-\infty}^{\infty} |\epsilon_{i,j}(\omega)|^2 d\omega = 2\pi \int_{-\infty}^{\infty} |\epsilon_{i,j}(t)|^2 dt \tag{B.164}$$

Problème d'optimisation L'idée est alors de trouver E qui minimise l'énergie de l'erreur. Le problème d'optimisation est présenté dans (B.165). La taille désirée pour le modèle réduit est notée n.

$$\begin{cases} \underset{E}{\text{minimize}}\ \boldsymbol{\epsilon_{i,j}} = \displaystyle\int_{-\infty}^{\infty} |\epsilon_{i,j}(\omega)|^2 d\omega \\ \text{subject to } E \in \mathbb{E}_{\epsilon_{participation}},\ tr(E) \leq n \end{cases} \tag{B.165}$$

Ce problème étant discret, il est résolu en utilisant un algorithme génétique.

Conclusion du chapitre

Ce chapitre a présenté les 3 méthodes développées. Elles sont basées sur deux principes communs: la résidualisation et une approche modale.

Ensuite chaque méthode adopte une stratégie différent pour choisir les variables à résidualiser/les pôles à supprimer:

- la première supprime les pôles les plus rapides.

- la seconde résidualise les états qui participent dans les pôles liés aux états les moins commandables et observables dans la réalisation équilibrée.

- la troisième minimise un critère d'erreur.

Chapitre 4: application des méthodes pour la simulation et l'analyse de réseaux de transport à forte pénétration d'électronique de puissance

Dans ce chapitre, les méthodes développées dans le chapitre 3 sont appliquées à des cas tests réalistes basés sur les modèles du chapitre 2.

Cas simple à un convertisseur grid forming connecté à un réseau infini

La figure B.8 présente le système étudié.

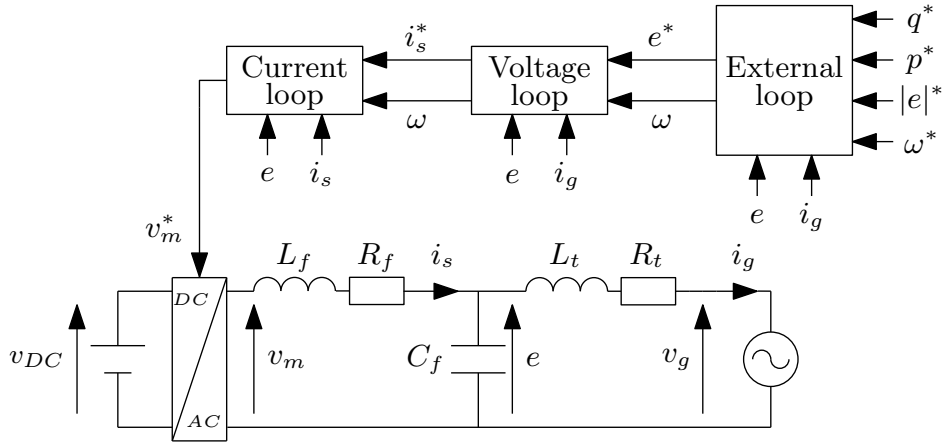

Figure B.8: Structure du système étudié

Ce système est modélisé par le système d'équations dans (B.166).

$$\begin{cases} \dfrac{dx_{diff}}{dt} = f(x_{diff}, x_{alg}, u) \\ 0 = g(x_{diff}, x_{alg}, u) \\ y = h(x_{diff}, x_{alg}, u) \\ x_{diff} = \left(i_{s_d}\ i_{s_q}\ e_d\ e_q\ i_{g_d}\ i_{g_q}\ p_m\ \theta\ q_m\ M_{CL_d}\ M_{CL_q}\ M_{VL_d}\ M_{VL_q}\ M_{AD_d}\ M_{AD_q}\right)^T \\ x_{alg} = \left(v_{m_d}\ v_{m_q}\ v^*_{m_d}\ v^*_{m_q}\ p\ \omega\ q\ e^*_d\ e^*_q\ i^*_{s_d}\ i^*_{s_q}\ v_{g_d}\ v_{g_d}\right)^T \\ u = \left(v_{g_{d_g}}\ v_{g_{q_g}}\ \omega^*\ p^*\ q^*\ |e|^*\right)^T \end{cases} \tag{B.166}$$

Groupes d'états/de valeurs propres Les valeurs propres du système linéarisé et les facteurs de participation sont calculés et donnés dans le tableau B.14.

	M_{CL_d}	M_{CL_q}	M_{VL_d}	M_{VL_q}	M_{AD_d}	M_{AD_q}	i_{s_d}	i_{s_q}	i_{g_d}	i_{g_q}	p_m	q_m	θ	e_d	e_q
$\lambda_1 = -1.4$	0.18	0.08	0.5	0.24	0	0	0	0	0	0	0	0	0	0	0
$\lambda_{2,3} = -1.5 \pm 0.1i$	0.16	0.34	0.16	0.34	0	0	0	0	0	0	0	0	0	0	0
$\lambda_4 = -1.7$	0.5	0.24	0.18	0.08	0	0	0	0	0	0	0	0	0	0	0
$\lambda_{5,6} = -15.5 \pm 28.2i$	0	0	0	0	0	0	0	0	0	0	0.5	0	0.5	0	0
$\lambda_7 = -16.2$	0	0	0	0	0.4	0.6	0	0	0	0	0	0	0	0	0
$\lambda_8 = -17.2$	0	0	0	0	0.6	0.4	0	0	0	0	0	0	0	0	0
$\lambda_9 = -31.4$	0	0	0	0	0	0	0	0	0	0	0	1	0	0	0
$\lambda_{10,11} = -21 \pm 134i$	0	0	0	0	0	0	0.25	0.25	0.25	0.25	0	0	0	0	0
$\lambda_{12,13} = -759 \pm 3330i$	0	0	0	0	0	0	0.13	0.13	0.12	0.12	0	0	0	0.25	0.25
$\lambda_{14,15} = -790 \pm 3820i$	0	0	0	0	0	0	0.12	0.12	0.13	0.13	0	0	0	0.25	0.25

Table B.14: Facteurs de participation

Le critère de participation $\epsilon_{participation} = 0.99$ est choisi, ce qui permet d'identifier les états qui participent le plus dans chaque valeur propre, ce qui est fait dans le tableau B.15.

Valeur propre	Etat
$\lambda_1 = -1.4$	M_{CL_d}, M_{CL_q}, M_{VL_d}, M_{VL_q}
$\lambda_{2,3} = -1.5 \pm 0.1i$	M_{CL_d}, M_{CL_q}, M_{VL_d}, M_{VL_q}
$\lambda_4 = -1.7$	M_{CL_d}, M_{CL_q}, M_{VL_d}, M_{VL_q}
$\lambda_{5,6} = -15.5 \pm 28.2i$	p_m, θ
$\lambda_7 = -16.2$	M_{AD_d}, M_{AD_q}
$\lambda_8 = -17.2$	M_{AD_d}, M_{AD_q}
$\lambda_9 = -31.4$	q_m
$\lambda_{10,11} = -21 \pm 134i$	i_{s_d}, i_{s_q}, i_{g_d}, i_{g_q}
$\lambda_{12,13} = -759 \pm 3330i$	i_{s_d}, i_{s_q}, i_{g_d}, i_{g_q}, e_d, e_q
$\lambda_{14,15} = -790 \pm 3820i$	i_{s_d}, i_{s_q}, i_{g_d}, i_{g_q}, e_d, e_q

Table B.15: Etats qui participant le plus dans chaque valeur propre

Ce tableau permet de créer les groupes de valeurs propres et leurs groupes d'états associés dans le tableau B.16.

Valeurs propres	Etats	Nom du groupe
λ_1, $\lambda_{2,3}$, λ_4	M_{CL_d}, M_{CL_q}, M_{VL_d}, M_{VL_q}	P_1
$\lambda_{5,6}$	p_m, θ	P_2
λ_7, λ_8	M_{AD_d}, M_{AD_q}	P_3
λ_9	q_m	P_4
$\lambda_{10,11}$, $\lambda_{12,13}$, $\lambda_{14,15}$	i_{s_d}, i_{s_q}, i_{g_d}, i_{g_q}, e_d, e_q	P_5

Table B.16: Groupes d'états et de valeurs propres

Ce tableau donne les modèles réduits possibles qui sont résumés dans le tableau B.17.

Ordre	Nom	Groupes résidualisés	Groupes gardés
0	0	P_1, P_2, P_3, P_4, P_5	
1	1	P_1, P_2, P_3, P_5	P_4
2	2a	P_1, P_3, P_4, P_5	P_2
2	2b	P_1, P_2, P_4, P_5	P_3
3	3a	P_1, P_3, P_5	P_2, P_4
3	3b	P_1, P_2, P_5	P_3, P_4
4	4a	P_2, P_3, P_4, P_5	P_1
4	4b	P_1, P_4, P_5	P_2, P_3
5	5a	P_2, P_3, P_5	P_1, P_4
5	5b	P_1, P_5	P_2, P_3, P_4
6	6a	P_3, P_4, P_5	P_1, P_2
6	6b	P_2, P_4, P_5	P_1, P_3
6	6c	P_1, P_2, P_3, P_4	P_5
7	7a	P_3, P_5	P_1, P_2, P_4
7	7b	P_2, P_5	P_1, P_3, P_4
7	7c	P_1, P_2, P_3	P_4, P_5
8	8a	P_4, P_5	P_1, P_2, P_3
8	8b	P_1, P_3, P_4	P_2, P_5
8	8c	P_1, P_2, P_4	P_3, P_5
9	9a	P_5	P_1, P_2, P_3, P_4
9	9b	P_1, P_3	P_2, P_4, P_5
9	9c	P_1, P_2	P_3, P_4, P_5
10	10a	P_2, P_3, P_4	P_1, P_5
10	10b	P_1, P_4	P_2, P_3, P_5
11	11a	P_2, P_3	P_1, P_4, P_5
11	11b	P_1	P_2, P_3, P_4, P_5
12	12a	P_3, P_4	P_1, P_2, P_5
12	12b	P_2, P_4	P_1, P_3, P_5
13	13a	P_3	P_1, P_2, P_4, P_5
13	13b	P_2	P_1, P_3, P_4, P_5
14	14	P_4	P_1, P_2, P_3, P_5
15	15		P_1, P_2, P_3, P_4, P_5

Table B.17: Modèles réduits possibles

Maintenant que tous les modèles réduits possibles sont connus, les trois méthodes développées aident à choisir le modèle le plus adapté.

La taille voulue pour le modèle réduit est arbitrairement fixée à 6.

Première stratégie L'application de la première stratégie est plutôt directe et donne comme modèle réduit le modèle $6a$.

Deuxième stratégie La fonction h est choisie afin que les sorties du système soient les courants i_{s_d} et i_{s_q}.

Les HSV sont calculées et données dans le tableau B.18.

	x_{b_1}	x_{b_2}	x_{b_3}	x_{b_4}	x_{b_5}	x_{b_6}	x_{b_7}	x_{b_8}	x_{b_9}	$x_{b_{10}}$	$x_{b_{11}}$	$x_{b_{12}}$	$x_{b_{13}}$	$x_{b_{14}}$	$x_{b_{15}}$
HSV (in %)	11.1	11	10.2	9.1	8.4	8.3	7.1	7	6.3	6.3	6.2	6.1	1.5	1	0.4

Table B.18: HSV du modèle

Une analyse des facteurs de participation dans la réalisation équilibrée et dans la réalisation physique permet de créer les groupes d'états et de valeurs propres. Ils sont présentés dans le tableau B.19.

Etats	Valeurs propres	Etats	Nom du groupe
x_{b_1}, x_{b_2}	$\lambda_{5,6}$	p_m, θ	P_2
x_{b_3}, x_{b_4}, x_{b_5}, x_{b_6}	λ_1, $\lambda_{2,3}$, λ_4	M_{CL_d}, M_{CL_q}, M_{VL_d}, M_{VL_q}	P_1
x_{b_7}, x_{b_8}, x_{b_9}, $x_{b_{10}}$, $x_{b_{11}}$, $x_{b_{12}}$	$\lambda_{10,11}$, $\lambda_{12,13}$, $\lambda_{14,15}$	i_{s_d}, i_{s_q}, i_{g_d}, i_{g_q}, e_d, e_q	P_5
$x_{b_{13}}$, $x_{b_{14}}$	λ_7, λ_8	M_{AD_d}, M_{AD_q}	P_3
$x_{b_{15}}$	λ_9	q_m	P_4

Table B.19: Groupes d'états et de valeurs propres dans les réalisations équilibrée et physique

Le critère $\epsilon_{HSV} = 50\%$ est choisi. Les états à garder dans la réalisation équilibrée sont x_{b_1}, x_{b_2}, x_{b_3}, x_{b_4}, x_{b_5} et x_{b_6}, les pôles à garder sont λ_1, $\lambda_{2,3}$, λ_4 et $\lambda_{5,6}$ et les états à résidualiser dans la réalisation physique sont les états dans P_3, P_4 et P_5.

Troisième stratégie Le problème d'optimisation suivant est résolu en utilisant un algorithme génétique :

$$\begin{cases} \underset{E}{\text{minimize}}\ \boldsymbol{\epsilon_{i,j}} = \displaystyle\int_{-\infty}^{\infty} |\epsilon_{i,j}(\omega)|^2 d\omega \\ \text{subject to } E \in \mathbb{E}_{\epsilon_{participation}},\ tr(E) \leq 6 \end{cases} \tag{B.167}$$

Dans le cas considéré, $i = 1$, la variable observée est i_{s_d} et $j = 1$, l'événement considéré est un changement de la tension du réseau $v_{g_{d_g}}$. Grâce à une analyse des facteurs de participation, $\mathbb{E}_{\epsilon_{participation}}$ est défini comme suit:

$$\begin{aligned}\mathbb{E}_{\epsilon_{participation}} = \{E \in \mathbb{R}^{15\times 15}/E = diag(\delta_i),\ \delta_i \in \{0;1\},\\ \forall (i,j) \in \{1,..,6\},\ E(i,i) = E(j,j),\\ E(7,7) = E(8,8),\\ \forall (i,j) \in \{10,..,13\},\ E(i,i) = E(j,j),\\ E(14,14) = E(15,15)\}\end{aligned} \tag{B.168}$$

L'optimisation trouve la matrice E suivante comme solution:

$$E = \begin{pmatrix} 0&0&0&0&0&0&0&0&0&0&0&0&0&0&0\\ 0&0&0&0&0&0&0&0&0&0&0&0&0&0&0\\ 0&0&0&0&0&0&0&0&0&0&0&0&0&0&0\\ 0&0&0&0&0&0&0&0&0&0&0&0&0&0&0\\ 0&0&0&0&0&0&0&0&0&0&0&0&0&0&0\\ 0&0&0&0&0&0&0&0&0&0&0&0&0&0&0\\ 0&0&0&0&0&0&1&0&0&0&0&0&0&0&0\\ 0&0&0&0&0&0&0&1&0&0&0&0&0&0&0\\ 0&0&0&0&0&0&0&0&0&0&0&0&0&0&0\\ 0&0&0&0&0&0&0&0&0&1&0&0&0&0&0\\ 0&0&0&0&0&0&0&0&0&0&1&0&0&0&0\\ 0&0&0&0&0&0&0&0&0&0&0&1&0&0&0\\ 0&0&0&0&0&0&0&0&0&0&0&0&1&0&0\\ 0&0&0&0&0&0&0&0&0&0&0&0&0&0&0\\ 0&0&0&0&0&0&0&0&0&0&0&0&0&0&0 \end{pmatrix} \tag{B.169}$$

Résultats de simulation Le modèle complet d'ordre 15 et le modèle réduit d'ordre 6 sont considérés ici.

Tout d'abord, on remarque dans la figure B.9 que comme voulu, certains pôles ont été supprimés et les autres très peu modifiés.

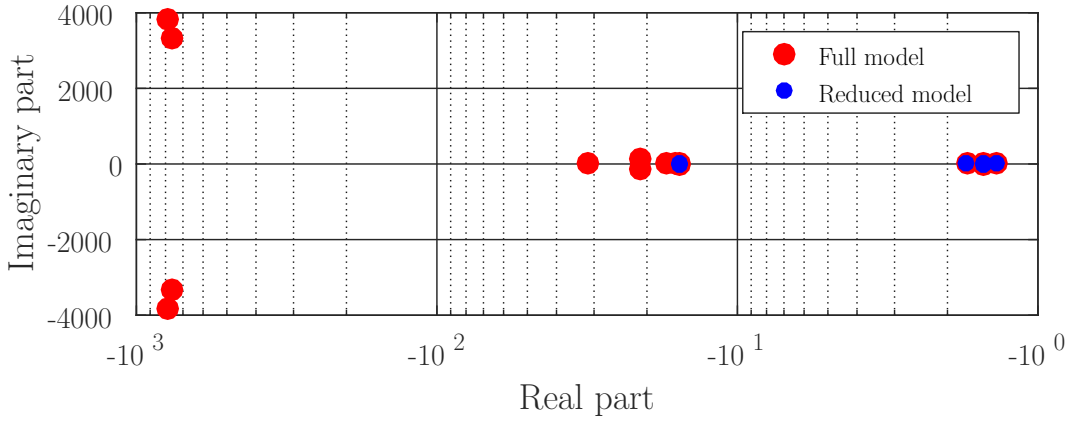

Figure B.9: Comparaison des pôles des modèles complet et réduit

Un court-circuit au niveau du réseau est simulé puis éliminé après $150ms$. Le courant dans le convertisseur est observé dans la figure B.10.

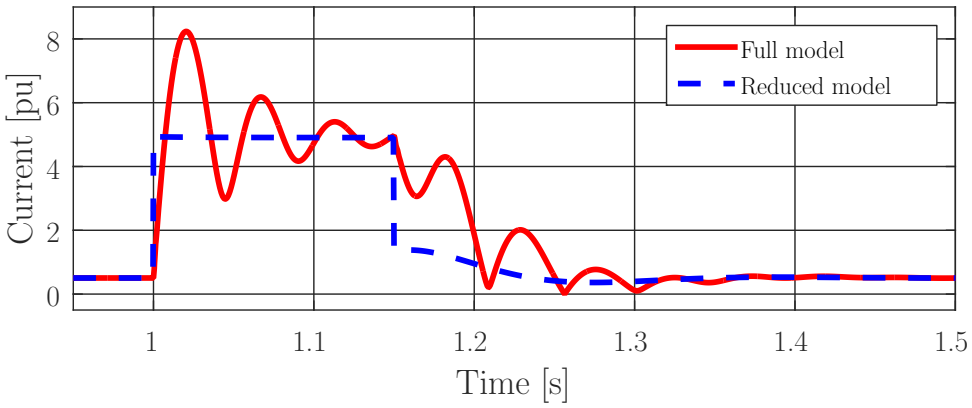

Figure B.10: Comparaison du courant dans le convertisseur pour les modèles complet et réduit

On remarque que l'allure générale du courant est préservée.

Cas d'un réseau de transport

Le réseau de transport irlandais est considéré. Ce système est composé de 47 charges, 14 convertisseurs, 85 lignes, 6 condensateurs shunt et 40 transformateurs. Le modèle est d'ordre 906. Une représentation de la structure est donnée dans la figure B.11.

Figure B.11: Structure du réseau de transport irlandais

Un court-circuit est simulé au niveau d'une charge à $t = 0.1s$ (Dunstown sur la carte). Le courant dans un convertisseur proche (Shellybanks sur la carte) est observé. Seule la troisième stratégie est appliquée.

Habituellement, l'approximation phaseur est effectuée, ce qui mène à un modèle d'ordre 210. L'idée ici est de trouver un modèle réduit de même taille et de le comparer au modèle complet et à ce modèle phaseur.

Dans le modèle réduit obtenu en appliquant la stratégie 3, certains convertisseurs sont réduits, d'autres non, de même pour les lignes.

Le tableau B.20 donne l'ordre du modèle pour chacun des convertisseurs du réseau.

Converter	1	2	3	4	5	6	7	8	9	10	11	12	13	14
Order (strategy 3)	12	12	12	12	12	12	12	12	6	6	6	6	6	6

Table B.20: Ordre du modèle pour chaque convertisseur

Sur la figure B.12, la partie du réseau en EMT et la partie en phaseur sont représentées. On peut remarquer que les lignes proches du convertisseur observé et de l'événement simulé sont en EMT.

+

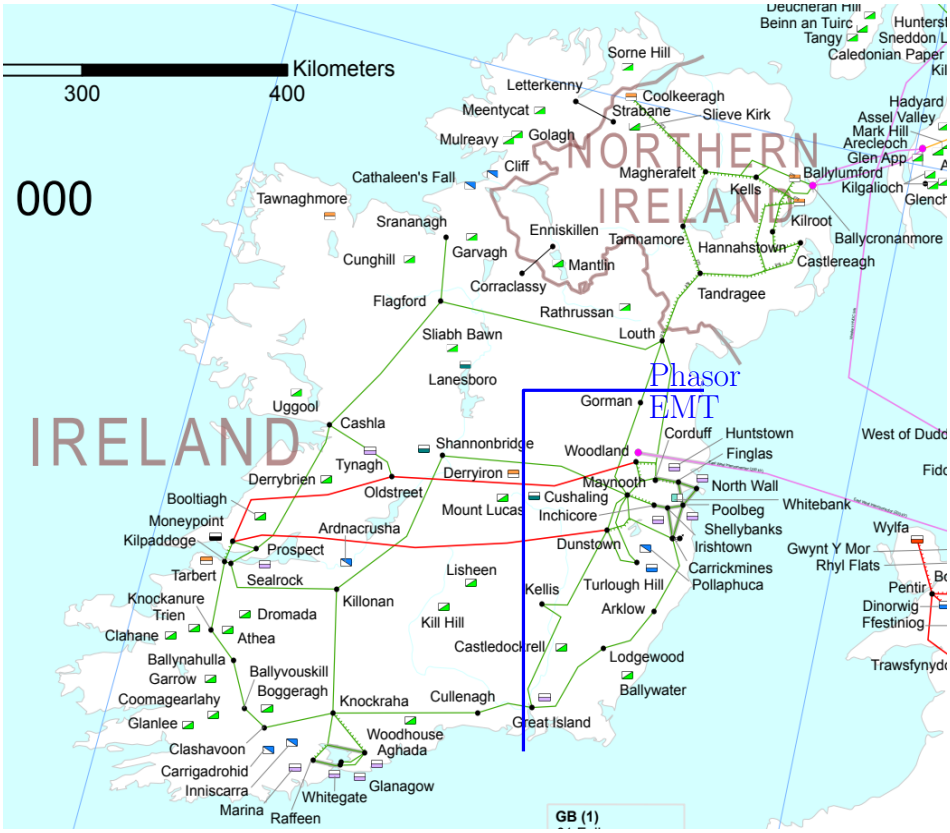

Figure B.12: Structue du réseau de transport irlandais après la réduction de modèle

La figure B.13 représente le courant dans le convertisseur pendant le court-circuit pour les trois modèles : complet, phaseur et réduit.

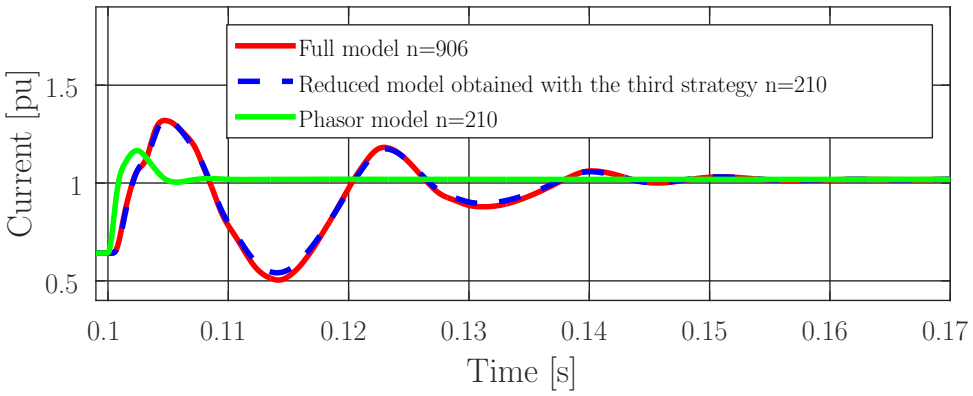

Figure B.13: Comparaison du courant dans le convertisseur pour les modèles complet, réduit et phaseur

On peut remarquer que le modèle phaseur ne prend pas en compte le pic de courant alors que le modèle réduit oui. Globalement, ce dernier est plus précis que le modèle phaseur.

Conclusion

Le contexte de cette thèse était la recherche de solutions techniques, telles que de nouvelles lois de commande, pour s'assurer que l'intégration massive de l'électronique de puissance dans les réseaux de transport n'entraîne pas une diminution de la stabilité et de la sécurité du système. L'objectif principal de cette thèse est rappelé et a consisté à développer de nouveaux outils et méthodes pour simuler et analyser des réseaux de transport à forte pénétration d'électronique de puissance. Le premier chapitre a présenté quelques outils communs qui sont utilisés aujourd'hui pour simuler et analyser les systèmes électriques. Grâce à cet état de l'art, un besoin de réduction de modèles a été identifié pour accélérer la simulation et simplifier l'analyse. C'est pourquoi la deuxième partie de ce chapitre a été consacrée à la présentation des méthodes classiques de réduction de modèles. La conclusion était que les méthodes classiques ne conviennent pas à la simulation et à l'analyse des réseaux électriques parce qu'elles utilisent des changements de base et des troncatures, qui modifient les variables et la structure du système. C'est pourquoi l'objectif de cette thèse était de développer des méthodes de réduction de modèle qui préservent les variables et la structure physique du système. Le deuxième chapitre a présenté les modèles des différents éléments d'un réseau de transport à forte pénétration d'électronique de puissance. Le troisième chapitre a présenté les méthodes de réduction développées. Ces trois méthodes sont basées sur la residualisation d'état, une approche modale et certaines caractéristiques inspirées des méthodes classiques présentées au chapitre 1. Comme souhaité, les méthodes développées préservent les variables du système, sa structure physique, la stabilité autour du point de fonctionnement et ont une erreur limitée. De plus, certaines d'entre elles donnent un modèle réduit qui est spécifique au cas test considéré, c'est-à-dire la variable observée et l'événement simulé. Comme les méthodes développées conservent la structure physique et les variables du modèle, l'analyse est simple, il est possible d'ajouter de nouvelles boucles de contrôle directement sur le modèle réduit et il est facile de mettre les modèles réduits dans les outils classiques de simulation. De plus, le temps de calcul est très réduit. Le quatrième chapitre a présenté les résultats de l'application des trois méthodes développées à des cas test réalistes.

Outils et Méthodes pour l'Analyse et la Simulation de Réseaux de Transport 100% Electronique de Puissance

RESUME :

Le développement des énergies renouvelables et des liaisons HVDC conduit à une augmentation de la pénétration de l'électronique de puissance dans les réseaux de transport d'électricité. Comme les convertisseurs possèdent des propriétés physiques différentes de celles des alternateurs synchrones, une évolution des contrôles employés s'avère nécessaire. Au vu de la taille des ensembles à simuler, la validation de solutions innovantes doit être réalisée par des simulations numériques et il est nécessaire d'être vigilant sur les outils utilisés afin d'éviter des temps de calcul prohibitifs. Dans cette thèse, des outils et des méthodes pour l'analyse et la simulation de réseaux de transport 100 % électronique de puissance sont développés. Une partie importante des travaux est consacrée à la modélisation des convertisseurs, ce qui permet de réaliser des simulations numériques plus ou moins précises en fonction du cahier des charges de l'étude et d'appliquer ou de développer des méthodes d'analyse de stabilité. Un modèle simplifié du réseau Irlandais est utilisé comme réseau exemple de façon à valider les méthodes et outils développés dans le cadre de la thèse.

Mots clés : Analyse des réseaux de transport, 100% Électronique de Puissance, Simulation de réseaux électriques, Réduction de modèles

Tools and Methods for the Analysis and Simulation of Large Transmission Systems Using 100% Power Electronics

ABSTRACT:

The development of renewable generation and HVDC links lead to an important increase of the penetration of power electronics in the transmission systems. As Power Electronics converters have completely different physical behavior than synchronous machines, an evolution in the way TSOs control transmission systems is needed. It is impossible to build a real size prototype of a transmission system. The validation of the solutions must be done using dynamic numerical simulations. Because of the size of the studied systems, we have to be careful with the simulation tools that we use, in order to reduce the computation time. In this PhD tools and methods for the analysis and simulation of large transmission systems using 100% power electronics are developed. An important part of the work looks at the models of the converters. Those models allow us to do numerical simulations and to apply and develop stability and performance analysis methods for the considered system. A simple model of the Irish network will be used as an example in order to assess the developed methods.

Keywords : Power Systems Analysis, 100% Power Electronics, Power System Simulation, Model order reduction

Arts et Métiers Sciences et Technologies

HESAM UNIVERSITÉ